CHALMERS

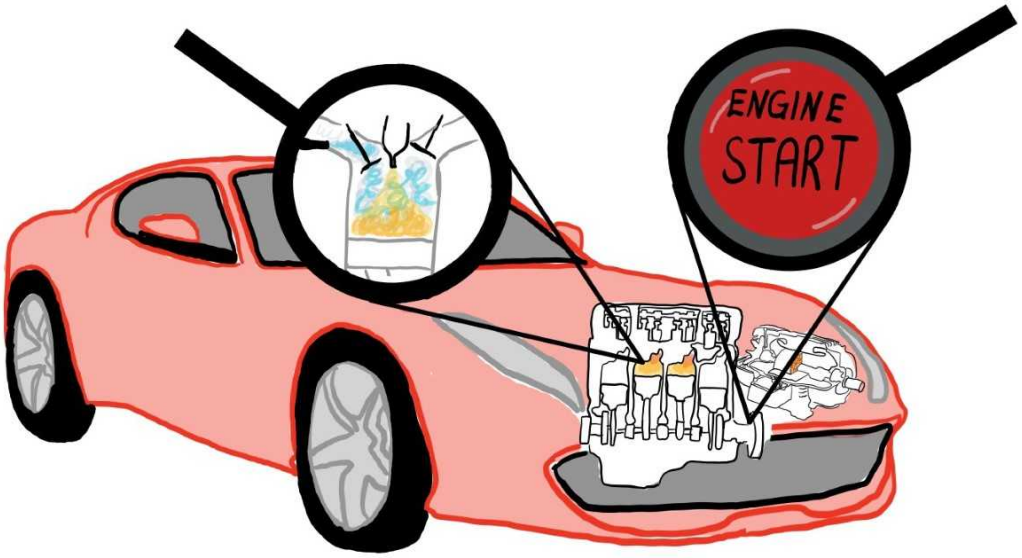

Towards High Efficiency Powertrains

An investigation into technologies to improve powertrain efficiency

JAYESH KHATRI

Department of Mechanics and Maritime Sciences
CHALMERS UNIVERSITY OF TECHNOLOGY
Gothenburg, Sweden 2022

Thesis for the degree of Doctor of Philosophy

Towards High Efficiency Powertrains

An investigation into technologies to improve powertrain efficiency

Jayesh Khatri

Department of Mechanics and Maritime Sciences
CHALMERS UNIVERSITY OF TECHNOLOGY
Göteborg, Sweden 2022

Towards High Efficiency Powertrains
An investigation into technologies to improve powertrain efficiency
Jayesh Khatri
ISBN 978-91-7905-609-4

Doktorsavhandlingar vid Chalmers tekniska högskola
Ny serie nr 5075
ISSN 0346-718X

Department of Mechanics and Maritime Sciences
Chalmers University of Technology
SE–412 96 Göteborg, Sweden
Telephone + 46 (0) 31 – 772 1000

Cover: The two technologies, Water Injection and Cleaner Engine Starts in SI engines, investigated as part of this dissertation. Designed by Annabelle Jerre in Notability© (from Ginger Labs, Inc.)

Typeset by the author using LaTeX.

Printed by Chalmers Reproservice
Göteborg, Sweden 2022

to perpetual learning..

Abstract

In recent years there has been a great shift whereby conventional vehicles powered by an internal combustion (IC) engine are being partially or completely replaced by electrified alternatives; almost all major automotive manufacturers have made statements indicating a shift towards electrification. This shift has been driven in large part by concerns about climate change, which have prompted lawmakers to introduce increasingly strict regulations limiting vehicular emissions, particularly of carbon dioxide (CO_2). Hybrid electric vehicles (HEVs) that combine an electric motor with an efficient downsized spark-ignited engine offer a viable solution to these challenges.

This thesis presents studies on two different strategies with the potential to improve the efficiency of spark-ignited engines and, by extension, that of hybrid systems. The first strategy is water injection, which was studied as part of a project seeking to optimize an SI engine for use in a high efficiency hybrid powertrain. The second strategy is cleaner engine starts, which was studied as part of a project seeking to improve the efficiency and reduce emissions during engine starts.

Downsizing SI engines makes it possible to reduce fuel consumption and improve efficiency without loss of power output. However, downsizing while maintaining high thermal efficiency leads to high cylinder pressures and temperatures, which increases the propensity for knocking combustion. Water injection (WI) has been used to mitigate knock and was therefore investigated during the first phase of the project. Experiments were conducted on a 3-cylinder 1.5L turbocharged engine with a port water injection (PWI) system to assess the effects of water injection on knock and efficiency. To account for the variation in the research octane number (RON) of commercially available gasoline blends, experiments were performed using gasoline blends with RONs of 91, 95, and 98. The first test campaign showed that WI enables stoichiometric operation and advancement of ignition timing while suppressing knock. A follow-up experimental campaign focused on investigating the effect of the relative humidity (i.e., the water content of the ambient air) on the efficiency benefits of WI. The engine was operated at three different humidity levels, which were established and maintained using a humidity control system developed in-house. This campaign revealed that the knock suppressing effect of WI in the studied engine was mainly due to charge dilution; the charge cooling effect due to the injected water's heat of vaporization was insignificant. Finally, a simulation study was performed in GT-Suite to assess the feasibility of using WI in a hybrid vehicle. The simulations showed that the improvement in BSFC due to WI was maximized in highly downsized engines.

Engine starts were investigated during the second phase of the project. Since, any driving event in a hybrid vehicle will inevitably involve multiple engine starts and/or restarts, the objective during this phase was to develop methods to study engine starts and to use these methods to find ways of improving the engine's starting efficiency. The first investigations in this area were conducted on a hybrid system; later experimental work focused on an isolated engine setup. The hybrid system featured a 1.5L turbo-charged SI engine with Port Fuel Injection (PFI) in a P2.5 Hybrid architecture. Tests were performed under various drive cycles including WLTC and RTS95. The start events were categorized into three different categories (cold, mild, and warm starts) based on the initial three-way catalyst (TWC) temperature, and it was found that warm starts were most common. The second campaign therefore investigated electric motor (EM)-assisted warm engine starts in a Gasoline Direct Injection (GDI) engine. EM-assisted starts were modeled by performing dynamometer-assisted starts on the engine test bed. During this work, methods were developed for categorizing, understanding, and optimizing engine starts for different powertrain architectures. On the basis of a simple case study of a hybrid system, it was estimated that engine start optimization could reduce CO_2 emissions by approximately 1.75 g per kilometer if comparing the most efficient conditions to the standard engine starting condition.

Keywords: Downsized spark-ignition engines, water injection, RON, knock mitigation, warm engine starts, hybrid powertrain, efficient engine starts

Acknowledgments

The length of this section shows how many people I have to thank for helping me reach the end of my PhD. In one way or another, everyone mentioned here (apologies to anyone I accidentally overlooked!) has helped me during this journey.

First and foremost, I appreciate the efforts of Lucien Koopmans and Ingemar Denbratt, who offered me this position. To my supervisor, Lucien, I am grateful for your expertise, assistance, guidance, and patience throughout this project. I also thank Ingemar, my co-supervisor, for his guidance and support in the project. I have learnt a great deal from both of them and am forever in their debt.

Besides my supervisors, I would like to extend my sincere gratitude to Petter Dahlander and Lars Jernqvist for their assistance with data collection and analysis. Special thanks are also owed to Robert Buadu, for his support during the hybrid tests in Cell H and for all of our varied discussions on subjects ranging from *nerdy* tech topics to political issues. I would also like to thank all the research engineers from the lab - Anders Mattsson, Alf-Hugo Magnusson, Timothy Benham, Patrik Wahlin, and Anders Bragée. In one way or another, I have learnt something from each one of them. And I certainly look forward to taking those 100 SEK from the board in the next Hanging (spinning) Bar Challenge! Please do send me the invite.

Additionally, I would like to mention Prof. David Blekhman and thank him for the insights he provided on PhD as an experience and for all our talks on shared interests ranging from hydrogen combustion to beautiful watches. I would also like to thank Prof. Bengt Johansson, for reading my thesis and providing valuable feedback and for the short yet interesting discussions about motorcycles.

I am especially grateful to the Swedish Energy Agency for funding this project, and to Volvo Cars, especially Thomas Bernichon and Fredrik Ekström, for the water injection hardware and your kind support. I sincerely thank CEVT Powertrain AB for providing the funding and hardware for the *Cleaner Engine Starts* project. I owe a great debt to the team behind this project - Johan Hellsing, Håkan Sandquist, Magnus Örngrip, and Simon Klacar. Thank you for all the input and our reference meetings. It was a challenging project, but I hope we were all satisfied with the results, including the ones that were rather unexpected!

I will also always be grateful to AVL List GmbH for their collaboration and support during the latter part of the PhD, and for giving me the opportunity to do my research exchange at Graz, where I not only conducted experiments but also got to meet some amazing professionals. Along with whole AVL team, I would especially thank Hans-Michael Koegeler, who made this journey with AVL possible and supported me during my research and in my efforts to get to grips with the AVL tool chain. I am also very thankful to the rest of the team - Harald Mayrhofer, Ganesh Balachandaran and Pierre Suchet.

I also have many people to thank from the administration team at Chalmers. To Angela Hillemyr and Robert Thomson, thank you for being such good leaders and providing a spectacular experience for all the PhD students at M2. To Anna-Lena Larsson, Åsa Eriksson, and Katrin Axelsson, thank you for all the support you provided during my PhD and the non-PhD work. Whenever I struggled with any protocol in the system, you always came through. Tack!

I must also acknowledge my colleagues; this will be a long paragraph. To Elenor Norberg, thank you for listening to my stories and quarter-life crises and helping me learn some Swedish. I remember the first thing you said when I came to you as a novice Swedish learner: Jag har alltid tid för dig. Now I see you literally meant it. Learning Swedish, both the language and the culture, has been an incredible experience, although sometimes a challenging one! *Stort tack till* Lars, Elenor *och* Sven Andersson for the anecdotes and for teaching me the subtleties of Swedish language and culture – your lessons greatly smoothed my integration with the highly social, albeit sometimes reluctant, Swedes! My fellow PhD students provided endless laughs and conversations at the lunch table and during *fika* breaks, as well as on some memorable trips we took together. I would particularly like to acknowledge my colleagues Victor Ebberstein, Ahfaz Ahmed, Nikhil Sharma, and Mindaugas Melaika for all of our conversations related to the project and about all manner of unrelated things. To Magnus Walander (M-dog), thank you for suggesting all the Adam Sandler movies to watch during the stressful times at work and coffee breaks towards the end of the PhD. I must also give a special shout-out to the Butterfly Boyz - from one proud member of the club to others: it has been a sheer pleasure!

Last but by no means least, I would like to thank my family for their moral support and all those phone calls, which never made me feel like I was 6000 km away from home. Special thanks are reserved for my grandparents: you are always keen to know what I am doing and how I am proceeding, although it is highly unlikely that you have ever grasped what it is all about! I hope I am making you proud.

Jayesh Khatri
Göteborg, December 2021

List of Publications

This thesis is based on the following appended papers:

Paper ??. Khatri, J., Denbratt, I., Dahlander, P., and Koopmans, L. (2019). *Water injection benefits in a 3-cylinder downsized SI-engine.* SAE International Journal of Advances and Current Practices in Mobility, 1(2019-01-0034), 236-248.

Paper ??. Khatri, J., Sharma, N., Dahlander, P., and Koopmans, L. (2020). *Effect of relative humidity on water injection technique in downsized spark ignition engines.* International Journal of Engine Research, 22(7), 2119-2130.

Paper ??. Khatri, Jayesh and Koopmans, Lucien (2020). *Water Injection System Application in a Mild Hybrid Powertrain.* SAE Technical Paper, 2020-01-0798.

Paper ??. Khatri, J., Koopmans, L., Sandquist, H., Örngrip, M., Hellsing, J., Mayrhofer H., and Koegeler, H.M. (2021). *Methodology Development for Investigation and Optimization of Engine Starts in a HEV Powertrain.* submitted as SAE Technical Paper in *WCX* 2022.

List of Acronyms

AFR	–	Air Fuel Ratio
AKI	–	Anti knock Index
aTDC	–	after Top Dead Centre
BEV	–	Battery Electric Vehicle
BMEP	–	Break Mean Effective Pressure
BSFC	–	Brake Specific Fuel Consumption
bTDC	–	before Top Dead Center
bBDC	–	before Bottom Dead Center
CAD	–	Crank Angle Degree
CO	–	Carbon Monoxide
CoV	–	Coefficient of Variation
CO_2	–	Carbon dioxide
C_p	–	Specific Heat Ratio at constant Pressure
CPC	–	Condensation Particle Counter
Cv	–	Specific Heat Ratio at constant Volume
DAQ	–	Data Acquisition
DCT	–	Dual Clutch Transmission
ECU	–	Electronic Control Unit
EGR	–	Exhaust Gas Recirculation
EOI_w	–	End of Water Injection
EV	–	Electric Vehicles
HEV	–	Hybrid Electric Vehicle
HVO	–	Hydrotreated Vegetable Oil
ICE	–	Internal Combustion Engine
IMEP	–	Indicated Mean Effective Pressure
IVO	–	Intake Valve Opening
KLSA	–	Knock Limited Spark Advance
KPI	–	Key Performance Indicator
LCA	–	Life Cycle Analysis
LD	–	Light Duty
LHV	–	Lower Heating Value
MBT	–	Maximum Brake Torque
MEP	–	Mean Effective Pressure
MFB50	–	Mass Fraction Burn 50%
mg/cycle	–	milligram/cycle
MHEV	–	Mild Hybrid Electric Vehicle

NEDC	–	New European Drive Cycle
NO_x	–	Nitrogen Oxide
OI	–	Octane Index
P	–	Pressure
PHEV	–	Plug-in Hybrid Vehicle
PM	–	Particulate Matter
PWI	–	Port Water Injection
RDE	–	Real Drive Emission
RHS	–	Relative Humidity System
rpm	–	revolutions per minute
RON	–	Research Octane Number
RTS95	–	Standardized Random Test 95
SI	–	Spark Ignition
SOI	–	Start of Injection
TDC	–	Top Dead Center
THC	–	Total Hydrocarbon
TWC	–	Three Way Catalyst
V	–	Volume or Volt
WI	–	Water Injection
WLTC	–	Worldwide harmonized Light-duty vehicles Test Cycle
WOT	–	Wide Open Throttle

Contents

Part I

Introductory Chapters

Chapter 1

Introduction

1.1 Motivation

Climate change has become a major issue in recent decades as the ongoing increase in greenhouse gas (GHG) emissions has raised the average global temperature. Greenhouse gases, and Carbon dioxide (CO_2) in particular, have been identified as the main causative factors of this process: a 2014 report [1] released by the IPCC (Intergovernmental Panel on Climate Change) stated that CO_2 comprised 65% of total global greenhouse gas emissions during the year 2010, with the transportation sector alone being responsible for 14% of global greenhouse gas emissions, as shown in Figure 1.1.

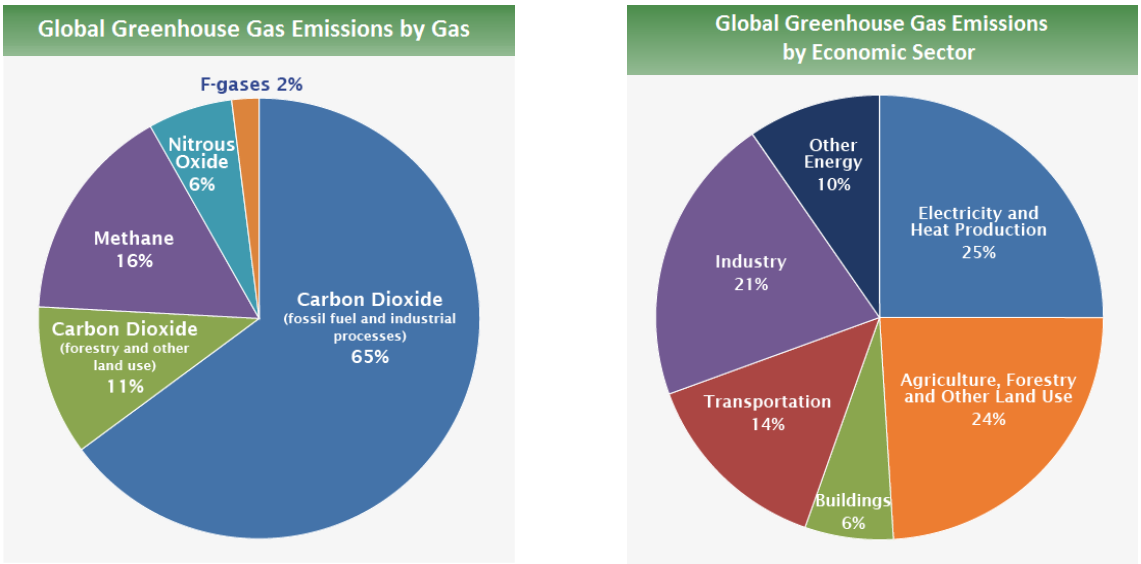

(a) by Gas (b) by Sector

Figure 1.1: Global greenhouse gas emissions sources in the year 2010 [1]

Since then, the transportation sector's share of greenhouse gas emissions has only increased: a 2017 EEA (European Environment Agency) report [2] found that 28% of total greenhouse gas emissions were attributable to transportation. As shown in Figure 1.2, almost 72% of greenhouse gas emissions attributable to the transport sector in the EU came from road transport, with 44% being specifically attributed to passenger cars. Consequently, there is an urgent need to reduce greenhouse gas emissions from passenger cars.

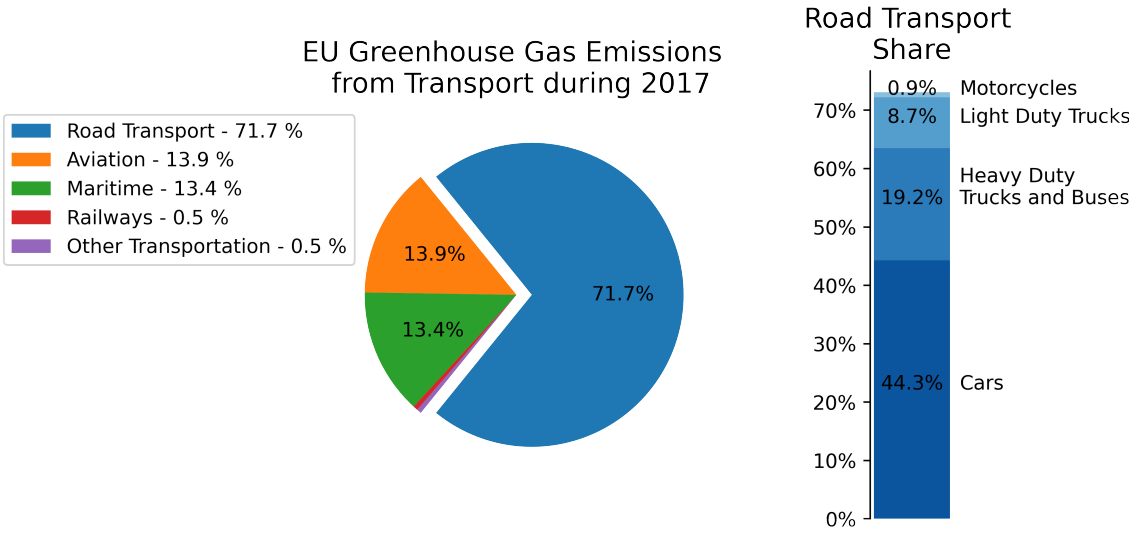

Figure 1.2: GHG emissions sources within the transportation sector in the EU during the year 2017 (Data Source: European Environment Agency [2])

Carbon dioxide emissions from vehicles are directly related to their fuel consumption: the greater the volume of fuel that is burned, higher the CO_2 is produced. Consequently, even small reductions in fuel consumption can have a significant impact on the global scale, and major efforts are being made to reduce CO_2 emissions by increasing engine efficiency. These efforts are further spurred by increasingly strict limits on CO_2 emissions imposed by legislative bodies, which (very rightly) place significant pressure on the automotive industry to reduce emissions.

Electrification of automotive powertrains is seen as the most viable way of reducing GHG emissions, so legislative bodies and policy makers tend to favor pure electric vehicles. Accordingly, a Life Cycle Analysis (LCA) comparing conventional and electric vehicles conducted by Hawkins et al. [3] compared that a small Battery Electric Vehicle (BEV) powered by electricity drawn from the European grid would have significantly lower GHG emissions over its life cycle than a comparable vehicle with a conventional internal combustion (IC) engine. However, the study also found that BEV production was linked to significant increases in human toxicity, freshwater eco-toxicity, freshwater eutrophication, and metal depletion. Similar conclusions were drawn in a separate report [4].

Andersson and Börjesson [5] recently published a life cycle analysis of vehicles' greenhouse gas impact, and suggested that plug-in hybrid could better enable automotive sector to achieve future climate goals than battery-electric vehicles. Figure 1.3 shows equivalent CO_2 in g/km for three different powertrains, with varying degrees of electrification.

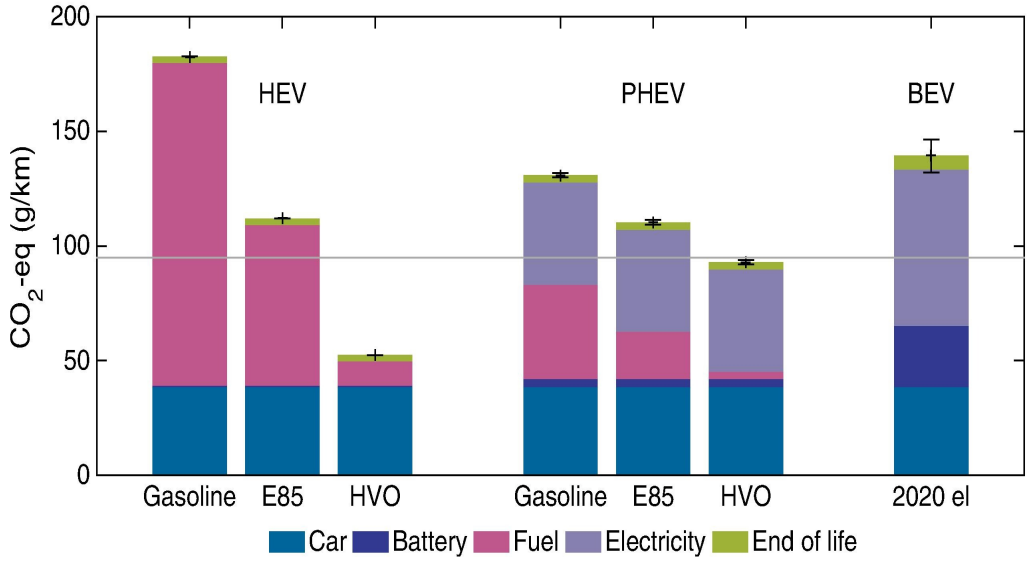

(a) using 2020 EU-28 electricity

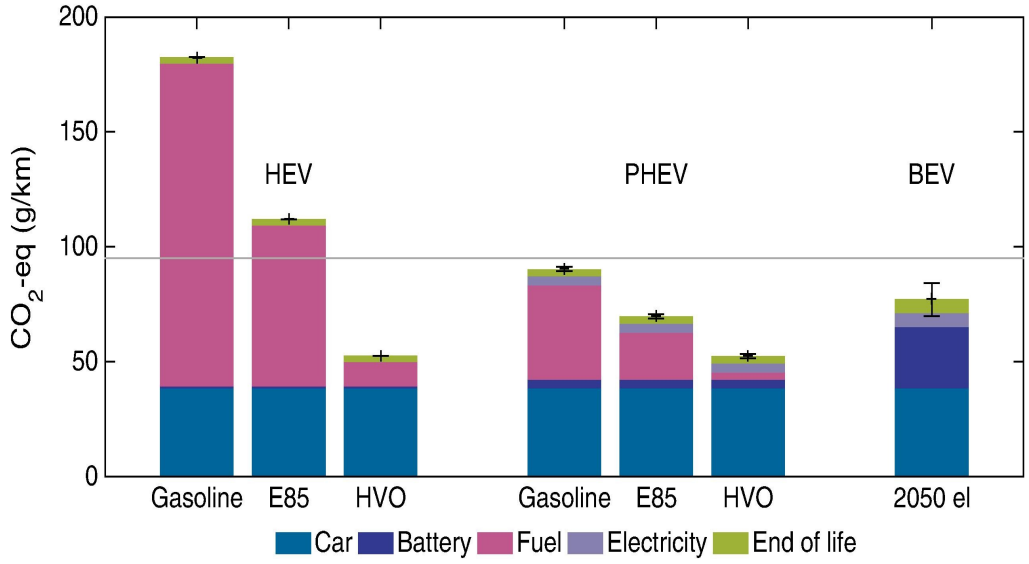

(b) using 2050 EU-28 electricity

Figure 1.3: Life cycle CO_2 emissions for a hybrid electric vehicle (HEV), plug-in hybrid electric vehicle (PHEV), and battery electric vehicle (BEV) [5]

The colors in figure 1.3 represent different sources of CO_2 emissions over a car's life cycle, from the manufacturing of the vehicle and its battery to the usage phase and finally the end-of-life emissions. The horizontal gray line in the figure represents the European fleet average limit of 95 g CO_2 per kilometer. Vehicle manufacturers incur a penalty if their fleets exceed this limit. However, the limit is not relevant

in the LCA context because the legal requirements apply only to tank-to-wheel emissions. Because current certification methods assume that BEVs produce no CO_2 emissions, the tank-to-wheel CO_2 emissions of HEVs and PHEVs are lower than those shown in the figure. HEVs generate both the lowest and highest lifecycle GHG emissions - highest when fueled with gasoline and lowest when fueled with Hydrotreated Vegetable Oil (HVO), a second-generation biofuel. The figure also shows that given the current EU electricity generation mix, electrification will not be sufficient to meet the 95 g per km CO_2 target from a life cycle assessment perspective. Moreover, both PHEV and HEV variants have lower total CO_2 emissions than a BEV when powered with biofuels; lifecycle emissions for a HEV using HVO as its fuel are significantly lower than those for a BEV.

Figure 1.3b shows the CO_2 emissions for the same vehicles with the expected EU electricity generation mix for 2050. Using the expected 2050 grid, the life cycle CO_2 emissions for BEVs fall below the 95 g per km target, largely because of the availability of sustainably generated electricity. Even though the life cycle emissions of HEVs in this scenario are identical to those predicted using the current generation mix, HEVs fueled with HVO still have a lower life cycle carbon footprint than BEVs.

The move towards electric vehicles is welcome if we assume that they are powered using electricity generated from renewable sources and that battery production can be made more sustainable than it currently appears to be. However, these conditions may not always be satisfied. Moreover, the energy density of currently available batteries is limited, their cost of production is high, and their charging times are relatively long, all of which place significant constraints on the use of pure electric vehicles. However, given the need to reduce carbon emissions to control climate change and comply with legal requirements, the continued use of conventional vehicles powered by an internal combustion engine (ICE) burning fossil fuels is clearly unsustainable. As such, hybrid vehicles are likely to play an important role for the foreseeable future and there is an urgent need to find new ways of increasing the efficiency of hybrid powertrains. To help meet this need, the work presented in this thesis focused on improving the efficiency of the IC engine component of a hybrid powertrain, where investigation of two technologies (water injection and engine starts) was performed.

Water Injection

It has been shown that hybrid powertrain architectures combining batteries and electric motors with SI engines could satisfy forthcoming emissions requirements, so much research has focused on improving the efficiency of SI engines in such systems under conditions where the electric motor (EM) cannot be used, and the SI engine must take over. Turbocharging and engine downsizing make it possible to ensure that when the SI engine must take over like this, it can do so maintaining a high compression ratio while operating in high efficiency regions of the engine map.

However, a major challenge of engine downsizing is the increased propensity for knock. Knock is the name given to the noise associated with the very rapid, high amount of heat release due to auto-ignition of the end gas ahead of the flame front, resulting in high pressure waves [6]. In the literature, several terms are used to describe this phenomenon - knock, knocking combustion, knocking and engine knock. For consistency, *knock* and *knocking combustion* are interchangeably used in this thesis. It is an inherent problem in combustion engines and can damage SI engines in different ways [7]. Because of its significant role in limiting efforts to improve combustion engines efficiency, knock has been studied extensively [7, 8, 9]. Knock is usually suppressed by retarding ignition, improving octane rating or mixture enrichment; retarding ignition reduces engine efficiency as the ignition timing moves away from maximum brake torque (MBT) timing and creating sub-optimal combustion phasing. Additionally, ignition retard under high load conditions exposes the exhaust after-treatment components to high exhaust gas temperatures. Under such conditions, fuel enrichment is used to reduce exhaust temperatures and suppress knock, but this significantly increases the fuel consumption or Brake Specific Fuel Consumption (BSFC). Additionally, recent standards have made it mandatory to maintain high three-way catalyst (TWC) conversion rates over the entire engine map, which requires stoichiometric engine operation. Figure 1.4 shows the engine map for a downsized engine to explain these challenges.

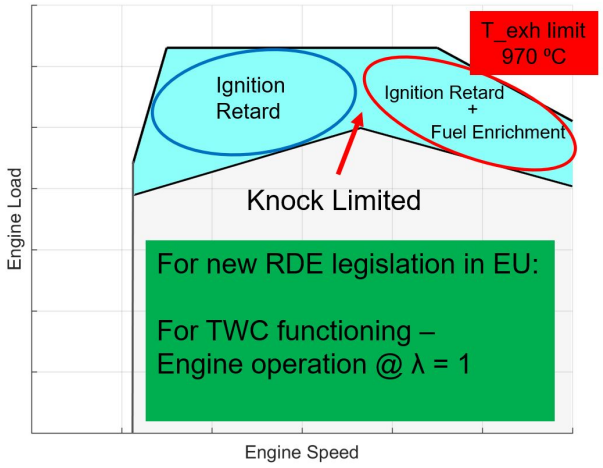

Figure 1.4: Engine map of a downsized SI engine showing the high load, high speed region in which fuel consumption is increased.

The high load region where knock must be controlled is shown in cyan. In the left-hand part of this region (which corresponds to high load but low or moderate engine speeds), ignition retard is used to reduce the cylinder pressure and temperature so as to prevent knock. The right-hand part of this region corresponds to operating conditions with high loads and high engine speeds. Under these conditions, ignition retard causes delayed combustion in the later part of power stroke and thus raises the gas temperature in the exhaust manifold. This is harmful to the exhaust after-treatment system, which cannot tolerate temperatures above 950-980 °C. Therefore,

fuel enrichment is used in this region (in addition to ignition retard) to induce a charge cooling effect and prevent damage to the after-treatment system. Unfortunately, this directly increases fuel consumption. Alternatively, water injection (WI) can be used in this region to suppress knocking combustion while still using a stoichiometric air:fuel mixture (i.e. $\lambda = 1$).

Water injection has been used in internal combustion engines since the 1940s. Although the reasons for its use have changed over time, the mechanisms responsible for its effects remain unchanged. In recent years, water injection technology has been investigated, developed, and used in IC engines for compact vehicles. The research on the subject is still limited and therefore, water injection was chosen as one of the research subjects for this project. The experimental work was performed on a 3-cylinder downsized engine, provided by Volvo Cars, and was equipped with a port-water injection system.

Engine Starts Investigation

Engine starts are highly transient events, and since a HEV will necessarily have multiple engine starts during any drive event, any minor improvement in fuel consumption will result in significant energy saving over the total life cycle of a vehicle. Hence, it becomes important to understand the engine starts from a system's perspective. During the benchmarking of the hybrid powertrain under the engine starts investigation, it was noted that most starts during a drive event are warm starts (especially in HEVs). In a study by Eckl et al [10], the authors predicted that a hybrid vehicle goes through about 0.6 million engine (re-)starts during its lifetime. Additionally, given the NVH benefits of starting the engine with EM assistance, increasing numbers of OEMs (including CEVT [11]), now intend to use clutch starts rather than a 12V starter motor in their future HEVs. And considering the high attention already given to cold starts, the scope of the research was further narrowed to consider only warm starts with EM assistance. Figure 1.5 shows how engine starts can be classified based on the starting temperature (cold or warm) and the method of starting (clutch or 12V), illustrating the start types of interest.

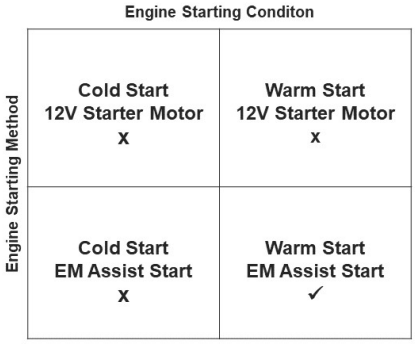

Figure 1.5: Classification of different start types showing the area of focus for the research presented in this thesis.

1.2 Objectives and Research Questions

This thesis presents research conducted within the framework of the *High Efficiency Hybrid Powertrain* project, funded by Swedish Energy Agency (*Energimyndigheten*). Its overall goal was to investigate strategies for improving efficiency of powertrain systems and the project was executed in two phases. Figure 1.6 outlines the scope phases and the work performed as part of this PhD project.

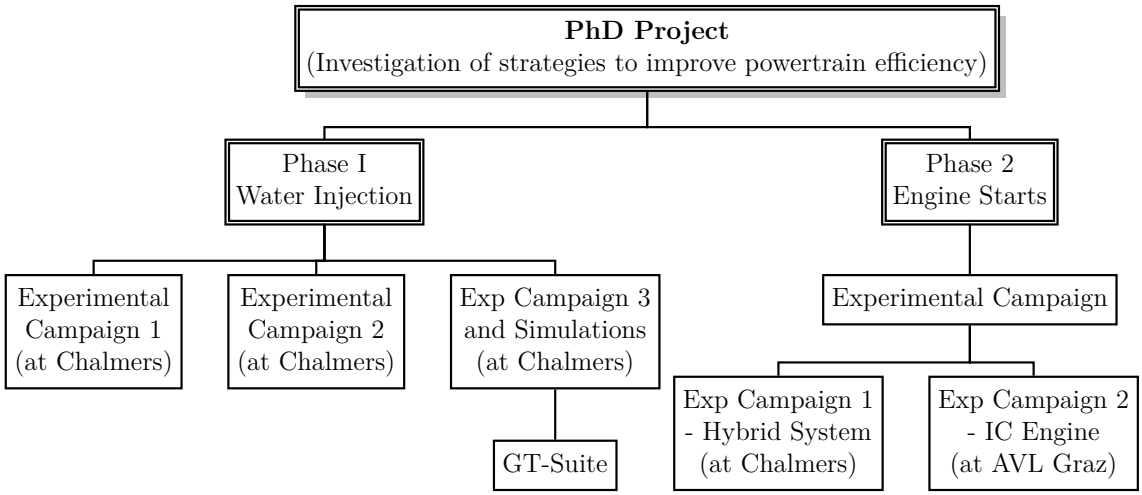

Figure 1.6: Scope of research work in this thesis

During the first phase of the project, investigation of water injection in spark ignited (SI) engines was carried out. Its objective was to analyze the benefits and underlying mechanism of water injection in SI engines - in particular, its potential to suppress knocking combustion and enable higher thermal efficiency. Additionally, the gasoline available in different parts of the world, varies in octane rating which consequently effects the knock tendency. Hence, it was identified as an important research topic to investigate how water injection behaves for different octane ratings of gasoline and the results were presented in Paper 1.

From the first experimental campaign of water injection tests, one of the conclusions was that the high latent heat of evaporation of water, when injected had a significant charge cooling effect and subsequently better knock suppression. Also, during the first campaign it was observed that the inevitable daily variation in the ambient temperature, pressure, and humidity had notable effects on basic engine performance and other parameters. With high water content in the air, the rate of evaporative cooling decrease which will affect the charge cooling effect of the injected water. Under high humidity conditions, how is water injection performance affected? What is the underlying mechanism during those conditions? Would it be charge dilution or still the heat of vaporization? These questions (hypotheses) motivated the second experimental campaign and the content for paper 2. The experiments conducted during this phase took advantage of hardware and support provided by the Swedish car manufacturer Volvo Cars.

Effective use of water injection requires quantitative data on its effects on fuel efficiency. Therefore, the results obtained in the experimental campaigns were used to support the development of a simulation model that could be used to predict the improvement in fuel efficiency for an SI engine with water injection over different drive cycles. Hence a GT-Suite simulation model developed at the division of Combustion and Propulsion Systems at Chalmers, was used to simulate the benefits and consumption of water injection in a HEV powertrain. The simulation model was based on a 48V hybrid vehicle, which is currently a popular technology for hybrid vehicles among automotive manufacturers. The results from this campaign were presented in paper 3.

Finding ways to make IC engines cleaner and more efficient, during engine (re-)start events was one of the objectives of investigating engine starts. Engine starts are relatively easier to study in engines in isolation, however, as the system complexity increases with electrified powertrains, it becomes challenging. Hence, as an initial objective, development of a methodology to ease engine start investigations was targeted. The work on engine starts investigation was performed in collaboration with the Gothenburg-based CEVT AB (China Euro Vehicle Technology) division of the Geely group. The combined objective of this collaboration was to study engine starts and develop ways of achieving a more efficient start strategy (in a system where one can choose ICE or EM) independent of driving event. The hardware used in this phase was a hybrid powertrain with a state-of-the-art 7-speed dual clutch transmission (DCT) and was provided by CEVT. The experiments in this phase were performed under two test campaigns. Experiments in the first campaign were performed on Chalmers university's hybrid testbed. Later in the project, the Austrian powertrain consulting company AVL List GmbH joined the collaboration, to provide support in the use of their AVL CAMEO toolchain to prepare and automate tests and data collection when performing experiments. As part of this collaboration, the author also visited AVL in Graz to use the company's engine testbed in order to refine experimental methods, which constituted the second test campaign of phase 2 (engine starts) of the project. A vast amount of data was collected to investigate the engine starts from both test campaigns, using hybrid and engine testbeds. The relevant data was filtered, post processed and presented in the fourth publication.

Research Questions

From the above objectives, following research questions were formulated:

- **What advantages does water injection offer considering the efficiency and performance of IC engines?**
- **How does the water content in atmosphere (relative humidity) affect the functioning of water injection? What are the mechanisms behind the effects of water injection?**

- **Is it worth having a water injection system in a car?**
- **How can engine starts in different powertrain architectures be studied more effectively?**
- **How can the developed methodology be used in the optimization of engine start for warm start conditions?**

1.3 Thesis Outline

This thesis is organized into seven chapters. The current chapter provides an overview of the problems caused by greenhouse gas emissions as well as the contribution of the automotive sector (and passenger cars in particular) to those emissions. It also outlines the problems facing the automotive industry as it strives to reduce the CO_2 emissions of new vehicles. These two factors constitute the motivation for efficient engines and powertrain; and the work presented in the subsequent chapters is an attempt to achieve this goal. Also mentioned in the first chapter are the objectives and the research questions within the framework of this PhD project. Chapter 2 provides a brief introduction to water injection, the first technology investigated in the project. Key publications and theoretical considerations pertaining to water injection are summarized, and a brief history of the technology in recent decades is presented. This chapter also illustrates the varied historical applications of this technology, including its uses in military aircrafts (fighter jets). Chapter 3 introduces the issues surrounding engine starts and their effects on emissions. Both cold and warm starts are discussed with reference to previous literature. Chapter 4 presents the experimental setups and methods used in the two research phases. It also includes a discussion of the simulation environment used to analyze the potential benefits of water injection in hybrid vehicles. In chapter, 5, a brief summary of all the appended publications, on which this thesis is based, is presented. Chapter 6 presents and discusses the main findings and results from the test campaigns and appended publications. Chapter 7 summarizes the conclusions drawn from the work presented in this thesis and provides a conclusive summary along with answers to the research questions put forth in section 1.2. Finally, Chapter 8 proposes some future research directions that could build on the work presented herein and summarizes the lessons learned during this research work.

Chapter 2

Water Injection

The efficiency of IC engines is mainly limited by knocking combustion, so for decades researchers and engineers have sought ways to prevent knock. Water injection is one technique that has been shown to be able to suppress knock without increasing BSFC. Moreover, it allows the engine to be operated at MBT or near-MBT timings with a stoichiometric air-fuel ratio (AFR) over the entire engine map, with direct beneficial effects on fuel consumption and CO_2 emissions. For example, a 13% reduction in fuel consumption was reported by Pauer et al [12]. Water injection is therefore seen as a promising option for increasing the efficiency of SI engines, especially downsized engines operating under high load conditions.

An early study on the benefits of water injection concluded that "with water addition to the emulsion, the research octane number rose from 91.2 to 100 for a 40 weight percent water emulsion [13]." Other authors have also concluded that water injection can increase the effective octane number of the fuel and improve its anti-knocking qualities, leading to reduced knock sensitivity, because of the cooling effect of water vaporization in the cylinder [14]. However, the effects of water injection have not been studied systematically using fuels with different octane ratings in a single experimental campaign. High RON (Research Octane Number) fuels are commonly used to provide knock resistance. However, high RON fuels are more expensive than lower octane fuels and are not available in all markets. Alcohol fuels have high latent heats of vaporization (e.g. 952 kJ/kg for ethanol) and octane numbers (>100), making them promising options for mitigating knock and enhancing performance. Alcohol fuels are also combustible and act as anti-freeze agents for water. Various water injection strategies using 50/50 blends of water with an alcohol such as methanol [15] and other non-gasoline fuels (e.g., LPG and hydrogen) have been studied [16, 17, 18]. Water injection system for internal combustion engines can be divided into two groups depending on whether the water is injected into the intake manifold or directly into the cylinder. Several publications have assessed the pros and cons of different water injection strategies [12, 14, 19, 20, 21] and the effects on cylinder charge properties resulting from injecting water into the intake manifold or directly into the cylinder.

2.1 Background

2.1.1 Historical Background

Water injection technology has been used in aircraft engines since the 1940s [22, 23, 24, 25, 26]. Its historical development is summarized visually in figure 2.1. Following its introduction by Harry Ricardo in the 1930s, the technology was mainly used in aircraft engines between the 1940s and 1960s. It was also used intermittently by automotive manufacturers such as General Motors (GM) and Saab in the later parts of the 20th century, and was recently (in 2015) used in a production car by BMW.

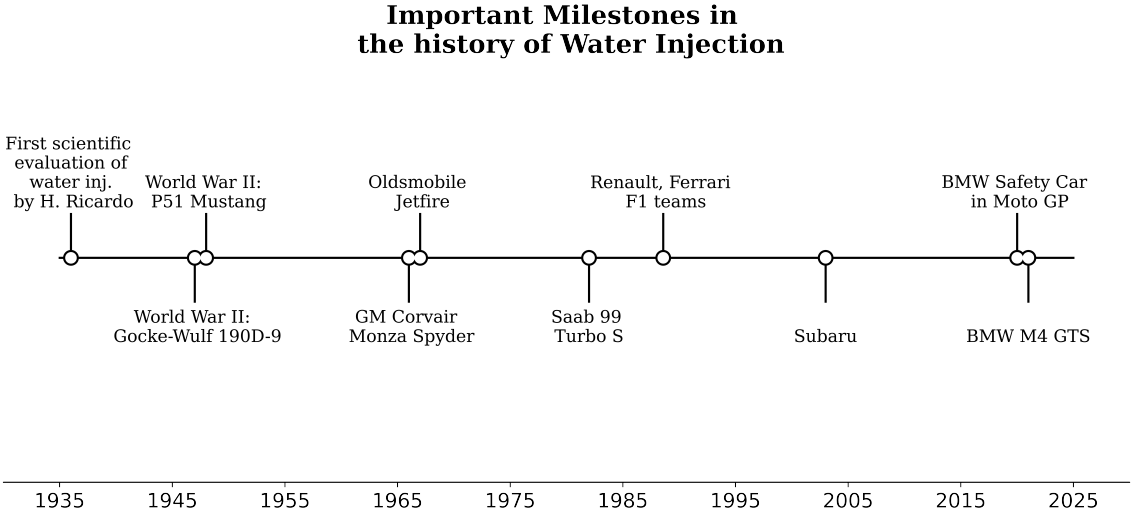

Figure 2.1: Historical timeline of water injection research and milestones

The technology was famously used in two iconic 1940s air-cooled radial aircraft engines: the 41.8-liter, 14-cylinder BMW 801 [27], which powered the Focke-Wulf 190, and the 18-cylinder Pratt & Whitney R2800 [28] used in the Republic P-47 Thunderbolt and Chance-Vought F4U Corsair. In 1950, the stock R2800 engine produced 2400 hp (1790 kW), but water injection allowed it to achieve power outputs as high as 3400 hp (2535 kW) under emergency combat conditions [29]. This engine is shown in figure 2.2.

The liquid-cooled, 35.7-L, V12 DB 605 engine from Daimler-Benz, which powered the World War II Messerschmitt Bf 109 fighter aircraft, used a MW50 (50% water-50% methanol) water injection [31] as a power-boosting anti-detonant agent that provided a charge-cooling effect and enabled the supercharged engines to use higher boost pressures for short time periods (approximately five minutes). As a result, the aircraft achieved hundreds of extra horsepower in combat situations [32].

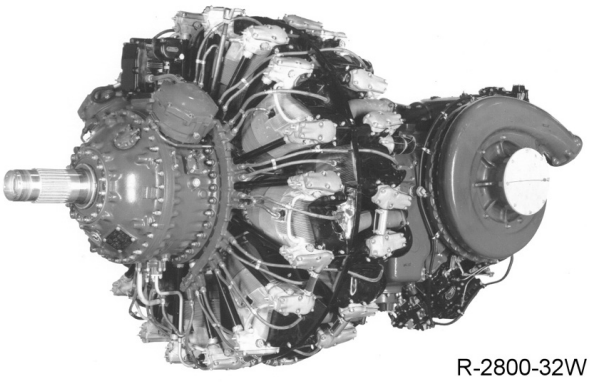

Figure 2.2: The iconic 18-cylinder Pratt & Whitney R2800 radial series engine that powered U.S. Thunderbolt and Corsair fighters, showing its water injection system. [30]

2.1.2 Application in Automotive Vehicles

Water injection has seen less use in passenger cars. Its first commercial application in this context occurred in 1962, when Oldsmobile developed a high compression ratio (10.25:1) turbocharged engine known as the Turbo-Rocket, which was rated at 215 hp. The high compression ratio created problems due to knocking combustion, which were overcome by using a novel water-injection system to spray distilled water and methyl alcohol into the air intake system [33]. A cross-section diagram of this *jetfire* engine is shown in figure 2.3. The Swedish automotive manufacturer Saab also developed a water injection system in the late 1970s for their Saab 99 Turbo S model; this system increased the engine's maximum power by 15-20 hp [34].

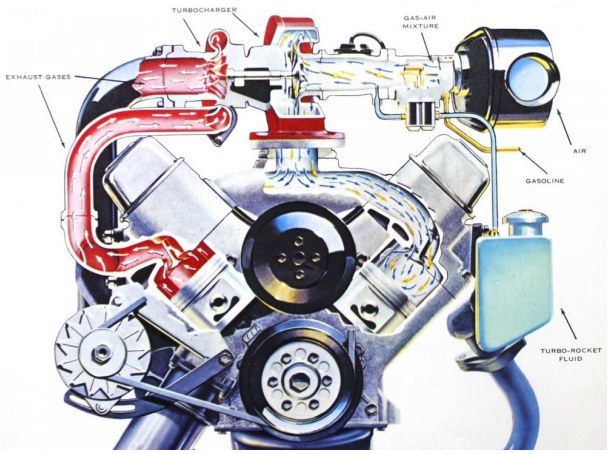

Figure 2.3: The 1962 Oldsmobile Jetfire V8 engine. The "turbo rocket fluid" used was a blended water-methanol mixture. [35]

2.2 Theory and Literature

Earlier aircraft and automotive engines were limited in raw power, but advances in engine technology obviated the need for water injection for some time. The technology has recently attracted fresh interest from manufacturers because of its knock-suppressing capabilities. Water's latent heat of vaporization (2250 kJ/kg) greatly exceeds that of gasoline (397 kJ/kg for RON95 E5 gasoline), so injected water should absorb more heat from the charge than gasoline, thereby reducing the charge temperature and the likelihood of knock. Water also has a higher specific heat capacity (C_p) than air, so water injection changes the thermodynamic properties of the charge during the compression and expansion strokes. Several authors have argued that the benefits of water injection are mainly due to charge cooling effects caused by evaporation [36, 37].

Another potential benefit of water injection in SI engines is reduction of tailpipe NO_x and CO emissions [16, 18, 20, 38]. The effects of water injection on NO_x and CO emissions at different values and engine speeds were therefore investigated in this work. Another important type of pollution emitted by vehicles is particulate matter (PM). In-cylinder water injection has been shown to substantially increase potential engine torque output, which directly affects particulate formation. For example, Hermann et al. [39] reported that increasing the water:fuel ratio in the combustion chamber can reduce PM emissions. However, increasing the water:fuel ratio in stoichiometric regions can also increase PM emissions by reducing the in-cylinder temperature because of the heterogeneous distribution of water droplets [40, 41]. Adding further complexity, the vaporization of liquid water together with localized increases in the specific heat of the gas surrounding the flame may reduce particulate emissions. The timing of the water injection can also have important effects on Brake Specific Fuel Consumption (BSFC) and particulate emissions: Tajima et al. [42] found that water injection during the latter half of the fuel injection period reduced soot formation within the flame. It is thus clear that much work remains to be done in order to clarify the effects of water injection on particulate emissions from SI engines.

A cause-effect diagram illustrating the benefits of water injection in spark-ignited engines is shown in figure 2.4. WI causes both direct and indirect improvements in fuel efficiency and engine performance. The underlying effect is due to a reduction in the in-cylinder charge temperature, which leads to knock suppression.

The major factors responsible for the knock-suppressing effects of water injection are evaporative cooling, flame temperature reduction, and changes in the specific heat properties of the charge mixture. However, water also acts as a diluent, extending and slowing combustion; this increases the time needed for the flame front to reach the end-gas and thus increases knock propensity. Another effect (not investigated here) stems from the dissociation of water molecules at high pressures and temperatures, which results in the formation of molecular oxygen. This would alter the mixture's

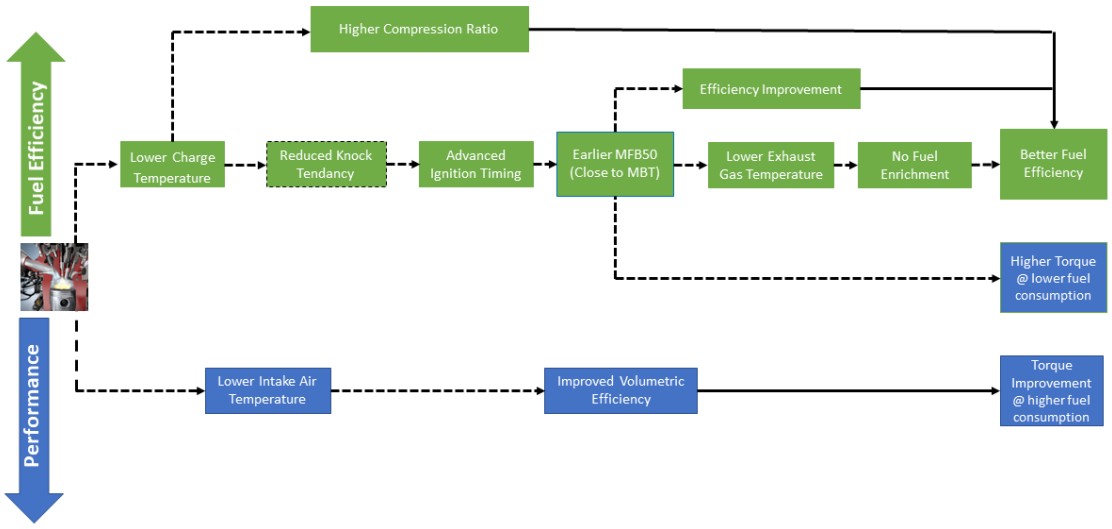

Figure 2.4: Cause-effect diagram outlining benefits of water injection in SI Engines [12]

properties and thus affect the combustion process, although the effect is assumed to be very small. To author's knowledge, a single study on the analysis of competing effects of different factors is lacking at the time of writing this thesis.

2.2.1 Water Injection Fundamentals

Thermodynamics

The thermodynamic properties of the working fluid significantly affect engine performance and must therefore be considered carefully. The main working fluids in an SI engine are usually air and fuel (gasoline). Both fluids consist of several different components, with water being an important component of air that is particularly relevant to any discussion of the benefits of water injection. Figure 2.5 below, shows the influence of water vapor on various thermodynamic properties of air.

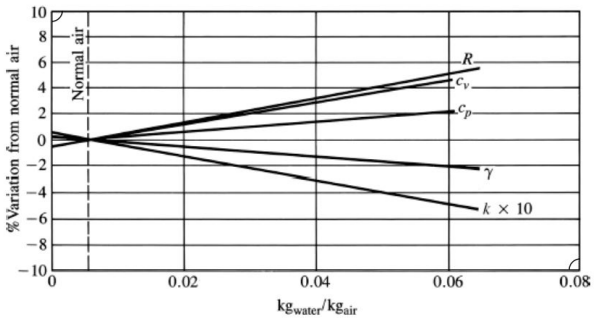

Figure 2.5: Effects of humidity on the properties of air. (From Taylor [43])

The figure shows that water vapor increases the specific heat capacity of the mixture and therefore reduces fuel-air-cycle efficiency. Equation 2.1 [6] describes the

relationship between fuel conversion efficiency and the specific heat ratio (κ or γ) of the mixture. The presence of water slows down combustion and increases time losses unless the spark is properly advanced as humidity (water content) increases, as discussed by Gardiner et al [44].

$$\eta_{f,i} = 1 - \frac{1}{r_c^{\gamma-1}} \tag{2.1}$$

The indicated fuel conversion efficiency ($n_{f,i}$) increases as the compression ratio (r_c) increases and decreases as the mixture's specific heat ratio (γ) decreases[6]. The indicated thermal efficiency varies with the fuel-air ratio but is also sensitive to the influence of water vapor on the thermodynamic properties of the working fluid (cylinder charge) before and after combustion. Figure 2.6 shows how humidity affects indicated thermal efficiency under no-knock conditions with constant fuel injection and spark timings [43].

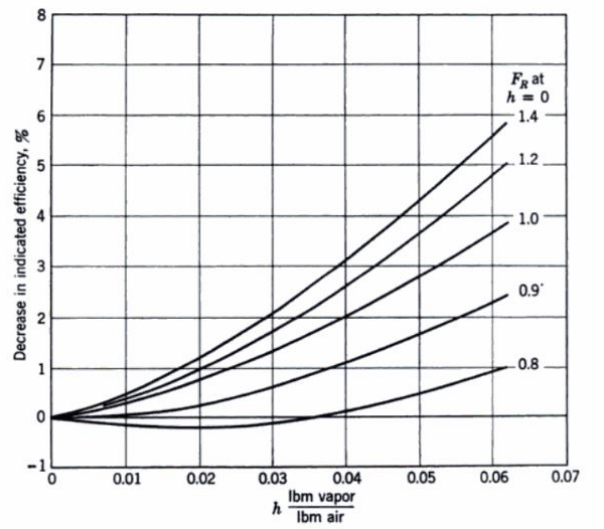

Figure 2.6: Effect of humidity on indicated thermal efficiency. (From Taylor[43])

Depending on the effectiveness of evaporation and charge cooling, the cycle efficiency may either increase or decrease. Pressure-volume diagrams for an SI engine in the standard and water-injected cases are shown in figure 2.7 to illustrate the effect of water injection on cycle work. The diagrams are based on the assumption that the water is fully vaporized at 170° bTDC. This causes the cylinder pressure to fall during the compression process, which reduces the compression work. However, water addition also reduces the peak cylinder pressure during combustion, resulting in a reduction in cycle work during combustion. As shown in the figure 2.7, the expansion work is similar in both cases. Thus, the work gained during compression is lost during the combustion process. In fixed compression ratio tests, water injection increases engine efficiency in some segments of the cycle and reduces it in others, resulting in little to no overall effect on cycle efficiency [13]. However, Taylor et al. [43] noted that "when spark-ignition engines are run near the detonation limit

humidity seems to act as a knock suppressor". A similar conclusion was drawn in a more recent publication [45], which found that water acts as an anti-knock agent when added to the air:fuel mixture. In effect, the injected water increases the fuel's effective octane rating, provided that the ignition/spark timing is adjusted to maintain MBT or near-MBT timing.

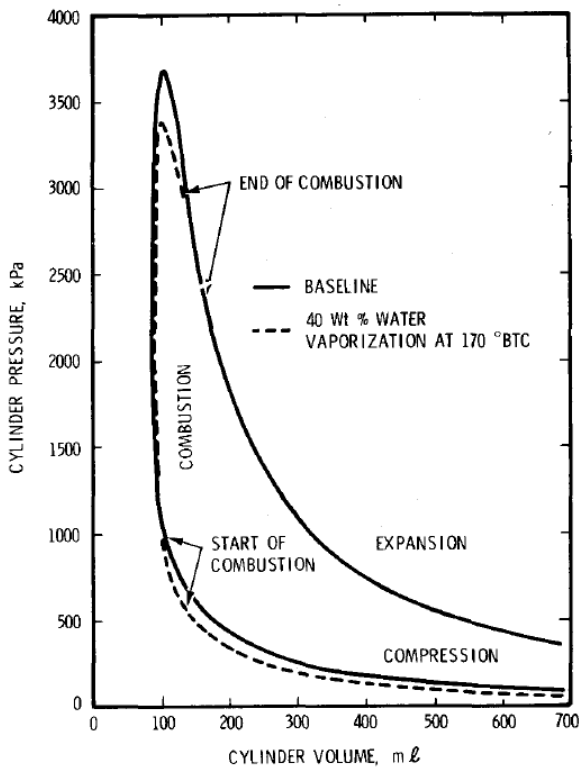

Figure 2.7: Calculated effect of water on the indicated pressure-volume curve. [13]

Effect of Atmospheric Variables

Variation in ambient atmospheric conditions can cause variation in engine power output. This is important because individual vehicle models may be sold and used in diverse geographical locations where they will be subject to significantly different climatic and atmospheric conditions including different temperatures, pressures, and humidity levels. Changes in atmospheric conditions (relative humidity) will affect the composition and properties of the engine inlet air and could potentially affect the engine's thermodynamic and anti-knock properties. In the 1960s [46], Ingamells et al. performed several experiments to investigate the relationship between the octane number requirements of IC engines and selected atmospheric variables including the humidity. They reported a linear relation between humidity and octane requirement, stating that an increase in absolute humidity reduced the required octane number. A more recent study conducted by the author of this thesis [45] found that water acts as an anti-knock agent, mitigating knock and enhancing performance. The impact of variation in atmospheric humidity on engine performance was investigated

by Gardiner [44], who suggested the use of a correction factor for moisture. In his book [43], Taylor also discusses the effects of atmospheric conditions (temperature, pressure, and humidity) on the performance of SI engines. Using Dalton's law of partial pressures and the ideal gas law, Taylor suggests that the density of the inlet air can be assumed to equal the density of air at a given temperature (T_i) and pressure(P_i), multiplied by a correction factor that accounts for variation in humidity, as shown in equation 2.2.

$$\rho_a = \frac{29p_a}{RT_i} = \frac{29p_i}{RT_i}\left(\frac{1}{1 + F_i(29/m_f) + 1.6h}\right) \tag{2.2}$$

where $_a$ = partial pressure of air
p_i = total pressure
R = gas constant
T_i = temperature
F_i = mass ratio of fuel vapor to dry air
m_f = molecular weight of the fuel vapor
h = humidity

The correction factor is shown in parentheses and includes the humidity term h.

Humidity is defined as the mass of water vapor per unit mass of dry air in an air-water mixture [47] and can be expressed as

$$\omega = \frac{0.622P_v}{P - P_v} \qquad \text{(kg water vapor/kg dry air)} \tag{2.3}$$

where P is the total pressure and P_v is the partial pressure of water

This quantity is the so-called absolute or specific humidity. However, it is more common to discuss the relative humidity, which gives the values of moisture content based on the ambient temperature. Assuming constant temperature, low relative humidity point means a low content of water in the air and a high humidity means a high water content. Relative humidity depends on a number of factors including the saturation pressure and partial pressure of water. A system with 100% relative humidity is said to be saturated. Water added to an unsaturated mixture will evaporate, increasing the moisture content of the air until it can hold no more moisture. Any further water added to the air after that point will condense. In SI engine applications, water injection is used to exploit water's high latent heat of vaporization in order to reduce the in-cylinder temperature and achieve charge cooling via evaporation. However, no evaporation will occur if the air/charge is saturated, which could weaken or eliminate the expected knock mitigation effect. Variation in ambient atmospheric conditions could thus affect engine performance [43]. A recent simulation study [48] suggested that intake air humidification could be

used as a knock suppression strategy. However, further research is needed to make such strategies generally useful because the combined effects of water injection and variation in ambient humidity on engine operation remain poorly understood.

Chapter 3

Engine Starts

In this chapter, the theory and background of engine starts is discussed.

3.1 Background

Engine starts are usually highly transient operations and major source of emissions during any driving event. Whereas SI engines in conventional non-hybrid vehicles are usually only started once per journey, a journey in a HEV may require multiple engine starts, which presents challenges in terms of emissions control. Depending on the choice of hybrid control strategy, which is usually governed by the battery's state of charge (SoC) or the vehicle's velocity demand, the IC engine may be activated occasionally or frequently to meet high power demands, to charge the battery, or both [49]. Starting the engine causes fuel consumption and generates emissions. Unfortunately, it is difficult to determine and inject the exact quantity of fuel needed during transient events such as engine starts. This may lead to the injection of an excessive mass of fuel, leading to incomplete fuel consumption and the generation of pollutants such as CO, unburnt hydrocarbons, and NO_x . The term NO_x refers to a a wide range of nitrogenous species, the most prevalent being nitrogen oxide (NO) and nitrogen dioxide (NO_2). NO_x is formed by the oxidation of atmospheric nitrogen (N_2) at high temperatures, as shown in equations 3.1 and 3.2:

$$N_2 + O_2 \leftrightarrow 2NO \tag{3.1}$$

$$NO + 1/2O_2 \leftrightarrow NO_2 \tag{3.2}$$

The combustion process in IC engines is inhomogeneous because air-fuel mixing is imperfect and the temperature inside the cylinder varies. Consequently, the efficiency of fuel combustion is below 100%, resulting in partial combustion and the emission of CO, NO and unburnt hydrocarbons (HC). NO is formed at high combustion temperatures, usually above 1500 °C. Upon cooling, NO can be further oxidized to NO_2 [50]. To minimize emissions of these harmful substances, the exhaust gases are passed through a TWC in which the CO and HC are oxidized into non-harmful gases (equations 3.3 and 3.4). In contrast, the conversion of NO_x requires reduction

(equation 3.5). Note that the stoichiometric equations presented below are not balanced and are only shown to illustrate the processes taking place within the TWC.

$$CO + 1/2O_2 \rightarrow CO_2 \tag{3.3}$$

$$C_xH_y + (x + y/4O_2) \rightarrow xCO_2 + y/2H_2O \tag{3.4}$$

$$CO + NO/NO_2 \rightarrow N_2 + CO_2 \tag{3.5}$$

The formation and control of emissions in SI engines are described in detail in the chapter written by Wade and Farrauto [50] in *Metropolitan Sustainability* and in *Chapter 11* of *Internal Combustion Engine Fundamentals* by Heywood [6]. A particularly important parameter affecting engine-out and tailpipe emissions is the air-fuel equivalence ratio, or λ. This quantity is a normalized form of the actual air to fuel ratio, and is calculated using the equation below:

$$\lambda = (A/F)_{actual}/(A/F)_{stoichiometric} \tag{3.6}$$

Here, A/F_{actual} is the actual ratio of the mass of air in the cylinder to the mass of fuel, while $(A/F)_{stoichiometric}$ is the *stoichiometric* air-fuel ratio. If $\lambda = 1$, the mass of air in the cylinder contains exactly the amount of oxygen needed for complete combustion of the mass of fuel in the cylinder and the air-fuel mixture is said to be *stoichiometric*. If $\lambda < 1$, the mass of air in the cylinder does not contain enough oxygen for complete combustion of the mass of fuel in the cylinder and the air-fuel mixture is said to be *rich*. Conversely, if $\lambda > 1$, the air in the cylinder contains more oxygen than is needed for complete combustion of the fuel and the air-fuel mixture is said to be *lean*. The excess air during lean operation can facilitate the oxidation of CO and HC, but it also tends to increase NO_x emissions. On the other hand, under oxygen deficient (*rich*) conditions, NO_x emissions are reduced but CO and HC emissions increase.

The TWC for spark-ignited gasoline engines was introduced in 1980 to control tailpipe emissions of CO, HC, and NO_x by converting these substances in the engine-out exhaust into CO_2 , H_2O and other less harmful compounds. Efficient operation of the TWC requires stoichiometric conditions, which can be maintained by using an oxygen (also referred as lambda) sensor mounted at the catalyst inlet. Figure 3.1 shows how the efficiency of CO, HC, and NO_x conversion in a modern TWC varies with the air-fuel ratio; it is only under stoichiometric or near-stoichiometric conditions that all three pollutants are efficiently converted. In the insufficient air zone corresponding to rich operation, NO_x is efficiently converted due to the presence of elevated levels of CO. Rich operation also inhibits the formation of NO_x during combustion because it tends to reduce combustion temperatures. In contrast, in the excess air (lean operation) zone, CO and HC are efficiently converted by oxidation due to the increased abundance of oxygen, but the conversion of NO_x is significantly reduced. Oxidation of CO and HC in the TWC is catalyzed by Pt and Pd, while NO_x reduction is catalyzed by Rh [51].

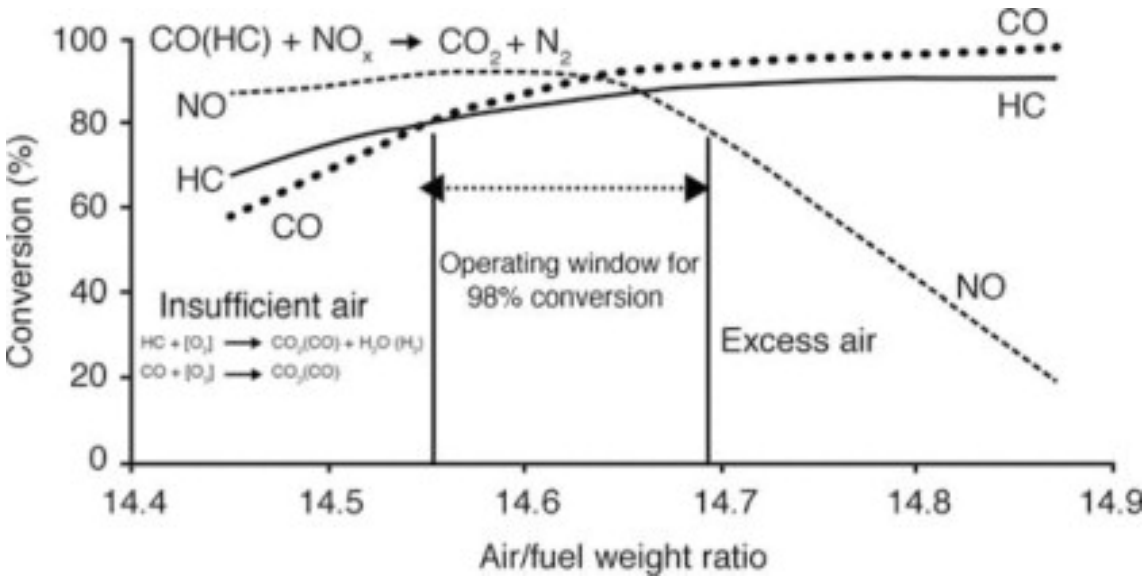

Figure 3.1: TWC conversion efficiency profiles for CO, HC, and NO_x as functions of the air-fuel ratio [50].

Although the use of oxygen sensors at the catalyst inlet allows the mass of injected fuel to be adjusted to maintain stoichiometric operation, there is inevitably some lag between the measurement of λ and the fuel injection response. This leads to oscillation between rich and lean conditions. Modern TWCs therefore also contain oxygen buffering compounds such as CeO_2 that allow them to store and release oxygen to compensate for transient changes in λ. The use of oxygen storage capacity in TWCs has been discussed extensively [51, 52].

Modern electronic fuel injection systems and oxygen storage compounds together with the high efficiency of current TWCs have greatly increased the scope for controlling the delivery of fuel to the engine and the air-fuel ratio. However, the problem of high emissions during transient engine operation is not fully solved, and periods of transient operation continue to be major sources of emissions. This problem is especially pronounced under real driving conditions, especially during engine starts. Additionally, the conversion efficiency of the TWC is significantly reduced when it is below its ideal operating temperature, which is usually only reached some time after engine start. These issues are discussed in more detail below.

3.2 Theory and Literature

Most engine start events can be classified as either cold starts or warm starts. According to the current regulations issued by the European Commission [53], the cold start period covers the first 5 minutes after the initial start of a combustion engine or the period before the coolant temperature first reaches 70 °C following the engine start. A significant fraction of the emissions produced during driving events are generated during the cold starts because of the coldness of the engine

and the exhaust after treatment system, especially the TWC. The first engine start in a driving event is usually a cold start because there is no residual heat to keep the catalyst above its light-off temperature of ~300°C. However, engine restarts after the first cold start also generate increased engine-out emissions, especially of unburned hydrocarbons (THC) and carbon monoxide (CO), because of incomplete combustion resulting from poor air-fuel mixing. The high emissions during cold starts are thus attributable to both increased engine-out emissions and sub-optimal catalyst operating conditions.

For conventional IC engines and HEVs equipped with combustion engines, the first cold start determines whether or not a vehicle will pass its emission test. It is therefore essential to either reduce the engine out emissions or shorten the time needed for the catalyst to reach its light-off temperature during cold-starts. Much work has been done to find solutions to these problems, and the literature in this area has been reviewed by Roberts et al [54]. Several groups have investigated the relationship between engine temperature and emissions during cold starts [55, 56, 57], while others have examined the benefits of heating the engine oil and lubricant before starting the engine [58, 59, 60]. There have also been studies on the use of fuel alcohols such as methanol and ethanol as gasoline substitutes or additives to reduce cold start emissions [57, 61, 62, 63]. Alcohols are attractive for this purpose because of their high oxygen content and relatively low boiling temperatures, which cause them to evaporate quickly. Song et al. [62] found that a blend containing 30% methanol (by volume) blend in gasoline yielded a significantly shorter flame development period during cold starts in an SI engine than pure gasoline. Fuel or hardware heating to increase the volatility of the injected fuel and thus the combustion efficiency has also been suggested as a way to reduce cold start emissions [64, 65].

Another important strategy for reducing tailpipe emissions during cold starts is to quickly bring the TWC up to its light-off temperature. Accordingly, both conventional and electric catalyst heating methods have been investigated [66, 67, 68]. Conventional heating strategies for cold starts usually involve retarding the ignition timing and operating the engine at high load to increase the heat flux through the exhaust after treatment system. A variant of this approach developed for a PHEV (Plug-in Hybrid Electric Vehicle) with a 2.0 liter GDI engine was investigated by Chambon et al. [69], who achieved a 12% reduction in HC emissions (relative to a conventional cranking start) by using an electric machine to drive the engine and injecting fuel only once the engine speed reached 1100 rpm. The authors also noted that a combination of high idle speed, elevated load, and retarded spark timing can accelerate catalyst heating by up to 30%. However, these measures also reduce engine efficiency and increase fuel consumption. Additionally, their work was primarily focused on cold starts because a PHEV may require multiple cold starts during a single driving event. In contrast, a HEV powertrain will usually require only one cold start per driving event, with the remaining starts being warm starts; consequently, fuel consumption during the start event becomes an important consideration. More recently, Thomas et al. [70] investigated engine behavior in two different hybrid

vehicles during on-road testing and reported the effects of cold starts and start-stop behavior on emissions.

In addition to the widely recognized cold and warm starts, a third intermediate engine start category was defined during this project. These "mild" starts occur when the catalyst temperature is between the light-off temperature (300°C) and the ideal operating temperature (500°C) at the beginning of the engine start event. Figure 3.2 shows the WLTC operation of a hybrid system on a powertrain test bed. Each start event is categorized into one of the three categories - cold, mild, or warm - based on the catalyst temperature during engine start.

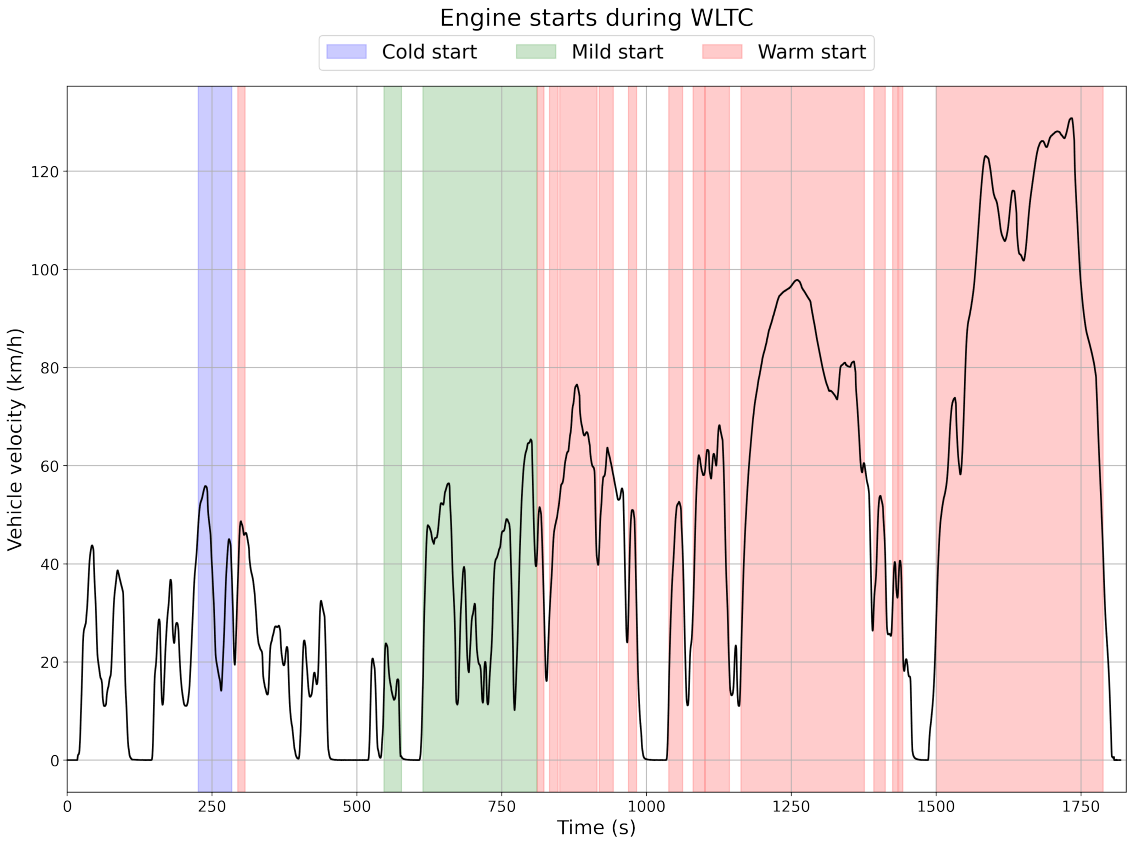

Figure 3.2: Engine start categories in WLTC

The first engine start is a cold start, with both the catalyst and the engine being at the ambient temperature. Usually, during a cold start, the catalyst heating strategy is used at the expense of fuel consumption to maximize the heat flux through the exhaust after treatment system in order to quickly heat up the catalyst. The engine was operated for approximately 55 seconds after the first start; by the end of this period, the catalyst temperature had risen above 500°C, which is the point at which its conversion efficiency exceeds 95% and the catalyst can be considered fully heated.

The next engine start was categorized as *warm* (indicated by a red background) because the catalyst temperature at the beginning of the start event was still above 500°C. After the second engine start, the powertrain operated on pure electric drive for about 250s, long enough for the catalyst to cool to below 500°C but still above the light-off temperature. Consequently, the third start was classified as a mild start (indicated by a green background). Because the duration of the engine's operation after the third start was quite low (only 30s), the heat from combustion was not sufficient to heat the catalyst to 500°C. Consequently, the next engine start was also a mild start. However, after this fourth start the engine remained in operation for approximately 200s, and at the end of this period the catalyst temperature was 650°C. As a result, the fifth start event was a warm start. The catalyst temperature remained above 500°C over the remainder of the drive cycle, so all subsequent engine starts were also warm starts. As a result, using the standard/base calibration, the tested hybrid powertrain underwent 1 cold start, 2 mild starts, and 14 warm starts over the WLTC driving cycle. The test was conducted under SoC (state of charge) neutral conditions: the SoC of the HEV battery was 61.3% at the start of the cycle and 61.62% at its end.

Another factor influencing engine starts in modern hybrid vehicles is the engine starting procedure. The engine of a HEV can be started using either a conventional 12V cranking motor or with assistance from the electric motor. The use of the 12V starter motor and EM assistance during start events in the HEV testbed over the WLTC is shown in figure 3.3.

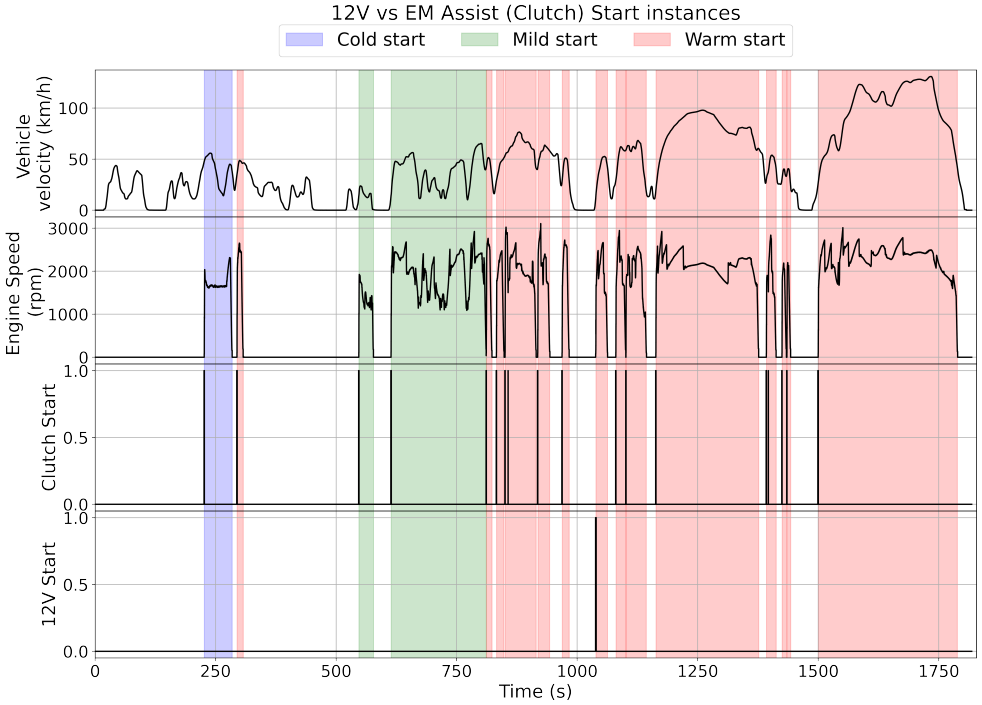

Figure 3.3: 12V cranking motor vs electric motor assisted (clutch) engine starts in WLTC

Vehicle and engine speed over the WLTC are plotted in the top part of the figure, while the bottom two graphs show the instances when the engine was started via the clutch (i.e., with EM assistance) and using the conventional starter motor; the black vertical lines in the clutch graph indicate starts in which EM assistance was used to start the engine, while the black lines in the 12V graph indicate starts in which the 12V starter motor was used instead. The conventional 12V cranking motor start has been described in detail by Wellman et al [71]. Because EM assistance offers significant benefits in terms of noise, vibration, and harshness (NVH) as well as smoother engine starts, OEMs are increasingly favoring EM-assisted or Clutch starts. A recent publication by the Geely Group [11] presented a new modular hybrid system featuring two electric motors, one of which is primarily used as a generator unit and to start the engine, replacing the 12V cranking motor entirely.

Table 3.1 shows the total number of engine starts for the HEV testbed with its base calibration over the WLTC along with the number of starts using the starter motor and EM assistance. There was only one conventional start during WLTC operation (approximately 1100 seconds into the cycle).

Table 3.1: No. of engine starts using the conventional starter motor and EM assistance.

Drive Cycle	**No. of Engine Starts**		
	Conventional 12V Starts	Electric Motor assisted Starts	Total
WLTC	1	16	17
RTS95	8	15	23
FTP75	11	9	20
NEDC	0	6	6
US06	7	0	7
SC03	3	3	6
RDE	11	61	72

Similar results were observed when the powertrain was operated on other drive cycles with the exception of the US06 cycle, for which all seven engine starts used the conventional 12V starter motor. The high number of engine starts using EM assistance indicates the importance of optimizing these events.

Chapter 4

Test Setup and Methodology

This chapter outlines the experimental setups and instrumentation used to study the effects of water injection along with the simulation model used to simulate various drive cycles with water injection. Experimental Setup and methodology used to investigate engine starts, first on a hybrid powertrain and later on an engine setup, are also discussed in this chapter.

4.1 Water Injection

The study of water injection tests was performed in three experimental campaigns and using a simulation model based on data collected from the final campaign.

4.1.1 Experimental Setup

Engine and Hardware

All water injection experiments presented in this thesis were performed using a 3-cylinder 1486 cc turbocharged engine from Volvo Cars. A sketch of the engine showing its basic components is shown in Figure 4.1. In the experimental setup, fuel was injected directly into the cylinder (direct injection) and water was injected into the intake runner via three dedicated injectors, one for each cylinder. This system configuration is commonly referred to as port water injection (PWI). The engine's specifications are given in Table 4.1.

For in-cylinder pressure measurements, high resolution piezo-electric pressure transducers (Kistler A6045) were installed in each cylinder. Their output was post-processed using AVL IndiCom. Two-point thermodynamic pegging was used in all experiments. Top Dead Center (TDC) was determined by setting a thermodynamic loss angle of 0.7 CAD and running the engine. The auto-calibrate function of AVL indiCom was then used for TDC calibration; TDC was taken to be equal to the timing of maximum indicated cylinder pressure plus the thermodynamic loss angle. Intake and exhaust pressures were measured with Kistler 4007C pressure transducers. Temperatures were recorded at multiple points in the engine using standard K-type

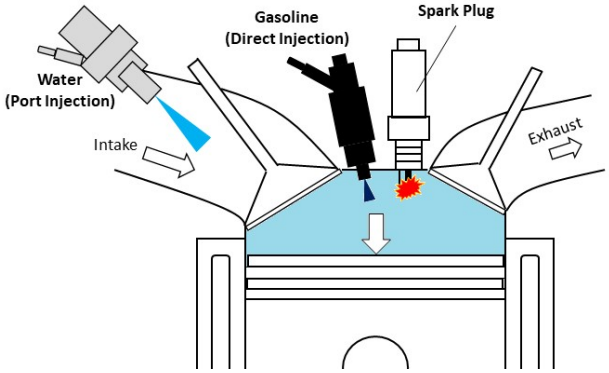

Figure 4.1: Diagram of the water-fuel injection system installed in the engine

Table 4.1: Volvo GEP3 Engine Specifications

Specification	**Value**
No. of cylinders	inline, Three-cylinder
Displacement Volume	1476 cc
Bore x Stroke	82 x 93.2 mm
Compression Ratio	10.5:1
Max Torque	265 Nm
Max Power	132 kW @ 5500 rpm

thermocouples, a CSM Thermo-Scan Mini module, and INCA Addon. The engine load was controlled by varying the throttle position and turbocharger boosting, and was measured using a National Instrument DAQ system controlled with LabVIEW. Engine speed was controlled by an AC dynamometer. The experimental setup in the test cell is shown in figure 4.2.

The fuel flow to the engine was measured with a coriolis-type mass flow sensor. The air-fuel ratio (λ) was controlled and measured based on the feedback from two wideband O2 sensors installed upstream and downstream of the TWC. A separate water injection system was installed upstream of the intake valves, in the intake manifold.

The engine exhaust gases were sampled before the TWC via a 180°C heated line and fed to a conditioning unit maintained at 190°C in the emission analyzer. Concentrations of NO_x , unburnt HC, CO-CO_2, and O_2 in the exhaust were measured using an Eco-physics chemiluminescence analyzer, a flame ionization detector, separate non-dispersive infrared radiation detectors, and a magnetic susceptibility analyzer, respectively.

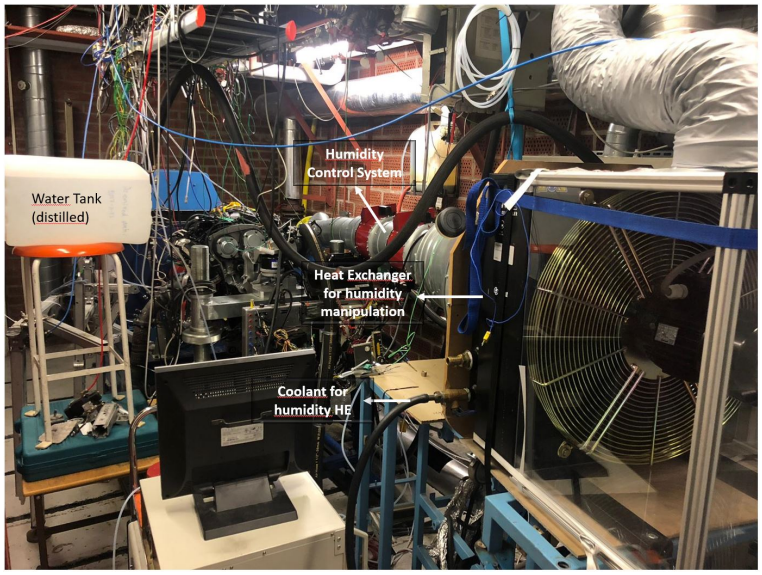

Figure 4.2: The experimental setup in the test cell comprising the GEP3 Engine and the water injection system

In addition to the engine hardware, a humidity control system was developed and fabricated to manipulate the relative humidity of the air entering the engine. The following section briefly explains this system's design and operation.

Water and Humidity Control System

The humidity control system was developed during the second experimental campaign to study the influence of airborne moisture on the effects of water injection. The system was fabricated to enable testing of engine performance and the benefits of water injection at different humidity levels. The relative humidity and temperature were measured using sensors placed at three different positions in the test setup. The locations of these sensors are indicated by the label RHS in Figure 4.3.

The objective was to record the absolute humidity (water content per kg dry air) of the air entering the engine, i.e. inside the intake manifold. A fan was used to force ambient air through a heat exchanger so as to establish an air temperature suitable for the desired humidity level. Three sensors from E+E Elektronik (two wall-type EE160 units and one probe-type EE210 unit) were used to measure the relative humidity and the air temperature.

The relative humidity was initially recorded immediately upstream of the air filter because the humidity there was assumed to be identical to that in the intake manifold. However, in retrospect it was noted that the turbocharger and/or the intercooler could potentially affect the humidity of air passing through them. Therefore, to see if the water content of the air in the intake manifold differed from that immediately upstream of the filter, another sensor was placed in the intake manifold. The air pressure in the manifold was approximately 2.3 bar, but the sensors used to measure

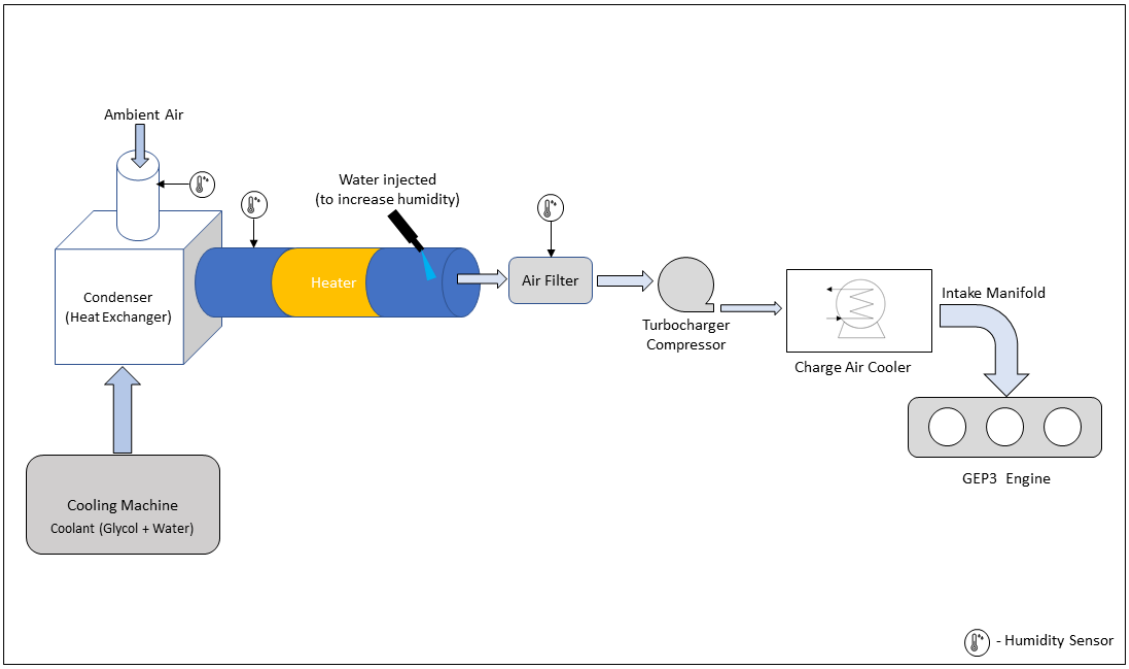

Figure 4.3: Humidity Control System

humidity were calibrated for atmospheric conditions. Therefore, air samples from the intake manifold were expanded into a container to enable humidity measurement at atmospheric pressure (after verifying that no condensation occurred during expansion). This revealed that the humidity in the manifold differed from that immediately upstream of the filter. It had been expected that the humidity in the intake manifold would be lower than that immediately upstream of the air filter because of condensation in the intercooler. In fact, the reverse was true. To determine whether this was due to a faulty sensor, the sensors at the two humidity measurement points were exchanged. This did not change the outcome, suggesting that both sensors were generating correct measurements and the humidity was indeed higher in the manifold. No plausible explanation for this outcome has yet been identified, so further investigations are needed to determine how the presence of a turbocharger and intercooler affects the distribution of humidity within an engine.

Based on the results discussed in the preceding paragraph, it was decided that humidity should be measured in the intake manifold rather than immediately upstream of the air filter. To achieve better control over the measurements several sensors were placed in a plastic container where they would be clearly visible to the test operator. The container was connected to the intake manifold via an insulated hose, allowing the air sample from the intake manifold to expand to ambient pressure. In addition to the humidity sensors (both EE160 models), pressure and temperature sensors were installed in the box to ensure that its conditions remained constant. In all of the experiments, the two humidity sensors generated virtually identical measurements, with negligible absolute differences in their outputs. The accuracy and reliability of the two humidity sensors was subsequently verified by comparing their

performance to that of an alternative humidity sensor that was developed in-house and which determines the humidity by measuring the dew point. This revealed that the accuracy of the original two sensors was consistent with that claimed by their manufacturer. During this testing process, the water content was measured indirectly by first measuring the relative humidity with sensors and then converting the measurements into absolute humidities using the standard equations. It was observed that the changes in the absolute humidity (water (g)/kg dry air) were more pronounced at lower relative humidity values and were very sensitive to the relative humidity.

The *water injection system* injected water into the intake manifold (port injection), where a Druck PMP 5000 series pressure transducer was installed to monitor the injection pressure. Fuel was injected directly into the cylinder at a pressure of 200 bar. Each cylinder was fitted with a port water injector operating at a pressure of 10 bar. Water injection parameters such as the injection timing and quantity of injected water were controlled using ETAS INCA. The positioning and orientation of the water injectors in the intake manifold profoundly affects the impact of water injection because it influences the rate of water vaporization and thus the amount of water that must be injected to achieve a given level of knock suppression. However, the positioning and orientation of the water injectors was not varied during these experiments.

4.1.2 Test Methodology

All tests were performed under controlled conditions. The humidity system was designed to control the moisture content of the intake air and determine how it affected the knock-suppressing effect of water injection. The relative humidity of the engine's intake air was manipulated using the humidity control system depicted in 4.3. Low-humidity conditions were established by passing coolant at temperatures of -2 to -5°C through the heat exchanger to remove water from the air by condensation and thereby reduce the humidity. High humidity conditions were established by spraying water into the intake air as shown in figure 4.3 to increase its water content before it entered the engine. The humidity control system was not used in experiments performed under ambient atmospheric conditions.

The tests were mainly performed at a high load of ~20 bar Indicated Mean Effective Pressure (IMEP) at engine speeds of 3600 or 4800 rpm because without water injection it was impossible to use the MBT ignition timing while keeping the exhaust temperature within safe limits when using a stoichiometric air-fuel mixture at higher speeds and loads. For all measurement points, the engine was operated with a stoichiometric air/fuel ratio using the Knock Limited Spark Advance (KLSA) ignition timing, which is not the same as the MBT timing. Before establishing the experimental operating conditions, the engine was operated at the planned test speed with a low load, and the load was gradually increased to the planned experimental value, initially at wide open throttle (WOT) and then with the waste

gate valve closed. Engine knock was detected with a knock sensor mounted on the engine and from the pressure traces recorded during the experimental measurements. Other relevant parameters were kept constant. All experiments in campaign 2 were performed using RON95 E10 gasoline. In campaign 1, experiments were conducted using this fuel and also with RON91 and RON98 gasoline.

The measuring equipment was regularly calibrated to ensure that its accuracy was maintained. The emissions measurement systems were calibrated before each test session. The results presented here are mean values based on 300 recorded cycles at each test point. To illustrate the accuracy of the experimental results, the spread of the measurements is also reported. Since the measurements were acquired under steady state conditions established by operating the engine at a single test point for an extended period until its behavior stabilized, the instruments' response times were not monitored.

4.1.3 Post Processing and Data Analysis

Polytropic Index (n) Calculation

The polytropic index is an important property of a thermodynamic system that can be used to describe and explain changes in the system's state. Within certain intervals, changes in the cylinder pressure during the compression and expansion strokes can be described very well in terms of polytropic compression/expansion. This means that the polytropic coefficient can be calculated from sampled cylinder pressure data using the polytropic expression $pv^n = c$. This method for calculation of polytropic calculation is discussed in detail by Tunestål [72].

It is possible to calculate crank angle resolved polytropic coefficients. This is done by taking the log of $pv^n = c$ and plotting log(v) against log(p); the slope of the resulting plot will be equal to the polytropic coefficient. The slopes of such plots typically appear to be almost constant even though the polytropic coefficient varies during both compression and expansion due to heat losses and changes in temperature. This is partly because the compression ratio profoundly affects the slope. To account for this, the effect of the cylinder head's dead volume must be taken into consideration. Because of this complication and the sensitivity of the polytropic coefficient to small changes in pressure, it cannot be computed directly from pressure measurements. Instead, to accurately detect small changes in the polytropic coefficient, a 5^th order polynomial must be fitted to the cylinder pressure trace. The computation of the polytropic index is therefore challenging and requires extensive numerical computation. To obtain reliable results, it is necessary to carefully determine the dependence of the results on the chosen numerical approach.

4.1.4 Simulation

HEV Simulation Model: GT Suite

To evaluate the impact of water injection on the fuel consumption of a mild hybrid, simulations were performed using a model representing a vehicle with a P2 parallel hybrid architecture. For this, a hybrid model developed in GT Suite at the division of combustion and propulsion systems, Chalmers [courtesy: Sarp Mamikoglu] was used to compute the BSFC benefits under different drive cycle operation. The specifications of the combustion engine unit for the 48V P2 Mild Hybrid architecture simulation model used in this work are given in Table 4.1. Selected vehicle parameters (drag coefficient, tyre radius, and rolling resistance) were kept constant. Vehicles with masses of 1350 kg and 1600 kg were simulated. The parameter settings for the simulated vehicles are given in Table 4.2.

Table 4.2: Parameter settings used in the vehicle simulation model

Specification	**Value**
Vehicle Mass	1350 & 1600
Drag coefficient (C_d)	0.27
Frontal Area (A_f)	2.1 m^2
Rolling Resistance (C_r)	0.007
Electric Motor Capacity	12, 15 & 20 kW
Drive Cycles Simulated	NEDC, WLTP & RTS95

The initial and final State of Charge (SoC) for the simulated hybrid's battery differed by no more than 1%. Parameters irrelevant to the powertrain were kept constant. All simulations were performed with a 7-speed dual clutch transmission and the same control strategy.

For the experiments in this campaign, BSFC was recorded at different operating points at stoichiometric conditions, with and without water injection. The test matrix with the operating points are shown in table 4.3. The operating points chosen had ignition timing other than MBT timing, for stoichiometric conditions.

Table 4.3: Operating Points for BSFC Measurement with and without Water Injection

Engine Load BMEP [bar]	**Engine Speed [rpm]** 1250	1500	1750	2000	2500	3000
6	✓					
8	✓	✓				
10	✓	✓	✓	✓		
12	✓	✓	✓	✓		
14	✓	✓	✓	✓	✓	✓
16	✓	✓	✓	✓	✓	✓
18	✓	✓	✓	✓	✓	✓

4.2 Engine Starts

4.2.1 Experimental Setup

The engine start research project involved two separate experimental campaigns. The first used a hybrid powertrain installed on a powertrain testbed, while the second used a four-cylinder engine installed on an engine testbed. Both of these setups are described in the following sub-sections.

Campaign 1: Hybrid System

A hybrid powertrain setup equipped with a 3-cylinder, 1.5 liter, PFI turbo-charged miller engine connected to a 7-speed dual clutch transmission was used in the first experimental campaign of phase 2. The hardware was installed on university's powertrain test bed. The specifications of the hardware in this system are presented in Table 4.4.

Table 4.4: CEVT HEV Powertrain Hardware [73]

Specification	Value
Engine Displacement	1477 cc
Maximum Torque	215 Nm @ 2500-4000 rpm
Rated Power	105 kW @ 5500 rpm
Fuel Delivery	Port injection
HV Battery Capacity	6.9 Ah
Total Energy	1.8 kWh
Nominal Voltage	194-295 V

In addition to the 12V battery, the HEV powertrain had a high voltage battery system to power the electric motor used to propel the vehicle and charge the high-voltage battery. The specifications of the electric propulsion system are given in Table 4.4. Additionally, the hardware had a state-of-the-art 7-speed, dual clutch gearbox with odd and even gears on two different shafts. This offers extra flexibility when operating the powertrain. The layout has been designated as P2.5 by hardware provider and OEM (CEVT AB). Figure 4.4 shows the power flow during engine starts in different vehicle operating modes i.e., a) when the vehicle is standing still and b) when the vehicle is running and in motion.

The engine can be started with the conventional 12V starter motor under conditions a) and b). However, EM-assisted starts are only permitted when the vehicle is moving above 12km/h when using the standard calibration.

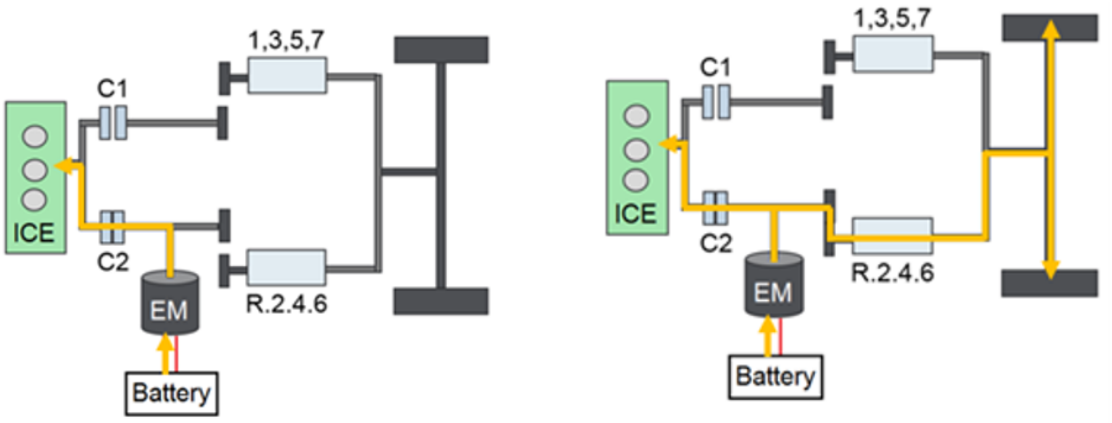

(a) when the vehicle is standing still (b) when the vehicle is running

Figure 4.4: Power flow in the HEV powertrain during engine starts under different vehicle operating conditions [73]

The HEV powertrain was installed on the Chalmers hybrid test bed with drive shafts connected to two AC Dynamometers with transient test capability and controlled via AVL PUMA 2.0 [74]. A sketch of the test setup layout is shown in Figure 4.5. The high voltage battery system was simulated with AVL E-Storage Battery Emulator using parameter settings of 160 kW, 800 V, and 600 A. The programmable Electronic Control Unit (ECU) and Transmission Control Unit (TCU) were accessed and controlled via ETAS INCA and the hybrid vehicle components were simulated using Vector CANOE.

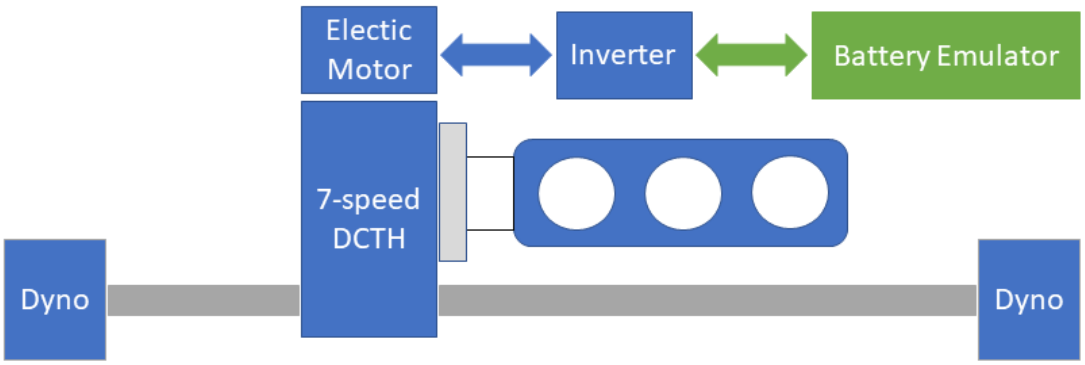

Figure 4.5: Hybrid test setup layout on the powertrain testbed

All of the regulated emissions were recorded at a sampling frequency of 5 Hz using FTIR from AVL. The recorded emissions were tailpipe emissions, i.e. emissions after passage through the catalyst. The only emissions analyzed in this work were CO, THC, NO_x , and CO_2 .

The HEV powertrain was operated on several drive cycles with its base calibration for benchmarking purposes and to investigate the engine start behavior as the first step in the test campaign. Basic details of each drive cycle are presented in Table 4.5.

Table 4.5: Details of the drive cycles used in the experiments

Drive Cycle	**Duration** $[s]$	**Total Distance** $[km]$	**Average Speed** $[km/h]$
WLTC	1800	23.25	46.5
RTS95	886	12.927	52.52
FTP75	1877	17.77	34.12
NEDC	1180	10.93	33.35
US06	600	12.8	77.90
SC03	600	5.8	34.80
RDE Landvetter	5100	-	-

WLTC was chosen as the reference test cycle for this campaign and was operated with an initial SoC of 61.30%. The final SoC for this cycle was 61.62%, which is within 0.5% of the initial SoC, meaning that the powertrain's operation was SoC neutral. Because the focus of the campaign was on engine starts only, the initial SoC was set to 61.3% for all drive cycles for the sake of simplicity. The powertrain was operated on a range of drive cycles to gather data on engine starts including cold and warm starts under diverse start conditions so as to capture as many different transient engine starts as possible.

Campaign 2: Engine Tests

The tests in this campaign were performed at AVL headquarters in Graz, on a 1.4L turbocharged GDI engine installed on an engine testbed with an active dynamometer. See table 4.6 for general engine specifications and figure 4.6 for the testbed layout.

Figure 4.6 shows the experimental layout for the test campaign with the 4-cylinder TGDI engine installed. Emissions were measured before and after the catalyst with an AVL AMA unit, providing both engine out and tailpipe emissions to study the effect of catalyst temperature. The transport delay was accounted for by adjusting the measured emissions based on the observed differences in transport delay times.

The testbed was controlled using AVL's state-of-the-art testbed control software PUMA 2. The testbed control software was accessible on the test operator side and was connected to the AVL CAMEO 4R3 and ETAS INCA programs. The tests were prepared in CAMEO with relevant boundary conditions and test operation ranges,

Table 4.6: Engine specifications for the second experimental campaign

Specification	Value
No. of cylinder	Four, in-line
Displacement	1395 cc
Bore x Stroke	80 x 74.5 mm
Compression Ratio	10.5
Max Torque	160 Nm
Max Power	103 kW
Fuel Delivery	Direct injection

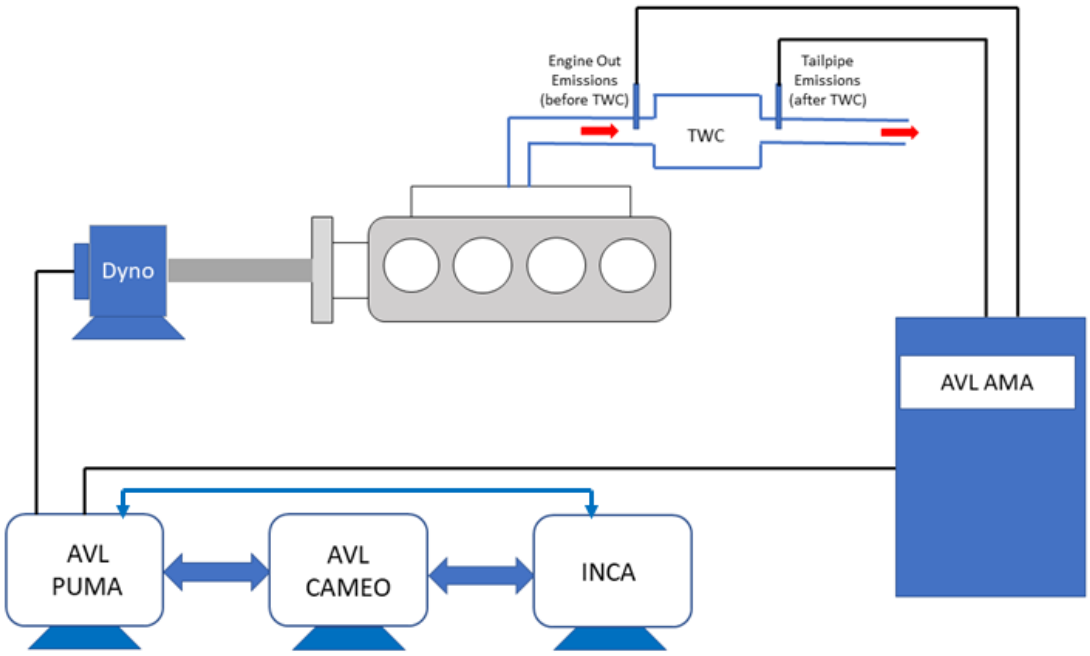

Figure 4.6: Test Setup with 1.4 TGDI Engine to Investigate Engine Starts

and were executed using PUMA, with CAMEO was acting as the master program. The resulting generated operating points are presented in figure 4.7.

To capture the engine's behavior during clutch starts, the engine was operated on the testbed with the AVL Dynoforce dyno serving as a stand-in for the electric motor present in a HEV powertrain. Dyno torque and speed were recorded in AVL Puma, and monitored in real time using AVL CAMEO. The real time dyno torque and speed were used to calculate integral power output from the dyno, which essentially served as a stand-in for the power provided by the electric motor in the HEV powertrain to start the engine. The methodology and test procedure used to investigate the engine starts are discussed in the following section.

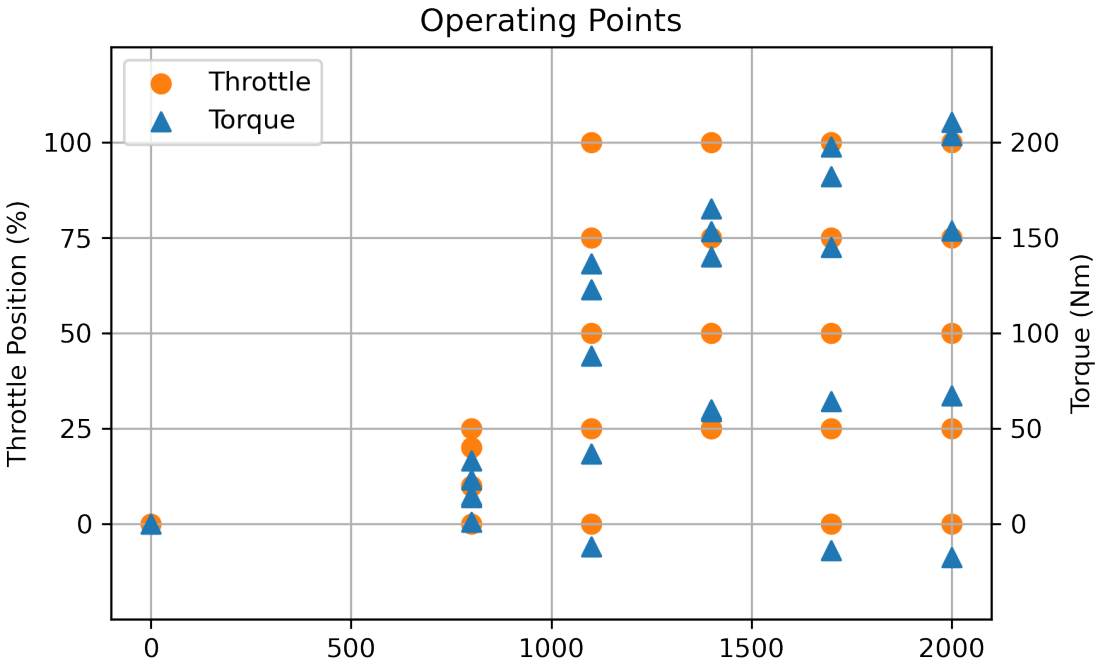

Figure 4.7: Operating points for the engine start investigation.

4.2.2 Test Methodology

Figure 4.8 shows the test methodology used to study engine starts in this campaign.

The first step in the test was to establish the desired engine speed, so the motor was used to bring the engine up to the desired speed and fuel was injected once the required operating speed was attained. In figure 4.8, 'n' represents the engine motoring or test speed, and 't' is the motoring time, i.e. the time after which fuel injection commences and combustion begins. For simplicity, the motoring time was kept constant for all operating points in this campaign. After the start of fuel injection, the load was controlled by the engine's throttle position, which was used as a test variable along with engine speed. After reaching the desired stable load point, the engine was operated at each point for a constant period of 10 seconds. Major regulated emissions and fuel consumption during the complete maneuver (10 seconds) were calculated using equation 4.1:

$$\int_{t_0}^{t_1} \frac{(fuel, emissions)}{Power * t_1} \tag{4.1}$$

where t_0 is the time at which fuel injection commenced and t_1 is the time at which fuel injection was stopped after recording. The engine starting effort, i.e. the energy consumed to start the engine, was calculated using equation 4.2:

$$E = \int_{t\_1}^{t_0} P = \frac{2\pi}{60} \int_{t\_1}^{t_0} N * T \tag{4.2}$$

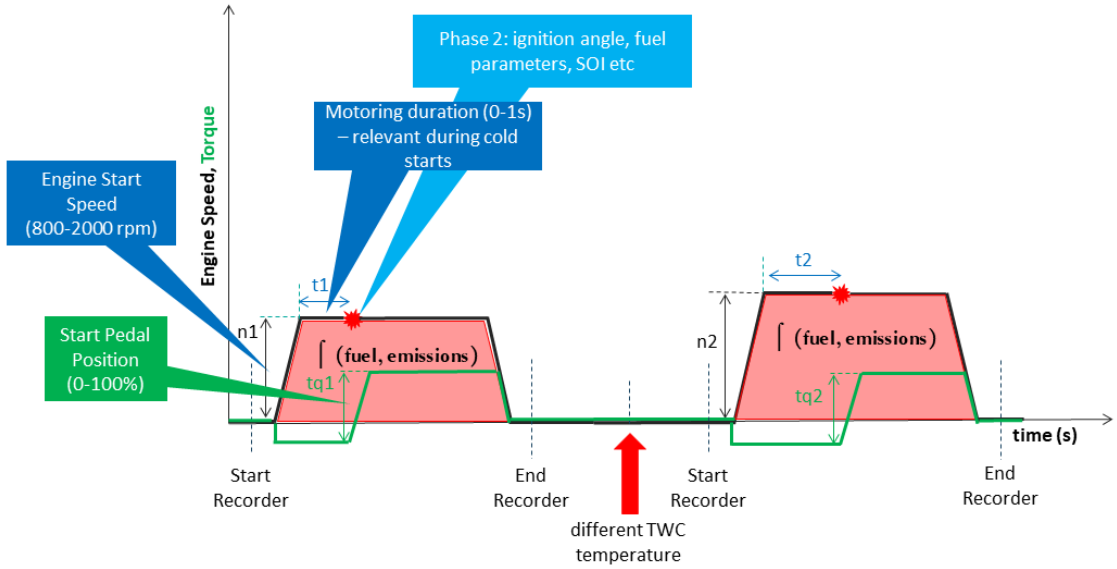

Figure 4.8: Test methodology used to investigate EM-assisted engine starts

where N is the engine speed in rpm and T (in Nm) is the torque provided by the dyno to start the engine. The equations used to calculate total emissions, fuel consumption, and the work done by the dynamometer over the 10-second test run were specified in CAMEO during test preparation. The PUMA and CAMEO recorders were started before the procedure and stopped after the data was recorded. The tests were repeated in the same way for all operating points and the full test series was automated using CAMEO to ensure good repeatability during the tests and measurements to avoid human-induced error.

4.2.3 Post Processing and Data Analysis

Experimental data were recorded with AVL PUMA, AVL CAMEO, and ETAS INCA. The recorded files were exported and analyzed using AVL Concerto and scripts written in the Python programming language. Only the relevant channels were imported into Python to save processing time and minimize data complexity. During data analysis, engine start events were separated from the overall powertrain operation during the drive cycles to better characterize the system's behavior during transient events. Engine start conditions were included in the script and the resulting starts were categorized as cold, mild, or warm based on the initial catalyst temperature. The engine and coolant temperature were ignored when defining these conditions because of their relatively low time-sensitivity.

Chapter 5

Summary of Papers

This chapter summarizes the contents of the appended papers on which this thesis is based. For all of the papers discussed in this chapter, the author was responsible for planning, preparing and conducting experiments and analyzing their results with guidance and support from the other authors. The author also wrote the reports and publications and presented the results wherever necessary.

5.1 Paper 1

Water Injection Benefits in a 3-Cylinder Downsized SI-Engine

Authors: **Khatri, J.**, Denbratt, I., Dahlander, P., and Koopmans, L.
SAE International Journal of Advances and Current Practices in Mobility 1(1),
`https://doi.org/10.4271/2019-01-0034`

Summary: Paper 1 discuss the benefits of water injection in downsized SI engines. The development of high efficiency downsized SI engines is limited by the knocking combustion. The issue becomes more complicated with the availability of different octane rating fuels in different parts of the world. The conventional methods used to suppress knock reduces the efficiency of the engine. Water injection enables knock-free operation even at stoichiometric conditions. This paper resolves some of the uncertainties regarding water injection and its benefits. Some of the parameters studied as part of this paper include effect of water injection when the engine is operating on different research octane rating (RON) fuels, advancement in combustion phasing, the effects of water injection timing, and the knock suppression capability of water in gasoline engines.

Author's Contribution: The author prepared tests and the experimental setup, operated the engine, monitored its performance during the tests, recorded and pre-processed experimental data, and finally analyzed the gathered data. With support from co-authors, the author analyzed the data obtained from the experiments, developed relevant figures, and presented them in the publication. Finally, the author wrote the manuscript for submission.

5.2 Paper 2

Effect of relative humidity on water injection technique in downsized spark ignition engines

Authors: **Khatri, J.**, Sharma, N., Dahlander, P., and Koopmans, L.
SAGE International Journal of Engine Research, 22(7)
https://doi.org/10.1177/1468087420940854

Summary: The purpose of this study was to determine how the atmospheric moisture content (i.e. the relative humidity) affects the performance, behavior, and emissions of internal combustion engines with water injection systems. To the author's knowledge, there were no previously published studies on this topic despite its potential importance: humidity varies widely between countries and seasons, so it is possible that a water injection strategy that was effective under a given set of climatic conditions would be ineffective or even harmful under others. These studies also helped reveal the mechanism responsible for the knock-suppressing effect of water injection, showing that it is primarily due to charge dilution and changes in the thermodynamic properties (particularly the specific heat ratio) of the fuel-air charge rather than local cooling. This finding may facilitate the design of more effective water injection systems and strategies.

The work presented in this paper also led to a collaboration with other universities on a fundamental assessment of water injection including a study of its chemical kinetics. This work is not published at the time of writing this thesis.

Author's Contribution: The author planned and prepared experiments and developed the humidity control system (with the assistance of laboratory engineers during its fabrication and testing). After performing the tests and analyzing the data, various hypotheses about the mechanism by which water injection suppresses knock were considered and evaluated. The author received support in computing the polytropic index and explaining the underlying theory from the co-authors of the paper. The measurement and evaluation of particulate emissions was performed by Nikhil Sharma. The author wrote the final manuscript.

5.3 Paper 3

Water Injection System Application in a Mild Hybrid Powertrain

Authors: **Khatri, J.**, and Koopmans, L.
SAE Technical Paper 2020-01-0798, 2020
https://doi.org/10.4271/2020-01-0798

Summary: The objective of this paper was to assess the benefit of water injection technology when used in a hybrid powertrain. Experiments were conducted using the water injection hardware previously used in Papers 1 and Paper 2 to investigate the gains in Brake Specific Fuel Consumption (BSFC) for load points other than those corresponding to Maximum Brake torque (MBT) timing. This was achieved through spark advancement, and it was shown that water injection enabled the use of MBT or near-MBT timings under conditions where this would otherwise be impossible. A BSFC map was generated for the load points mentioned in table 4.3.

The BSFC data (with and without water injection) for these load points were incorporated into a mild hybrid vehicle model developed in GT Suite at the division of Combustion and Propulsion Systems. Simulations were then performed to predict the BSFC and fuel consumption reduction potential of water injection technology for three different drive cycles.

Author's Contribution: The author prepared and conducted tests on the WI system and recorded data during the tests. The author then used a hybrid model developed in GT Suite by another PhD student at the department to assess the application and benefits of the technology in a complete powertrain. The author analyzed the data, developed figures, and wrote the paper presenting the results.

5.4 Paper 4

Methodology Development for Investigation and Optimization of Engine Starts in a HEV Powertrain

Authors: **Khatri, J.**, Koopmans, L., Sandquist, H., Örngrip, M., Hellsing, J., Mayrhofer, H., and Koegeler, H.M.
submitted to SAE World Congress 2022

Summary: The work presented in this paper comprised the second topic (project) investigated during author's PhD studies. The objective of this project was to develop strategies for cleaner engine starts in spark-ignited engines for hybrid powertrains. To this end, the work focused on developing a methodology to investigate and optimize engine starts.

Engine starts were first studied in a hybrid system to understand the behavior and characteristics of different engine starts. Tests were performed on a mild hybrid powertrain using six different drive cycles including a Real Drive Emissions (RDE) cycle on the university's hybrid test rig. Based on the obtained results, three different types of engine starts - cold, mild and warm - were identified. The only factor used to differentiate these start types was the catalyst temperature during engine start. Only one cold start was observed in each drive cycle; most of the observed starts were warm starts in which the catalyst was operating at or above its high conversion efficiency temperature. Because multiple cold starts occur in PHEVs but not in hybrid vehicles, where most starts are warm, the focus of the study shifted to the investigation and optimization of warm engine starts.

A hybrid system offers the flexibility to motor the engine up to a desired engine speed before starting combustion. This capability was used to investigate warm starts. Experiments were performed on an engine test bed in collaboration with AVL at their headquarters in Graz, Austria. The objective of conducting tests on an engine test bed was to have better control over engine starts and to mimic the engine motoring process, which is performed by the electric motor in a hybrid powertrain. Tests were designed to study engine starts at different speeds and loads, and selected responses (KPIs) such as fuel consumption, dynamometer work, and emissions were recorded. The results indicated that electric motor assisted starts can be divided into two parts: first the dyno (or EM in a HEV system) motors the engine to a predefined speed, then fuel injection (combustion) begins. The results from campaign 2 showed that for the hardware used, it was most beneficial to start the engine at a speed of 1700 rpm and a torque of 145 Nm. Finally, a simple case study was presented to calculate the CO_2 emissions that could be prevented by shifting from the least efficient starting point to the most efficient one.

Author's Contribution: The author devised the hypothesis and prepared the tests to understand the behavior of engine starts in a hybrid powertrain. In addition

to support from CEVT AB and his supervisor, the author received support from AVL List GmbH in the form of access to their *state-of-the-art* tool AVL CAMEO 4.3 to prepare and run tests on the hybrid test bed. The author planned and conducted tests for the second campaign using AVL. The data analysis and compilation of results from both campaigns was performed by the author, with valuable input from the co-authors.

Chapter 6

Results and Discussion

This chapter presents and discusses the main results obtained during the experimental work. The discussion is based on the work published in Papers 1-4.

6.1 Water Injection

This section summarizes the findings of the experimental campaigns focusing on water injection along with results from hybrid vehicle simulations.

6.1.1 Effect of water injection on engine operation when using fuels with different octane rating

Performance was measured by comparing torque levels achieved with a stoichiometric air:fuel mixture with and without water injection. Operation at full load points (high IMEP) causes the exhaust gas temperature to exceed the temperature threshold of the exhaust system components. Therefore, fuel enrichment (i.e., injecting more fuel than is needed for combustion such that $0.8<\lambda<0.9$) is often used to cool the exhaust. This imposes a significant penalty in terms of increased fuel consumption and emissions of CO and HC due to a deficit of oxygen in the cylinder.

The torque enhancements achieved with water injection for stoichiometric mixtures of different fuels are shown in figure 6.1. Results obtained with and without water injection at $\lambda = 1$ are plotted using dashed and solid lines, respectively. In cases without water injection, measurements were taken at the KLSA timing subject to a Turbine Inlet Temperature (TiT) limit of 970°C at all load points except when the engine speed was 1500 rpm, in which case the limit was determined by the maximum allowable ignition retard of 30°CA aTDC. At such low engine speeds, the limited mass of air entering the cylinder meant that the mass of fuel burned was insufficient to generate exhaust gas temperatures above 830°C.

In cases with water addition, the boost pressure and spark timing were adjusted to maximize torque subject to the previously specified temperature and knock limits

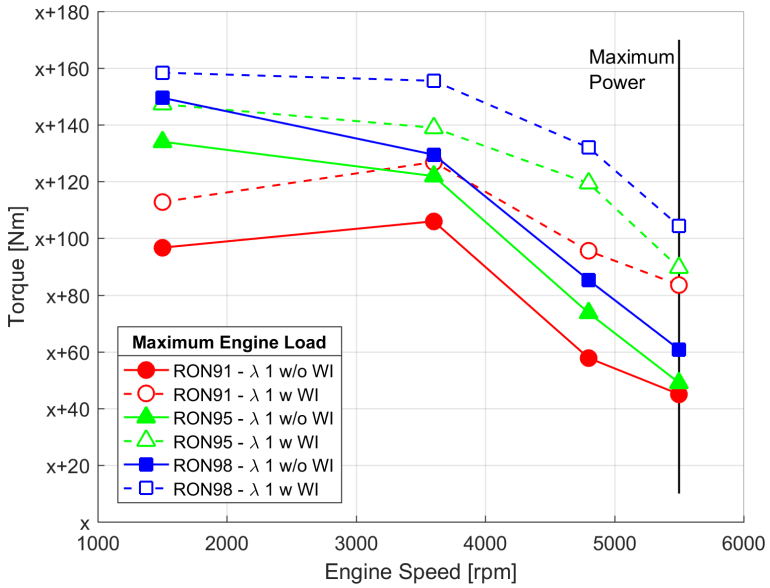

Figure 6.1: Improvements in torque using water addition for RON91, RON95 E10 and RON98 gasoline [45]

while ensuring that the Coefficient of Variation (COV) in IMEP remained below 3%. At 5500 rpm, where the engine power is maximized, both water addition and the RON of the fuel significantly affected the torque. When the engine was operated on RON91 with water injection, the torque at high engine speeds (4800 and 5500 rpm) was considerably higher than when using RON95 or RON98 without water addition. The maximum torque was achieved when using RON95 or RON98 with λ=1 and water injection; the torque under these conditions was comparable to that achieved with a rich mixture ($\lambda = 0.85$). The water/fuel ratio required to achieve the maximum torque values at specific load points for different fuels are tabulated in table 6.1. Based on these results, torque is maximized under stoichiometric conditions by using a water:fuel ratio of approximately 0.80 by mass.

Table 6.1: Water-fuel ratios required to maximize torque for gasoline fuels with different octane ratings

Engine Speed	**W/F Ratio**		
[rpm]	**RON91**	**RON95 E10**	**RON98**
1500	0.84	0.53	0.73
3600	0.54	0.70	0.71
4800	0.87	0.74	0.77
5500	0.89	0.72	0.80
Overall Average	0.80	0.67	0.75

It should be noted from table 6.1 that the amount of water:fuel ratio is consistently lower for RON95 E10 case, for achieving maximum load conditions. This can be due to the presence of ethanol in the fuel. Compared to gasoline, ethanol has high heat of vaporization which provides additional charge cooling effect. In a study by Kasseris et al. [75], the authors reported, from theoretical calculations, about 25K reduction in temperature due to charge cooling with 10% ethanol. Hence, the presence of 10% ethanol in the RON95 fuel, reduces the in-cylinder temperature and the propensity of knock, thus requiring relatively lower water quantity. The authors of [37, 36], have also claimed that the charge cooling effect of water injection is due to evaporation.

Operating the engine under stoichiometric conditions without water injection limits the maximum possible torque at the chosen engine speed, which would in turn limit vehicle performance and the scope for meeting customers' performance demands. The results presented in figure 6.1 show that water injection makes it possible to increase torque under stoichiometric operation, allowing the engine to use a stoichiometric mixture (λ=1) while maintaining maximum power.

To check the effect of the gasoline's octane rating, a λ vs water injection/fuel sweep was performed using three gasoline blends: RON91, RON95 E10, and RON98. In all cases, the engine was initially operated with $\lambda = 0.85$ and a water:fuel ratio (w/f) of 0 at a load point of 16 bar IMEP and 4800 rpm. The mixture was then gradually made leaner while increasing w/f to the minimum value required to sustain operation at the chosen load point until stoichiometric conditions (λ=1) were reached. The results are shown in figure 6.2.

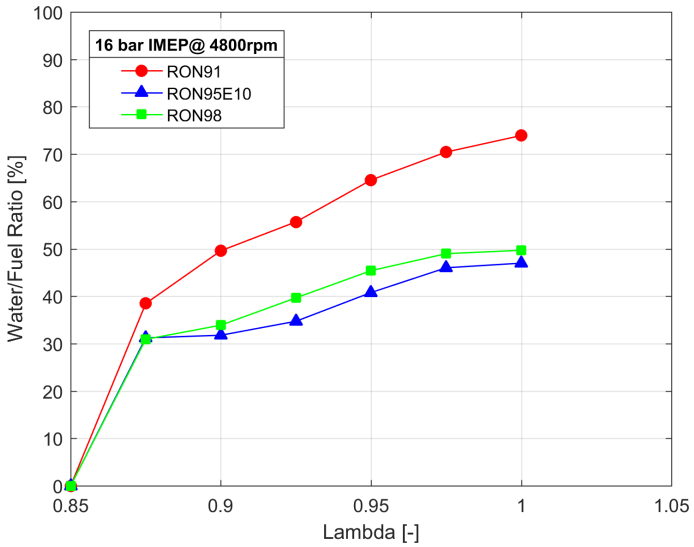

Figure 6.2: Minimum water:fuel ratios needed to maintain operation at a fixed load point with different λ values for three gasoline blends with different octane ratings [45]

The results presented in figure 6.2 show that at the chosen load point, the water:fuel ratio required to operate at the knock limit is highest for RON91 fuel followed by

RON 98 and RON95 E10; although the difference between the water:fuel ratio for RON95 and RON98 fuels is minor for all lambda values. As RON or MON alone are not good indicator of anti knock behavior of the fuel [6, 76], table 6.2 shows the different fuel properties for the three octane rating gasoline used in these tests.

Table 6.2: Fuel properties for gasoline with different octane ratings used in the WI experiments

Property	**Test Method**	**Fuel**		
		RON91	**RON95 E10**	**RON98**
RON	ISO 5164	91.2	95.8	98.2
MON	ISO 5163	83.5	85.3	87.8
Sensitivity (S)	calculated	7.7	10.5	10.4
Anti-knock Index (AKI)	calculated	87.35	90.55	93
Ethanol content (%V/V)	ISO 22854:2016		9.94	2.74
Water content (mg/kg)	ISO 12937:2000	35	230	85

It can be noted from table 6.2, that the sensitivity for RON95 E10 is very similar to that for RON98 gasoline. Moreover, the amount of water content present in the RON95 fuel is significantly higher than in RON98 fuel and perhaps this is why the water:fuel ratio required to operate at same conditions was lower for RON95 E10 as compared to RON98 gasoline. This, however, was not further investigated. The presence of higher ethanol content in RON95 E10 fuel provides additional charge cooling - which makes the operation at each point more resistant to knock and the higher water content makes the overall quantity of water higher than in RON98. These results are consistent with those obtained when operating the engine at maximum load, as discussed in the preceding section.

The AKI or Anti-knock index is defined as per equation 6.1 and is an indicator of the knock resistance of the fuel.

$$AKI = \frac{RON + MON}{2} \tag{6.1}$$

However, as per literature [77, 78, 79], octane index (OI) is a more accurate indicator of knock resistance and is defined as per equation 6.2.

$$OI = RON - K.S \tag{6.2}$$

$$S = RON - MON \tag{6.3}$$

where S is the sensitivity of the fuel and K is a constant (usually referred to K factor) which depends on the engine design and operating conditions (pressure-temperature of the unburned charge). The value of K is indicative of the octane

appetite of the engine at a particular operating point and is very hard to calculate for practical fuels. Historically, K value has been found to be positive and a value of 0.5 as K factor was commonly used in the USA. And a value of K=0.5 leads to OI equals (RON+MON)/2 or AKI [79]. However, for modern engines, especially boosted direct fuel injection SI engines, K value has been shown to be negative in many cases [76]. The results and effects presented here could be further explained by the study of K-factor but this was not investigated in this work.

Water injection also enables advancement of combustion phasing (MFB50) and thus the use of MBT- or close-to MBT timings, which improve BSFC. The effect of varying the fuel's octane rating was therefore investigated to see how the anti-knock properties of the fuel affect the improvement in BSFC. Figure 6.3 shows the advancement in MFB50 timing as a function of the water:fuel ratio for three fuels with different octane ratings.

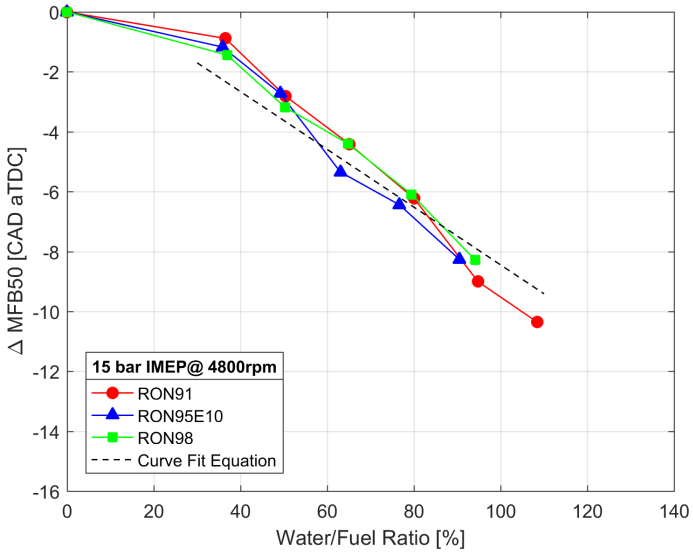

Figure 6.3: Advances in MFB50 as a function of the water:fuel ratio for three fuels with different octane ratings [45]

It was found that once the water:fuel ratio exceeded 30%, the relative advance in combustion phasing became almost linear and could be predicted using equation 6.4.

$$y = -0.0964x + 1.1945 \tag{6.4}$$

where y is the advancement in combustion phasing (ΔMFB50) and x is the quantity of added water expressed as a percentage by mass.

Effect of Water Injection Timing

To identify the mechanism responsible for the effects of water injection, water was injected at five different timings in the cycle. During these experiments the engine was operated at 15 bar IMEP and 4800 rpm, and the water injection timings were categorized into three intervals, as shown in figure 6.4: during Intake Valve Opening

(IVO, corresponding to the turquoise regions in the figure), at maximum valve lift (indicated by the yellow region), and when the intake valves were closed (indicated by the purple regions). Table 6.3 provides details of the test cases. The red and blue curves in figure 6.4 indicate the exhaust and intake valve lift profiles, respectively, for the chosen operating point.

Table 6.3: Water injection timings used when probing the mechanism responsible for the beneficial effects of water injection.

Case #	**Test Description**
Case 1	No water injection, ignition timing: 12.75 CAD bTDC C
Case 2	Water injection before IVO
Case 3	Water injection during IVO
Case 4	Water injection during maximum valve lift
Case 5	Water injection during IVC
Case 6	Water injection after IVC
Case 7	No water injection, ignition timing: 9.75 CAD bTDC C

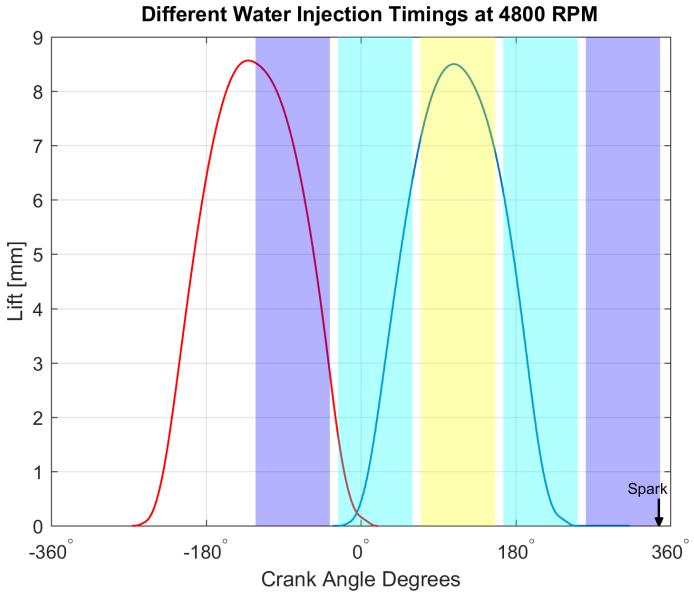

Figure 6.4: Valve lift profiles and water injection timing intervals for the experiments probing the mechanism of water injection [45]

The cycle-averaged cylinder temperature curves for all cases listed in table 6.3 are shown in figure 6.5. The temperature rise was highest for case 1, when no water was injected. Additionally, the temperature curve for case 6, when the water was injected after IVC, is very similar to that for Case 1. This might be because when water is injected after IVC, the charge is first cooled by evaporation of the injected water but is then re-heated by the hot cylinder walls before the next cycle begins, negating the benefit of water injection. This implies that it is not beneficial to inject water after the intake valve has closed.

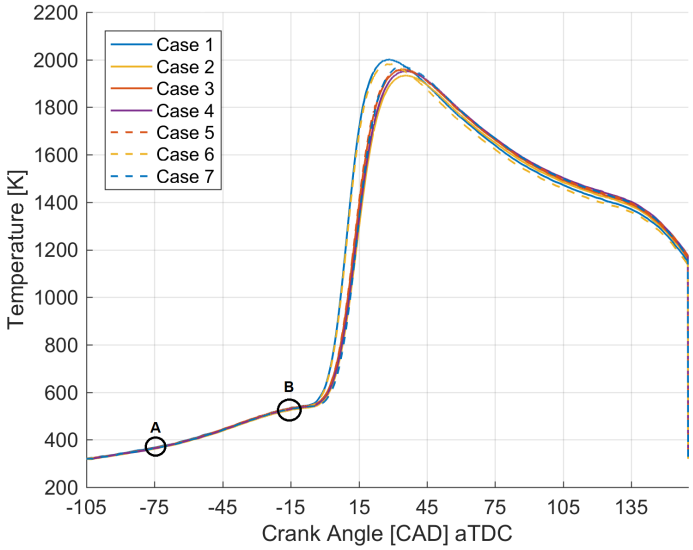

Figure 6.5: Cycle-averaged cylinder temperature curves for different water injection timings [45]

Points A and B in figure 6.5 correspond to two crank angle locations before combustion top dead center (75° and 15° bTDC, respectively) at which the in-cylinder temperatures for the 7 chosen cases were compared. Figures 6.6a and 6.6b show zoomed-in plots of the temperature traces for these points. Case 1 and Case 6 had similar temperatures at both points. The lowest in-cylinder temperatures at both points were achieved in Case 2, when water injection was performed before IVO. It thus appears that this is the most favorable water injection timing for the tested hardware. This effect is discussed in detail by the author in [45].

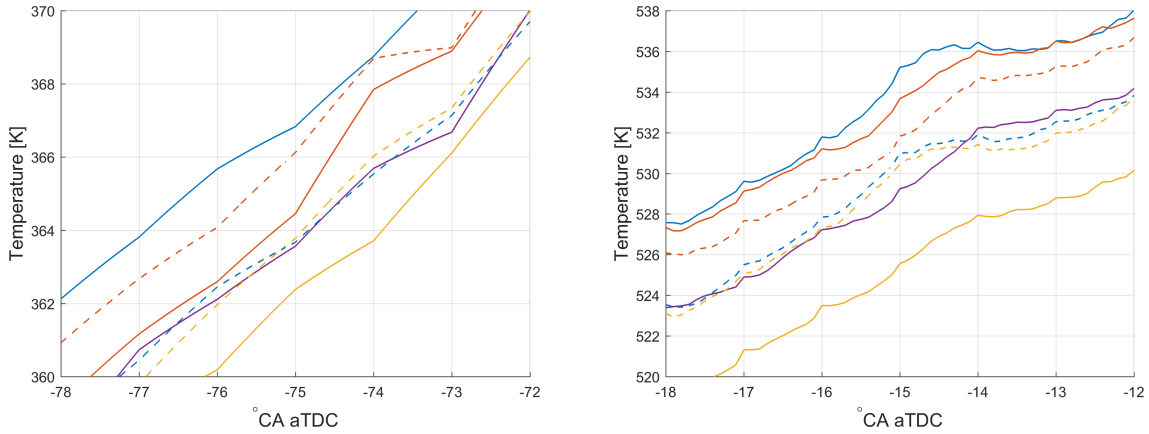

(a) at 75°CA before TDC (b) at 15°CA before TDC

Figure 6.6: In-cylinder temperature curves during the compression stroke with different water injection timings [45]

Netzer et al. [37] reported a temperature drop of ~10 K at 20 CAD before TDC with a 50% W/F ratio and port water injection. In keeping with the results obtained in this work, the use of a 63% water:fuel ratio reduced the temperature by ~9 K at

15 CAD bTDC when compared to the case without water injection case (Case 1). The temperature also decreased in other cases involving water injection, but to a lesser extent than in Case 2. These results show that with the tested hardware, it is most beneficial to complete the water injection just before IVO.

6.1.2 Effect of Relative Humidity

During the experimental campaigns described above, it was observed that the acquired measurements varied from day to day and the quantity of water content in the atmosphere affects the rate of evaporation. Additionally, it was also noted from the previous campaign that water injection has both direct and indirect effects in knock control through evaporative cooling and high specific heat capacity. This prompted an investigation into the effects of atmospheric variables on the engine's performance and the mechanism behind the working of water injection. The atmospheric variable expected to have the greatest influence was the moisture content of the air, i.e. the relative humidity.

Working Mechanism of Water Injection

Initially, experiments were performed to determine the minimum amount of water required to operate at a given load point for three different humidity levels - low, medium (ambient), and high. During each event, there were three sources of water of water inside the cylinder: the water from the moisture content upstream of the injector (humidity), the water injected by the experimentalist, and the water content from the internal exhaust gas recirculation (EGR) during valve overlap. The effect of water content from the EGR is not considered in this study. The working hypothesis for this experiment was that the minimum amount of injected water needed to maintain stable operation at the chosen load point should vary with the humidity of the inlet air and the degree of saturation and evaporation. Figure 6.7 shows the total quantity of water inside cylinder, along with the water content from atmosphere and the water injected by the experimentalist, required to maintain a constant load of 20 bar IMEP and 4800 rpm as engine speed.

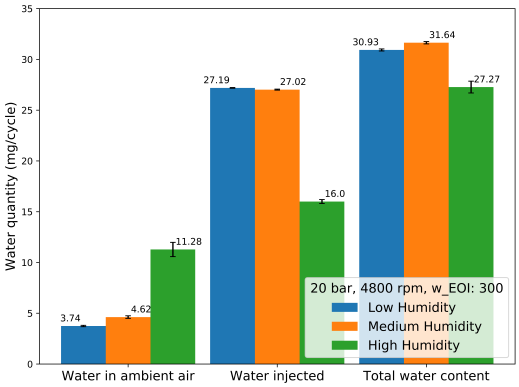

(a) when water is injected during valve opening (EOI_w = 300 CAD bTDC)

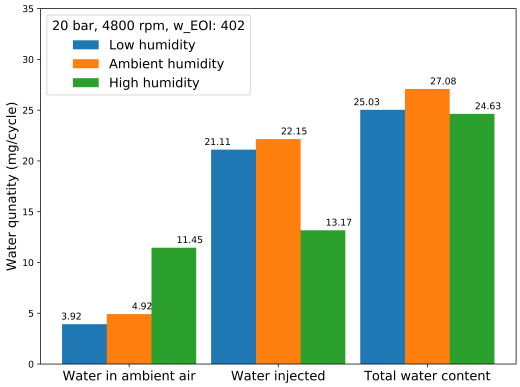

(b) when water is injected before valve opening (EOI_w = 402 CAD bTDC)

Figure 6.7: Amount of water in the cylinder for different humidity levels at 4800 r/min [80]

The histograms from figure 6.7 show the water content inside cylinder from different sources when the engine is operated at 20 bar IMEP and 4800 rpm with

water injection ending at 300 and 402 CAD bTDC. It can be seen noted from both figure 6.7a and 6.7b that the total quantity of water required to maintain the desired load does not vary significantly for different humidity values. This suggests that for the given conditions and the hardware used on this study, the effect of the latent heat of vaporization is insignificant and that it is the simply the total amount of water in the cylinder that determines performance. This may be because increasing the total water content of the cylinder causes charge dilution and also affects the specific heat ratio (κ) or polytropic index of the charge. The heat of vaporization might however be a major factor when the water injected directly inside the cylinder i.e. for a direct water injection hardware, where the injected water extracts heat from the cylinder charge. It can also be noted from figure 6.7a and 6.7b that the quanitity of water required to maintain constant load is lower when the water is injected before intake valve opens (EOI_w= 402) than for the case when it takes place during intake valve opening (EOI_w= 300). This is in agreement with the results obtained form the first experimental campaign and presented in section 6.1.1.

To assess the impact of water on the cylinder charge properties, polytropic index (n) was calculated for the conditions mentioned above, using cylinder pressure data. The value of polytropic index depends on the gas mixture properties including specific heat ratio of the mixture and heat transfer to and from the system, in this case cylinder. The compression and expansion processes can be fitted using polytropic equation, PV^n = constant, where P and V represents cylinder pressure and volume, and n is the polytropic index, however, this method is not applicable during combustion since combustion is not a polytropic process [6, 72]. Figure 6.8 shows the polytropic curves averaged over 300 cycles at different humidity conditions during both compression 6.8a and expansion stroke 6.8b of the cycle. The engine was operated at 20 bar IMEP and 4800 rpm with water injection ending 300 CAD bTDC (before IVO). The total amount of water for the low, ambient and high humidity cases were 30.93, 31.64 and 27.27 mg/cycle, respectively.

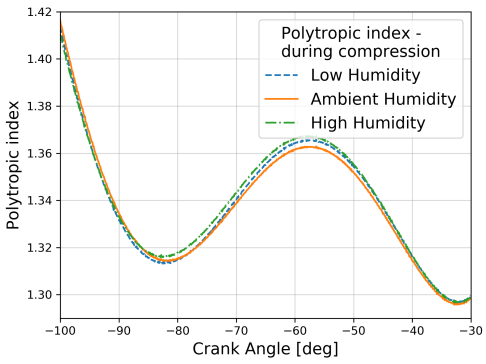

(a) polytropic coefficient during compression stroke

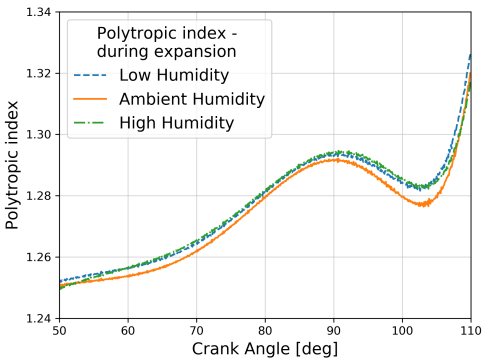

(b) polytropic coefficient during expansion stroke

Figure 6.8: Polytropic index computed during compression and expansion strokes for different humidity levels [80]

It can be noted from figure 6.8a that the polytropic coefficient evolves similarly for all the cases, independent of the humidity conditions, during compression stroke. The total amount of water in the cylinder is highest for the ambient humidity case which results in the lowest value for polytropic index between -85 and -30 CAD. This suggests that the effect of water on the polytropic index during the compression stroke is directly related to the total quantity of water in the cylinder.

Similar pattern is observed from figue 6.8b for the development of polytropic index for all cases during the expansion stroke. To further investigate this effect during the expansion stroke, experiments were conducted under conditions with low and high cylinder water contents. The polytropic index curves for these cases are presented in figure 6.9.

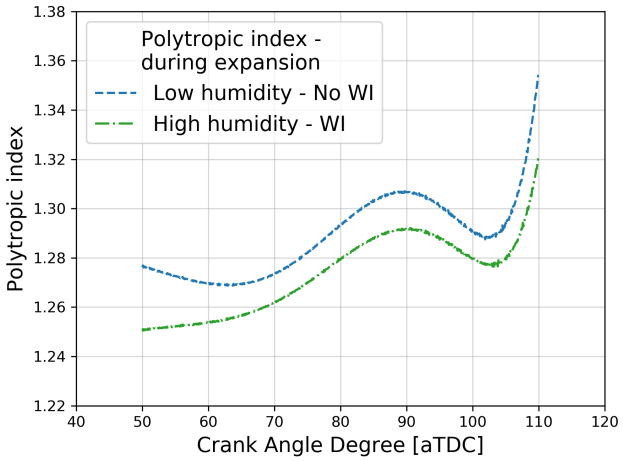

Figure 6.9: Variation in the polytropic index for the low and high cylinder water content cases during the expansion stroke [80]

The results in figure 6.9 show that water significantly affects the charge properties. The blue curve represents the results obtained without water injection under rich conditions ($\lambda = 0.9$). If a stoichiometric mixture ($\lambda = 1$) had been used instead, the difference between the blue and green curves would probably have been even more pronounced, as suggested by Klein [81]. Cycle-averaged pressure traces for the two cases showed that the cylinder pressure was lower for the high water content case (green curve), showing that extra water reduces the pressure and temperature inside the cylinder due to dilution effects [80].

Humidity and Combustion Phasing

Additional experiments were performed to investigate the effect of relative humidity on the degree of advancement of the ignition timing. Figure 6.10 shows the advancement in combustion phasing (in CAD aTDC) at different humidity levels and different water:fuel ratios.

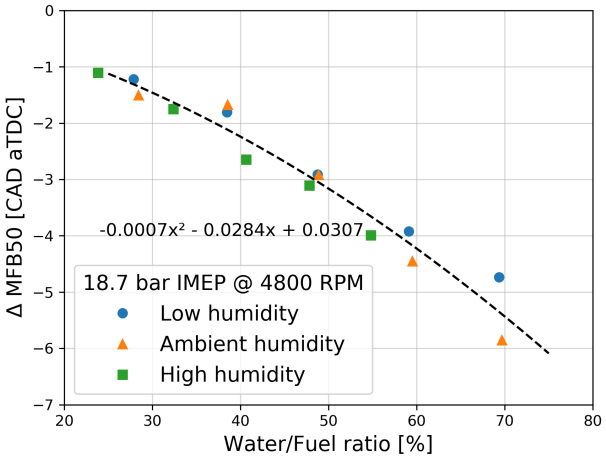

Figure 6.10: Ignition timing advance at different humidity levels [80]

The water:fuel ratios of the studied operating points are plotted on the x-axis, while the y-axis shows the advancement of the Mass Fraction Burn 50 (MFB50) in CAD aTDC. The engine was operated at ~18.7 bar IMEP and 4800 rpm in all cases. The results in the figure show that the advancement of MFB50 increases almost linearly with the water:fuel ratio and can be predicted with equation 6.5

$$y = -0.0007x^2 - 0.0284x + 0.0307 \tag{6.5}$$

where x is the water:fuel ratio in % and y represents the advancement of MFB50 timing in CAD. The equation suggests that the advancement in combustion phasing is essentially directly proportional to the total water content inside the cylinder and that variation in humidity has no direct effect other than insofar as it affects the total water content inside the cylinder.

6.1.3 Application in HEV - Simulation

Having clarified the benefits of water injection and the mechanism responsible for those benefits, a simulation study using GT-Suite was conducted to investigate its use in a full scale mild hybrid P2 vehicle. Details of the test setup and boundary conditions for this study are presented in Section 4.1.4. Initially, simulations were run in GT-Suite with a model of a 48V P2 mild hybrid equipped with a 15 kW electric motor to identify engine operating regions where water injection could potentially improve efficiency. Figure 6.11 shows the predicted engine operating time (expressed as a percentage of the total operating time) at different speeds and loads for three drive cycles with differing degrees of aggressiveness - NEDC, WLTC, and RTS95.

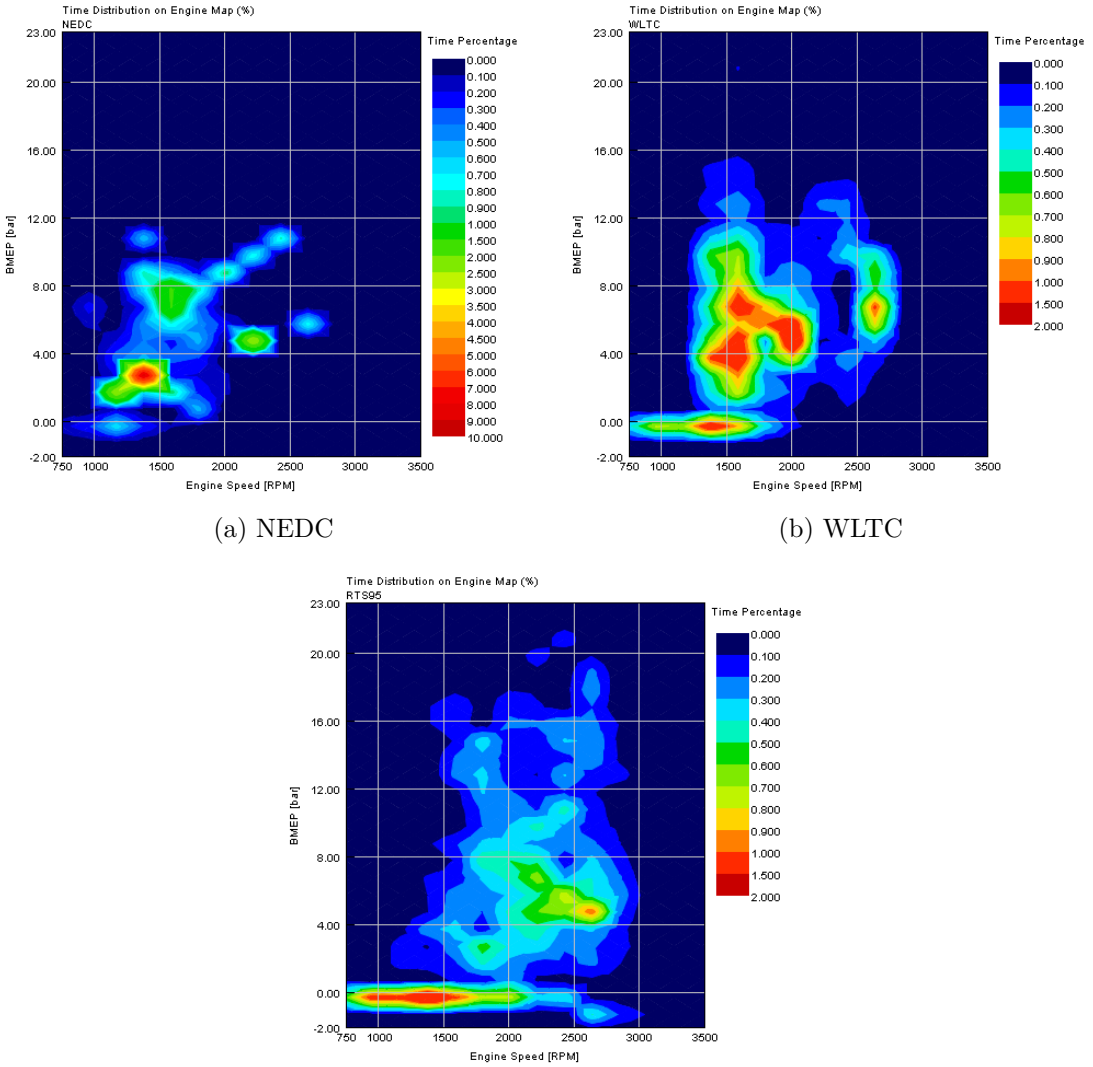

(a) NEDC

(b) WLTC

(c) RTS95

Figure 6.11: Engine operating time (as a percentage of the total operating time) at different loads and speeds for a HEV powertrain in three drive cycles [82]

Figure 6.11a shows that the engine mostly operates in the low load, low speed zone where its efficiency is significantly reduced by throttling and heat losses. As the aggressiveness of the drive cycle increases (from NEDC to WLTC and then RTS95), the engine operating points shift towards the high speed, high load zone where the engine is more efficient. In the RTS95 cycle, the engine load is spread throughout the operating zone, allowing the benefits of water injection to be exploited. Because real driving events tend to be more aggressive than most test cycles, it can be assumed that in a vehicle driven by a real customer, the engine would spend more time operating in the high load region than is suggested even by the RTS95 cycle. Operation in this region would also be favored by further downsizing of combustion engines in hybrid powertrains.

Using the information from figure 6.11 a test matrix (shown in table 4.3) was generated to evaluate BSFC with and without water injection. The improvements in BSFC (or fuel consumption) caused by water addition can be seen in figure 6.12.

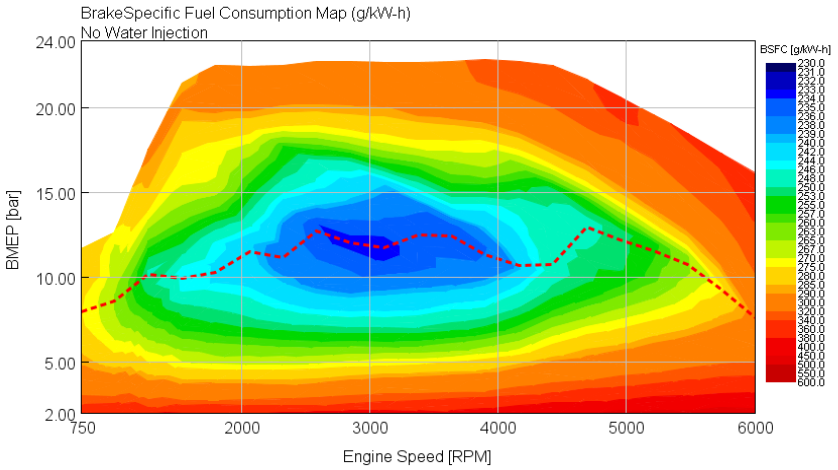

(a) without water injection

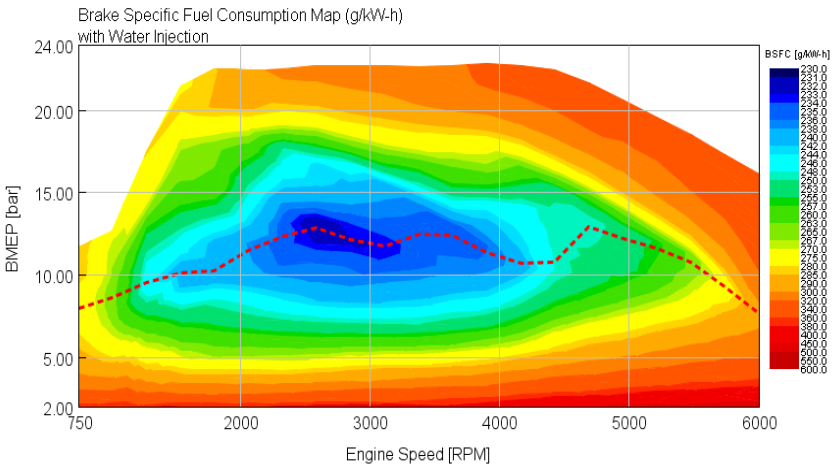

(b) with water injection

Figure 6.12: BSFC map of the engine in a mild HEV [82]

Water injection caused a clear improvement in overall BSFC, with a particularly notable improvement in the region around 20 bar BMEP and 2000 rpm, where the BSFC fell from about 300 g/kWh to ~280 g/kWh. Improvement in BSFC was also observed in the zone of lowest BSFC (i.e. the blue regions of the two maps), where the BSFC fell from 233 g/kWh without water injection to 231 g/kWh with water injection. The improvements observed in BSFC are due to the addition of water which shifts the knock limited spark advance towards or at MBT timing, and thus the engine can attain maximum torque. The dotted red line represents the best BSFC over the studied range of engine operating speeds. The greatest improvements in fuel efficiency due to water injection were observed at high load and low engine speed. Because the engine speed rarely exceeds 3000 rpm in compact passenger vehicles during standard drive events, simulations were only performed for engine speeds below 3000 rpm. However, further improvements could be achieved at higher engine speeds at full or near-full load. Water injection can also enable stoichiometric (or near-stoichiometric) operation in the high speed, high load region, where additional fuel would otherwise typically be added to keep the exhaust gas temperature within acceptable limits.

The BSFC benefits achieved through water injection are shown as percentages in the 3D plot presented in figure 6.13. Engine speed and load (BMEP) are presented on the x and y axes, respectively, and the improvement in BSFC (in %) over the operating range is shown on the z-axis.

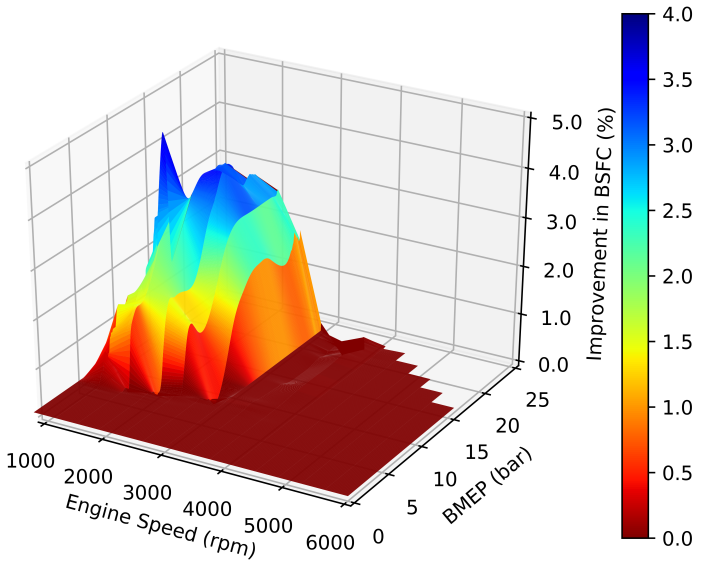

Figure 6.13: Improvement in BSFC due to water injection over the studied engine operating range [82]

Because simulations were conducted only at engine speeds below 3000 rpm, the curve is flat (red) in the region corresponding to higher speeds. Additionally, no simulations were conducted for load points at which the engine operated with MBT timing even without water injection. Figure 6.13 shows that most of the efficiency gains due to water injection are in the low speed, high load regions. This is because water injection enables advancement of combustion phasing, leading to higher efficiency when using a stoichiometric air-fuel mixture.

The updated BSFC values were then incorporated into the hybrid vehicle simulation model and the three previously mentioned drive cycles were simulated once more to evaluate the practical benefit of water injection in a mild hybrid powertrain. Simulation-based predictions of the vehicle's fuel and water consumption under different drive cycles are presented in table 6.4 and figure 6.14, in which the orange and blue bars respectively show the vehicle's fuel consumption in liters per 100 km without and with water injection. The cycle with the highest fuel consumption was RTS95, which is the most aggressive of the three studied cycles. The green bars show the fuel consumption benefit (i.e., the reduction in fuel consumption, expressed as a percentage of the fuel consumed in the case without water injection) of water injection, while the red bars show the volume of water consumed to achieve that benefit. Water injection caused small but consistent improvements in fuel consumption for all drive cycles, with the strongest improvement being seen for the RTS95 cycle.

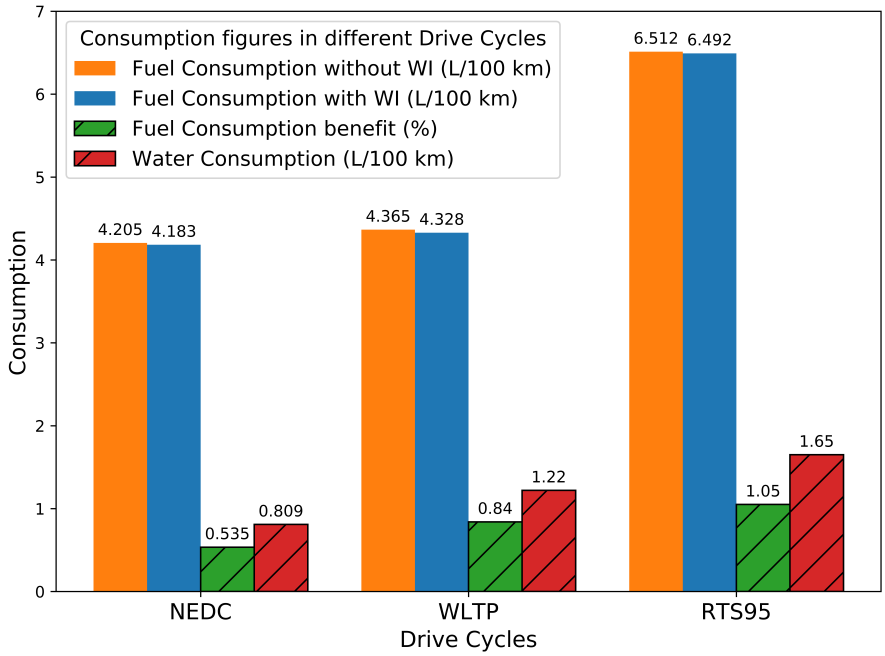

Figure 6.14: Reductions in fuel consumption when using water injection in a HEV powertrain for three driving cycles [82]

Table 6.4: Fuel and water consumption of a simulated mild hybrid vehicle under different drive cycles with and without water injection.

Drive Cycle	**Fuel Consumption**			**Water Consumption**
	w/o WI (L/100 km)	**with WI (L/100 km)**	**benefits (%)**	**(L/100 km)**
NEDC	4.205	4.183	0.535	0.81
WLTC	4.365	4.328	0.84	1.22
RTS95	6.512	6.492	1.05	1.65

The results in this section indicate that the benefits of water injection will be most pronounced for aggressive drive cycles resembling real driving events and for high performance powertrains. However, the quantity of water required will increase in proportion to the reduction in fuel consumption. Consequently, a vehicle with a 50 L of fuel tank would require an additional water tank with a capacity of around 10 L. This can be justified by using custom transmission and control strategies to operate the engine at high power output. Water injection technology will thus be most suitable for high performance hybrid vehicles equipped with highly downsized engines in which both engine and hybrid strategies can be used to maximize the benefits of water injection.

6.2 Engine Starts

6.2.1 Hybrid Setup - Investigation and Analysis

Drive Cycle Analysis

In the first phase of the engine start investigation, tests were performed with the hybrid powertrain in the Chalmers hybrid test bed. During post processing of the resulting experimental data, the first analysis and visualization step involved plotting the drive cycle in a way that highlighted the three different start categories (cold, mild, and warm starts), as shown in figure 3.2 in Chapter 3. Figure 6.15 shows the temperature variables that determine the nature of an engine start event along with the vehicle velocity profile for the WLTC. The start events of the hybrid powertrain during the WLTC are indicated by the colored bands in the figure: blue for cold starts, green for mild starts, and red for warm starts. For simplicity, the engine oil and coolant temperature were not considered when categorizing start events in this work. However, the trends in the engine oil and coolant temperatures were similar and aligned well with the engine start categories defined based on the TWC temperature, as shown in figure 6.15.

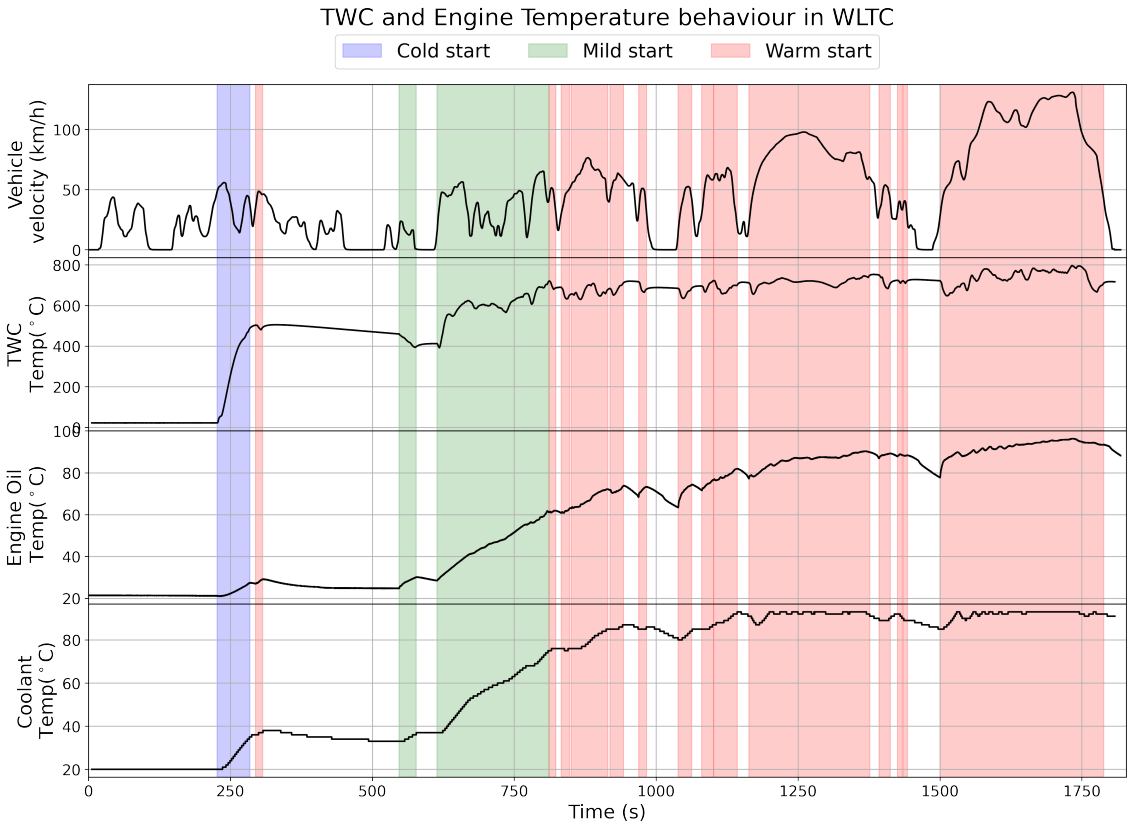

Figure 6.15: Engine and three-way catalyst temperatures in the hybrid powertrain during the WLTC.

When using the standard ECU/HCU calibration for the studied HEV powertrain, the engine coolant temperature first reaches 70°C at around 800 seconds into WLTC, towards the end of the fourth engine start. By this point, the catalyst temperature has already risen above 600°C (which is significantly above the catalyst light-off temperature). However, the engine oil temperature at this time is still in the range of 60°C. The engine's efficiency does not peak until it reaches around 90°C; below this temperature, fuel consumption is increased by friction between engine components. It should be noted that during the second warm start event in the WLTC, the initial engine coolant temperature reaches 70°C and so the engine is considered hot according to EU regulations [53]. However, the engine oil temperature at this point is still about 20°C below the value considered to represent normal operating conditions (80°C).

Because warm starts are often characterized by higher catalyst and engine temperatures than cold starts as well as lower engine-out and tailpipe emissions, finding ways to reduce fuel consumption was a major goal of the experimental work on warm starts. Conversely, because emissions are particularly high during cold starts, focus should be provided on finding ways to minimize emissions during cold starts. However, cold starts were not investigated as part of this work. An important benefit of distinguishing between cold, mild, and warm starts based on the temperature and conversion efficiency of the three-way catalyst is that it becomes possible to set individual emissions and fuel consumption targets for different start types, as discussed later on in this section.

The approach used to identify and characterize different start types in the WLTC was applied to six other drive cycles with different levels of aggressiveness. The results obtained in these measurement campaigns are summarized in table 6.5; figures showing the different engine start events during these cycles are provided in the Appendix.

Table 6.5: Engine start events and the initial and final state of charge of the hybrid powertrain for different drive cycles.

Drive Cycle	**State of Charge [%]**		**No. of Engine Starts**			
-	initial	final	Cold	Mild	Warm	Total
WLTC	61.30	61.62	1	2	14	17
RTS95	61.30	46.43	1	0	22	23
FTP75	61.30	39.32	1	0	19	20
NEDC	61.30	52.18	1	3	2	6
US06	61.30	60.80	1	0	6	7
SC03	61.30	47.78	1	0	5	6
RDE	61.30	69.18	1	1	70	72

The initial and final SoC values that define SoC neutral conditions depend on the driving conditions. However, because performing drive cycle tests is time consuming, it was decided that the initial SoC of the hybrid powertrain would be held constant at 61.3% for all studied drive cycles. The difference between the initial and final SoC values for a given cycle indicates the duration and intensity of the IC engine's operation during that cycle; if the final SoC is higher than the initial value, it means that the engine operated more frequently than was needed to maintain SoC neutrality. Conversely, if the final SoC is lower than the initial value, the engine runtime was less than would have been needed to recharge the battery and maintain SoC neutrality. In total, the experimental campaign generated a database containing information on 138 engine start events including 7 cold and 125 warm starts. As mentioned earlier, the low catalyst temperature during cold starts mean that reducing tailpipe emissions is a bigger challenge than minimizing fuel consumption.

Emissions vs Energy Consumption

As discussed in the previous section, the catalyst temperature during cold and mild starts is below 500°C, and cold starts are responsible for a majority of the tailpipe emissions during any driving event. Accordingly, figure 6.16 shows the tailpipe THC, CO, and NO_x emissions measured after the catalyst, normalized against the engine power and plotted in specific units (g/kWh). The exhaust gases reach their highest peaks during the first four start events (i.e., the cold and mild starts as well as the first warm start), and become significantly lower once the catalyst temperature rises above ~600°C. This is attributed to the fact that the catalyst reaches its maximum conversion efficiency at high temperatures.

The specific emission peaks are particularly high during the first four engine starts and became smaller as the catalyst reaches higher temperatures. High emissions are observed during the initial start period, irrespective of the engine start type. The peaks for CO and THC can be attributed to poor air-fuel mixing and non-homogeneous combustion, which are especially common during transient events such as engine starts [50]. However, there is no immediately apparent explanation for the peaks in specific NO_x emissions observed in this campaign.

For the warm start analysis, the first warm start event during the WLTC was ignored because it occurred while the coolant and oil were still below their normal operating temperatures. As mentioned previously, when the engine and catalyst are at their optimal temperatures, tailpipe emissions become non-significant. Consequently, rather than seeking to reduce emissions, the focus of the warm start research was on reducing the fuel consumption of the hybrid powertrain.

To summarize the preceding discussion, different categories of engine start events in a HEV powertrain can be defined based on the temperature of the three-way catalyst. These different engine start events can usefully be visualized by plotting changes in emissions and different aspects of the powertrain's behavior (e.g. the vehicle speed)

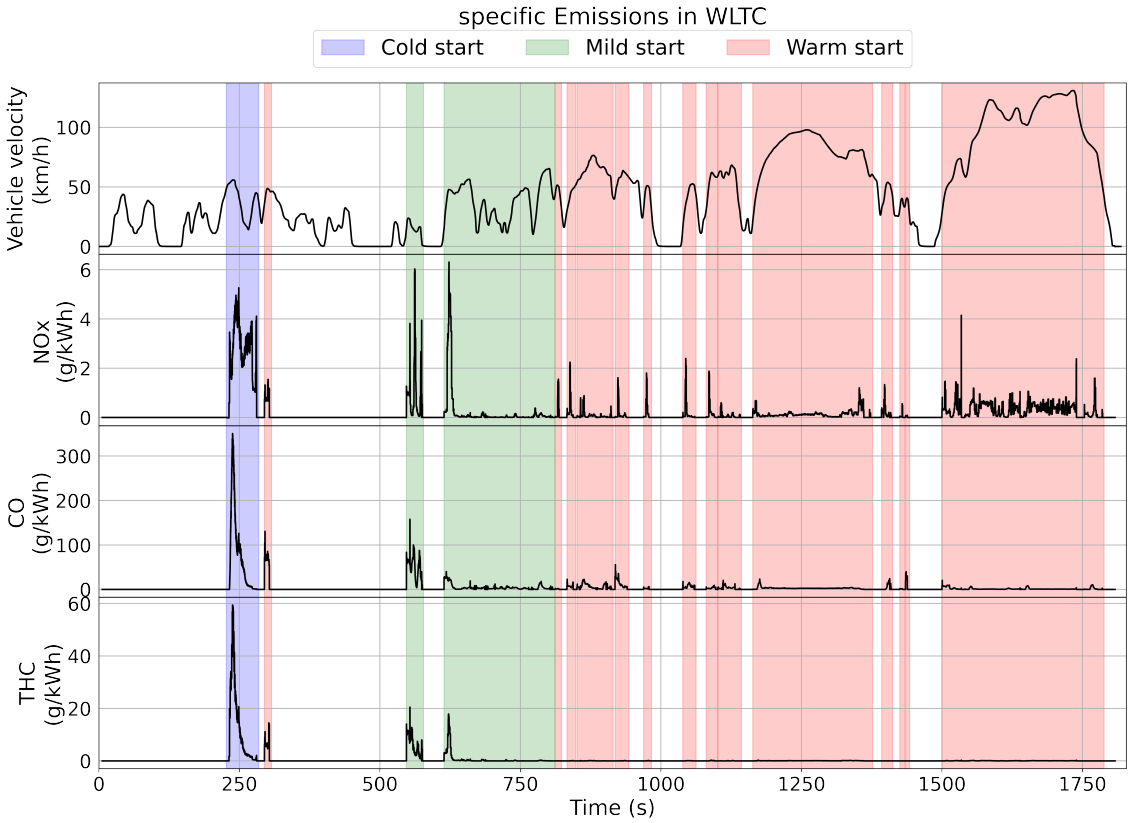

Figure 6.16: Specific tailpipe emissions (in g/kWh) of major regulated pollutants during the WLTC

over the course of a driving cycle and using different colored backgrounds to indicate periods corresponding to different start event categories. Because each start event category has unique characteristics, strategies for optimizing engine behavior in a HEV powertrain during start events must be chosen based on the nature of the start event. In the case of cold and mild starts, the energy management strategy (EMS) and HEV strategy should be chosen so as to minimize emissions (which may require increased fuel consumption to accelerate catalyst heating), whereas optimizing fuel or energy consumption should be the objective during warm starts. Taking these considerations into account, scripts were created to identify and classify start events, evaluate their duration, and determine whether fuel consumption or emissions reduction should be targeted during each event. The results obtained by applying these scripts to the WLTC data presented above are shown in table 6.6.

The time ranges specified in the top row of table 6.6 correspond to the parts of the WLTC in which the catalyst's conversion efficiency was suboptimal because its temperature was below 500°C. In such periods, tailpipe emissions will be high, so the EMS/HEV strategy should prioritize minimization of emissions. The time ranges specified in the second row correspond to parts of the WLTC in which the catalyst is at or above its efficient working temperature, allowing the use of fuel consumption optimization strategies. It is important to note that the results presented here

Table 6.6

Optimization Strategy	**Comments**	**Time during drive cycle (s)**
Emission Optimization	before the catalyst has reached its efficient working temperature (e.g., $T_{cat} < 500°C$)	(5.94, 290.74) (298.04, 312.44) (370.74, 626.44)
Fuel Optimization	after the catalyst has reached its efficient working temperature (e.g., $T_{cat} > 500°C$)	(290.74, 298.04) (312.44, 370.74) (626.44, 1818.35)

are only intended to serve as a proof of concept, and that the choice of strategies in a practical application will depend on both the hardware under consideration (including the TWC, the engine, and the HEV architecture) and the software used in the ECU and HEV/EMS.

To improve the robustness of optimization strategies and minimize complexity, they should only be applied in cases where their benefits will be realized for at least some minimum period of time. For example, the second time period listed in the first row of table 6.6 is only 14 seconds long. Thus, although in principle an emissions minimization strategy should be preferred in this period, in practice it is too short for such a strategy to be applied given that a fuel consumption minimization strategy would be called for immediately before it began and immediately after it ended. It should also be noted that the analysis presented herein is based on a predefined drive cycle that was known when the data post-processing was performed, and that the analysis was not performed in real time. Nevertheless, the data gathered during these tests can be used to develop emissions and fuel consumption optimization strategies suitable for use in diverse driving scenarios.

6.2.2 Engine Setup - Methodology and Optimization

Warm Engine Starts

In the second experimental campaign, tests were performed on a four-cylinder direct injection engine installed on an engine testbed. Experiments were performed at the operating points specified in figure 4.7. The target responses or Key Performance Indicators (KPIs) selected for this campaign were the regulated emissions (i.e., CO, NOx, and THC), the fuel mass integral, and the energy consumed while starting (or motoring) the engine. The chosen experimental variables were the engine speed (starting), engine load (throttle and/or torque), and the catalyst temperature during the engine start.

Figure 6.17 shows data for a start event at an operating point with an engine speed of 2000 rpm and an engine load corresponding to 75% throttle (or ~153 Nm torque). Initially, the engine is inactive; recording begins shortly before it starts being motored by the dynamometer, which occurs after about 10 sec in the figure. While the engine is being motored by the dynamometer, its torque output is negative. Expansions of the engine start period between 10 and 17 seconds are shown on the right of the figure. The calculations are initiated at the point when the engine speed rises above 0 rpm. However, because the initial increase in engine speed is driven by the dyno, the engine's torque is initially negative. Consequently, the calculation of the KPIs did not begin until the engine torque rose above zero Nm, indicating the start of fuel injection, the generation of power by the engine, and the transfer of power to the dynamometer.

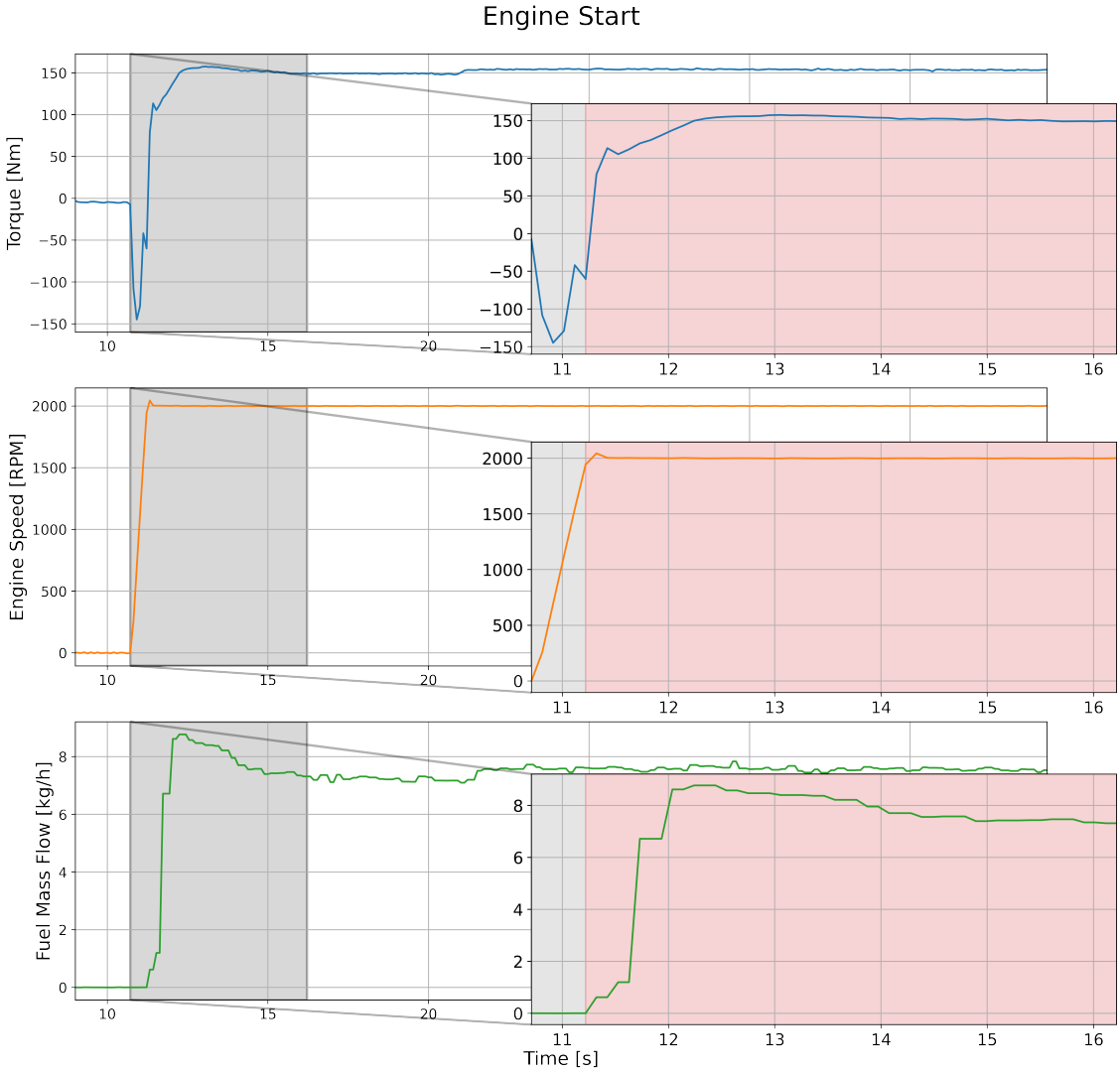

Figure 6.17: Changes in engine torque, speed, and fuel mass flow during a start event in which the engine was motored by the dynamometer.

The power was calculated by taking the integral of the engine speed (N) and torque (T) while the engine was being motored, which lasted for approximately 0.6 seconds for the operating point shown in figure 6.17. The bottom graph in figure 6.17 shows the fuel mass flow (kg/h), which starts rising when combustion begins after the desired engine operating speed has been reached.

Engine out emissions and fuel consumption were calculated only for the period after the initiation of fuel injection. Both of these variables were mass integrated over a stabilization period of 10 seconds. Figure 6.18 shows spider plots of the chosen KPIs for three different engine start (motoring) speeds and three different engine start loads (throttle values in %).

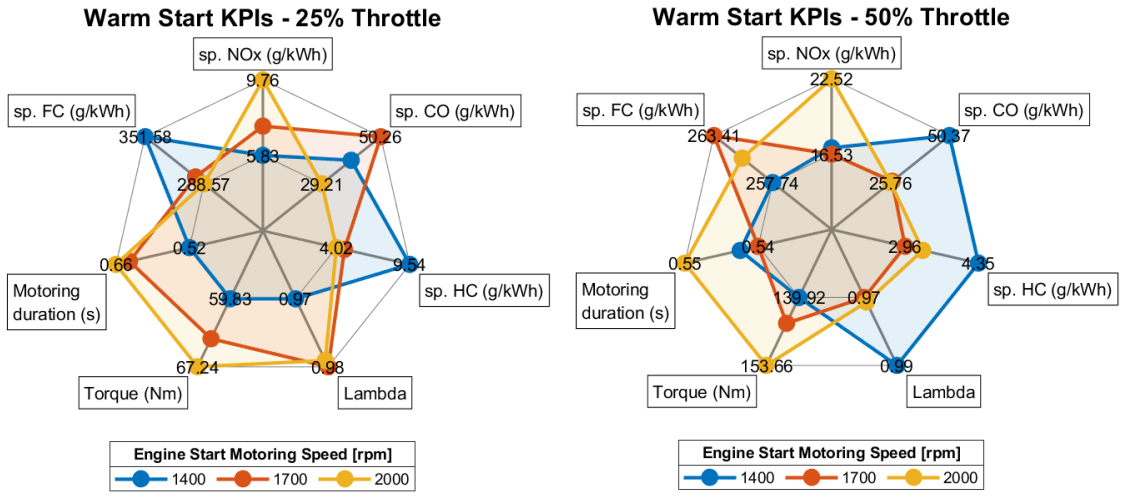

(a) Throttle: 25%

(b) Throttle: 50%

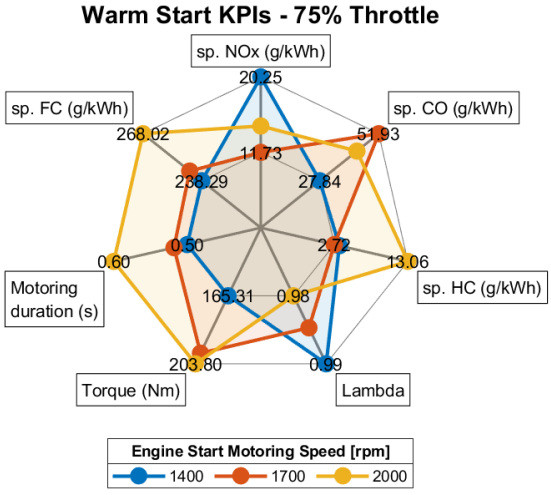

(c) Throttle: 75%

Figure 6.18: Spider plots of the chosen key performance indicators (KPIs) under different warm engine start operating conditions

Each plot in this figure shows the minimum and maximum values of each KPI. The KPIs shown are major regulated emissions (NO_x , HC, and CO) in g/kWh; along with corresponding torque and specific fuel consumption during the 10 second stabilization (recording) period for the maneuver described in the Test Methodology section and shown in figure 4.8. The spider plots clearly show that NO_x emissions generally increase with torque, although this was not true for the 75% throttle case, for which the NO_x emissions were unusually high. Overall, the results presented in the spider plots reveal no clear patterns in the KPIs that can be related to the chosen starting conditions. However, based on the data collected from the experiments, behavior models were generated in AVL CAMEO for various KPIs. The generated models were further used to identify optimal engine start conditions (engine speed and load) in the Optimizer function available in the tool. An example demonstrating this procedure is shown in Appendix.

The focus of the investigation therefore shifted to studying the efficiency of individual starts. The efficiency of a start was defined as the ratio of the energy output to the total energy supplied, and was calculated using the equation below:

$$\text{Engine Starting Efficiency} = \frac{\text{dyno energy output + fuel energy output}}{\text{fuel energy input + dyno energy input}} \tag{6.6}$$

The energy output is the energy required to motor the engine (supplied by the dyno or electric motor) and to start the engine (i.e. the energy in the injected fuel), with the duration of the engine start event being taken to be 5 seconds. The fuel and dyno input energy represent the total energy in the supplied fuel and the dyno or electric motor before losses, respectively. On the basis of the results presented in Figure 6.17, each engine start event was divided into two parts – the dyno motoring phase and the combustion phase, which began once the engine had reached the speed appropriate for the desired operating point. At each operating point, transient start events were repeatedly recorded until stable torque and fuel curves were obtained. Based on these measurements, the duration of a start event was assumed to be around 5 seconds. The starting efficiencies for the nine operating points examined in this test campaign are shown in figure 6.19.

In this figure, the efficiency of the engine start is indicated by the diameter of the circles (larger circles correspond to more efficient starts) and using the color scale shown on the right of the figure. The starting efficiency was lowest (29.45%) when the engine was started at 1700 rpm and 25% throttle, corresponding to ~65 Nm torque. The highest efficiency of 42.71% was obtained when the engine was started at 1400 rpm and 75% throttle, corresponding to ~165 Nm of torque.

Figure 6.19 indicates that for the selected hardware (four-cylinder, direct injection engine), it was optimal to start the engine at 1400 rpm and 75% throttle. The value of second best efficiency was approximately 1.5% lower at 41.22% - for 1700 rpm and

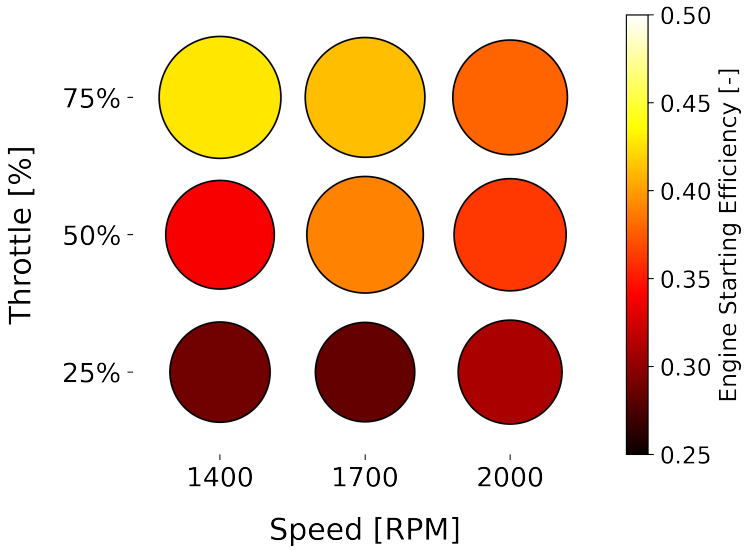

Figure 6.19: Warm engine starting efficiencies for the nine studied operating points.

197 Nm torque at 75% throttle. This indicates that engine starts with high loads and moderate speeds are more efficient. Starting an engine with an electric motor allows the engine to be started with the most efficient parameters, and depending on the requirements, any energy abundance or shortage can be compensated by the electric motor. A similar methodology will be applicable for different engines and powertrain systems and can be used to check the robustness of the developed methodology.

Engine Starts with Optimized ECU Calibration

The results presented in the spider plots in figure 6.18 were obtained in tests using standard ECU calibration. Since engine performance (gas exchange and dynamics) depends on the speed and load, the results presented in figure 6.18 do not represent the KPI values achievable under optimized engine start conditions. To properly assess the KPI values achievable at the chosen operating points, it was therefore necessary to optimize engine calibration variables such as the intake and exhaust valve timing and the fuel injection timing and pressure at each load point of interest. This was done during the second phase of the experiments, in which the calibration variables listed in table 6.7 were systematically varied at each of the chosen engine start speeds and loads while recording the KPIs of interest (i.e., emissions of CO, THC, and NOx as well as the consumption of fuel and energy). The test matrix was generated using s-optimal design and CAMEO's Active DoE methodology; the boundary conditions for the variables were chosen by the experimentalist.

The experimental data gathered during the second experimental campaign were then used to identify optimal engine settings that gave the most favorable KPI results at each load point of interest. This was done by performing optimization in AVL CAMEO using a Multiobjective Genetic Algorithm [83]. Separate optimizations were

Table 6.7: Engine calibration variables examined in experimental campaign 2

Variable	Unit	Base Value	Test Range
Engine Speed	rpm	0	850 to 2000
Throttle	[%]	0	5 to 40
Fuel - SOI	CAD bTDC	270	220 to 340
Fuel - Inj. Pressure	bar	150	100 to 200
Lambda	-	1	0.85 to 1.05
Intake Valve Timing	CADb TDC Int.	40	20 to 50
Exhaust Valve Timing	CAD bBDC Exh.	19	10 to 40
Ignition retard	CAD bTDC Pwr	0	0 to -6

performed for engine starts at speeds of 1400, 1700, and 2000 rpm and torques of 20, 40 and 60 Nm. The results of the optimization process for the three engine speeds mentioned above in the 60 Nm torque case are shown in the spider chart presented in figure 6.20.

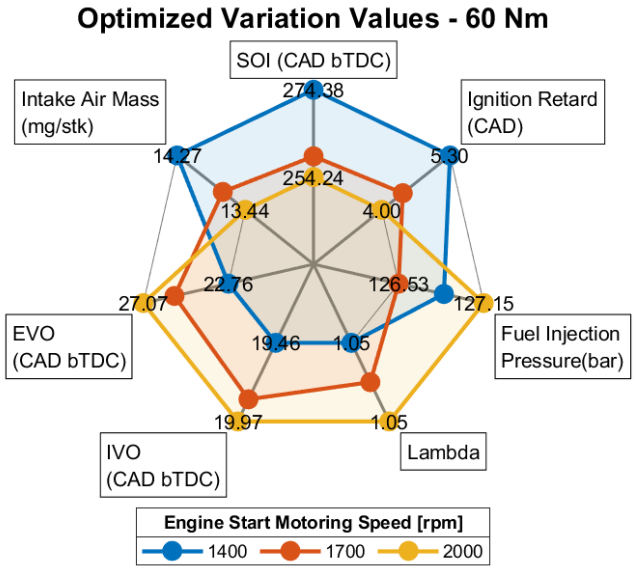

Figure 6.20: Optimized engine calibration variable settings for different engine start conditions.

In this chart, each vertex represents the optimized value for a specific engine calibration variable at the indicated engine speed. This approach makes it possible to identify engine settings that are optimal with respect to specific target responses (e.g., emissions during a cold start or fuel consumption during a warm start) at any starting speed and load of interest. The KPI values (i.e., fuel consumption and tailpipe emissions) achieved using the optimized calibration settings are not presented in this thesis, but the methodology presented herein can be applied to any engine type.

Energy Savings Achievable by Optimizing Engine Starts - A Case Study

To evaluate the benefit of engine start optimization in a HEV powertrain during drive cycle operation, the results obtained from the second experimental campaign were used to simulate the behavior of a hybrid powertrain. To this end, the drive cycle data from the first experimental campaign (discussed in section 6.2.1) was used together with the data from campaign 2. The WLTC was chosen as the drive cycle for this analysis because it had previously been used in the experiments performed using the HEV powertrain.

As discussed previously, the engine start time was assumed to be 5 seconds. The power and energy demand were calculated for each of the hybrid powertrain's 17 engine start events during the WLTC and then averaged over all 17 starts, giving an average start power of 12.981 kW and an average start energy of 0.01803 kWh. The average power was integrated over the five second engine start period to obtain the starting energy. Assuming that all starts have the same power (energy) demand, the total energy consumed to start the engine during WLTC operation is equal to the product of the average starting energy and the number of engine starts, or 0.3065 kWh. Table 6.8 compares the total starting energy requirements for seven drive cycles with and without optimization to maximize engine start efficiency. Note that the highest efficiency starting condition is compared with the starting characteristics of a stock (base or standard) calibration condition. The standard engine start had an engine starting speed of 1700 rpm and the starting engine load value is assumed at 50% throttle (corresponding to an engine start efficiency of 39%). The load (throttle) value is assumed in this case because in the stock calibration, load was not fixed and was dependent upon the vehicle power demand. Here it is assumed that the engine starting conditions can be fixed for each start, and compensated by the electric motor.

For each of the seven drive cycles, table 6.8 shows the average engine starting power and energy over the assumed 5 second engine starting time without optimization for efficiency, followed by the amount of energy required from the injected fuel to provide the engine start energy in two cases – when the engine starting efficiency is highest (1400 rpm, 75% throttle) and when an engine start for a standard calibration is used (1700 rpm, 50% throttle). The final two columns show the energy saved during each engine start and the total energy saved over each driving cycle. The

Table 6.8: Average energy requirements for engine starts and energy savings achievable through optimization of engine start for seven driving cycles

Drive Cycle	**No. of Engine Starts**	**Average Engine Starting** *(for 5 sec)*		**Energy input required when starting engine with** *(in Wh)*		**Energy saved during** *(in Wh)*	
		Power (kW)	Energy (Wh)	Base (39.05%)	Highest (42.72%)	Engine Start	Drive Cycle
WLTC	17	12.981	18.03	46.17	42.20	3.96	67.40
RTS95	23	15.852	22.02	56.38	51.54	4.84	111.36
FTP75	20	10.845	15.06	38.57	35.26	3.31	66.25
NEDC	6	11.514	15.99	40.95	37.43	3.52	21.10
US06	7	29.145	40.48	103.66	94.76	8.90	62.31
SC03	6	15.950	22.16	56.74	51.86	4.87	29.23
RDE	72	11.90	16.54	42.35	38.72	3.64	261.89

fuel energy consumption over the full WLTC would be approximately 0.0674 kWh lower if every engine start was performed under the most efficient starting conditions rather than the standard (stock ECU) condition. It should also be noted that the energy saving potential increases with the duration of the vehicle's duty cycle, as demonstrated by a Real Drive Emission (RDE) cycle used in this campaign: the total energy saved was around 0.261 kWh for all 72 engine starts in the measured cycle. To compute the energy savings achievable through engine start optimization, the following assumptions were made in this work:

- All engine (re-)starts consume the same amount of energy during all drive cycles. The additional energy demand or surplus is supplied or absorbed by the electric motor (and battery) in a hybrid system.
- A compact passenger car covers 152,137 miles (=244,841 km) over its entire lifetime [84]
- Based on the predictions from Eckl et al.[10], that there would be about 0.6 Million engine (re-)starts over the life of a hybrid vehicle, for this case study, the vehicle is assumed to perform 500,000 starts over its life.
- The engine operates for at least 5 seconds during each (re-)start.

- As per the US Environmental Protection Agency [85], 8887 grams of CO_2 is emitted per US gallon of gasoline, corresponding to 2347.6 g CO_2 per liter of gasoline.
- The energy content per liter of gasoline is 9 kWh, taking the density of gasoline to be 740 kg/m^3.
- The average starting energy saved during each engine start is 3.31 Wh based on the FTP75 cycle.

Using these assumptions, the reduction in emitted CO_2 and energy consumption achieved by operating with the highest starting efficiency rather than the lowest is:

- Energy saved during engine starts over the total life of a hybrid vehicle = 3.31 Wh * 500,000 = 1655 kWh
- Fuel energy saved over 500,000 engine (re-)starts = 1655 kWh / 9 kWh per liter gasoline = 183.88 liters of gasoline
- Average CO_2 emitted per liter gasoline = 2347.616782 g/l
- Total CO_2 saved over 500,000 engine (re-)starts = 2347.616782 g/l * 183.88 l = 431,700.64 grams
- Average distance traveled by a car during its life cycle = 244,841 km
- CO_2 saved per km = 431,700.64 g / 244,841 km = **1.76 g/km**

Note that this is a simple case with multiple assumptions and approximations. However, it shows that the methodology presented herein can be used to investigate, optimize, and better understand engine starts and to accurately analyze the energy saving potential of cleaner engine starts for hybrid powertrains.

Chapter 7

Conclusions

The work carried out in this study focused on two technologies, water injection and engine start optimization, that are intended to improve the efficiency of IC engines and subsequently efficiency of hybrid powertrains. The conclusions from the two projects are summarized below:

7.1 from Water Injection study

The objective of the first experimental campaign was to investigate the benefits of water injection in spark ignited engines and the effects of operating the engine on different octane rating fuels. The three ratings of fuel used for the tests in this campaign were: RON91, RON95 E10 and RON98. From the experiments at full load conditions and stoichiometric air-fuel ratio, it was found that RON91 gasoline with water injection can reach the same torque levels as RON95 without water injection. A similar pattern was observed for RON95 and RON98 fuels used in the study. This was possible due to the knock suppression with water injection. This allowed additional air-fuel mass induction by increasing boost pressure until knock was encountered again. Additionally, a λ vs water:fuel ratio sweep was performed for the three octane rating fuels, to find the amount of water required to operate the engine at same load (16 bar IMEP) and same air:fuel ratio for all three fuels. From the experiments it was noted that water injection enables stoichiometric operation ($\lambda = 1$) in high load regions without encountering knocking combustion. And, the water:fuel ratio required was highest for RON91 followed by RON98 and RON95 E10. The relatively lower water:fuel ratio requirement for RON95 fuel was because of the presence of ethanol in the fuel providing high heat of vaporization and knock resistance. An additional benefit of water injection was the advancement in combustion phasing at high loads which leads to MBT or close-to MBT timing and hence improvement in BSFC.

The second experimental campaign and the content of Paper 2 was motivated while performing experiments in campaign 1; when the effect of varying atmospheric conditions was noticed on the performance of water injection. Hence the research

question was formulated to investigate the effect of ambient humidity on the performance and thermodynamic behavior of water injection. At a fixed load point, the total quantity of water in the cylinder (i.e., the sum of the injected mass of water and the mass of water in the intake air) under stoichiometric conditions was independent of the relative humidity, indicating that the heat of evaporation does not contribute appreciably to knock mitigation and that the beneficial effects of water injection are mainly due to dilution. Upon analysis, it was noted that the polytropic coefficient decreases almost linearly as the total quantity of water in the cylinder increases. This effect is apparent during both the compression and expansion strokes for cases with water injection. Similar to finding of paper 1, water injection allows the ignition timing to be advanced independently of the humidity level, and the degree of possible advancement is directly proportional to the total amount of water in the cylinder.

In the third paper on water injection, the objective was to provide the benefits of water injection when used in a hybrid vehicle equipped with water injection system. The BSFC data for cases with and without water injection for different load points was used to simulate the BSFC gains in a GT Suite model of mild hybrid vehicle. The greatest benefits of water injection technology are observed during high load and high engine speed operation. Under these conditions, water injection can mitigate knock and enable advancement of the ignition timing towards the MBT timing while still using a stoichiometric air-fuel mixture. The fuel consumption benefits of water injection increase with the aggressiveness of the drive cycle. Simulations of a mild hybrid model in GT-Suite indicated that water injection reduced fuel consumption by 0.535%, 0.840%, and 1.05% in the NEDC, WLTC, and RTS95, respectively.

7.2 from Engine Starts study

Engine starts were studied in two experimental campaigns. The first used a hybrid powertrain at *Chalmers University's* powertrain testbed and the second used a 1.4-liter GDI engine on an engine testbed at *AVL Graz*. The project's objective was to develop more efficient and cleaner engine start strategies with a focus on applications in gasoline hybrid systems. The results from both campaigns were presented in the fourth publication. Initially, focus was to develop an effective strategy to study and investigate engine starts in a variety of powertrain setup. Tests were performed on different drive cycles (including WLTC and RTS95) to identify different types of engine starts in a hybrid powertrain. From data analysis, engine starts were classified into three distinct categories based on the catalyst temperature - cold, mild, and warm starts. These categories are defined as follows:

Cold Start: $T_{Cat} < 300°C$

Mild Start: $300°C < T_{Cat} < 500°C$

Warm Start: $T_{Cat} > 500°C$

This provided a better understanding of the engine starts and which starts should be considered based on the application. The decision of whether to optimize for minimization of fuel consumption or emissions can be made on the basis of the catalyst temperature at the beginning of the engine start event. It is reasonable to optimize a cold start event (where catalyst temperature is lower than 300°C) for emissions and for a warm start the optimization should be focused on fuel consumption. Since only one cold start was observed in each driving event while most of the starts were warm starts, the investigation focused on warm starts. During warm starts, tailpipe emissions are not of concern because the three-way catalyst is at its optimal operating temperature. Consequently, optimization of fuel consumption and efficiency was prioritized. With this objective, the tests were planned on an engine setup in AVL Graz to study warm starts. A method to calculate the engine starting efficiency was developed before the tests. For the specific engine used during this campaign, the maximum engine starting (energy) efficiency was achieved when the engine was motored to 1400 rpm using a dynamometer (replicating an EM-assisted start in a HEV) before starting fuel injection (combustion) with a starting load of ~165Nm (achieved with 75% throttle). Finally, to put things in a real scenario energy saving potential, a simple case study demonstrated that for a specific passenger hybrid vehicle, 1.76 g/km of CO_2 emissions can be reduced if the engine is always started under the highest efficiency conditions (1400 rpm, 165 Nm torque) rather than the condition (1700 rpm, 64 Nm torque) for stock (base) calibration. This calculation is based on the assumptions that the vehicle travels 244,841 kilometers over its life and performs 500,000 engine (re-)starts. Additionally, the engine starting power is assumed to be constant for all starts because it is assumed that the electric motor can compensate for the vehicle's varying power demand levels. Hence, as a result, a general test methodology applicable to a wide range of powertrain systems was developed to understand, investigate, and optimize engine starts.

7.3 Summary and Concluding Remarks

There is a significant potential to improve the overall efficiency of a hybrid system with a combination of available technologies. For one, internal combustion engine equipped vehicles operating in geographical regions where octane rating of available gasoline is lower (e.g., RON91), water injection can be used to achieve performance similar to those operating on higher octane rating gasoline (e.g., RON95). The power levels achieved were also possible for stoichiometric conditions without using fuel enrichment which causes CO emissions. Additionally, water injection also enables improved combustion phasing which subsequently improves BSFC of the engine. The simulation results showed gains in fuel consumption over several drive cycles, albeit with a significant consumption of water. Secondly, with the developed methodology to study engine starts, the opportunity of identifying and quantifying fuel saving potential in a hybrid system, adds to the overall goal of achieving high efficiency for hybrid systems. Although, an extended investigation and validation of the methodology on a full-scale hybrid powertrain is yet to be performed.

What advantages does water injection offer considering the efficiency and performance of IC engines?

- With water injection similar power output can be obtained for low octane rating fuels compared to relatively higher octane rating fuels operating without water injection.
- Water injection enables stoichiometric operation ($\lambda = 1$) in the high load, knock probable regions of the SI engines.
- Improvements in brake specific fuel consumption is achieved since water injection enables engine operation on MBT timing. This is because knocking combustion can be suppressed with the injection of water.

How does the water content in atmosphere (relative humidity) affects the functioning of water injection? What are the mechanisms behind the working of water injection?

- Water injection provides knock resistance due to charge dilution (change in polytropic coefficient) and is dependent on the total quantity of the water present in the cylinder charge.
- For same operating points, the benefits are related to the total water quantity, i.e. water from humidity plus injected quantity.
- The results indicate that for the hardware (Port Water Injection system) used in this campaign the charge cooling effect due to evaporative cooling was inappreciable. This might be because of heating and evaporation of water in the intake manifold, where the water extracts heat form hot surfaces in the intake system. However, the effect of charge cooling due to heat of evaporation might be more pronounced for direct water injection system.

Is it worth having a water injection system in a car?

- Water injection can increase the lambda=1 area of the engine hence avoid CO emissions in those regions where normally enrichment is applied for increased power. Also, there is a potential fuel-consumption benefit.
- Water injection technology is useful in the high load regions where either knock suppression is needed or improvement in combustion phasing (towards MBT timing) helps improve the efficiency. Hence, it is suitable in vehicles with highly downsized engines.
- Important to consider is that for the fuel consumption benefits the water quantity required on board also increases respectively.

How can engine starts in different powertrain architectures be studied more effectively?

- As part of this work, a methodology was developed to investigate engine starts in different powertrain architectures. The methodology can be used with AVL CAMEO to identify optimal engine starting condition (load and speed) for specific conditions - cold and warm starts .
- The engine starts were classified into three categories (cold, mild and warm starts) based on the catalyst temperature. More engine parameters such as oil and coolant temperatures can also be included in the step, however, for sake of simplicity only one parameter (TWC temperature), was considered in this work.
- Cold starts are more relevant for emissions and the optimization of the warm-start event and the number of warm-start events during driving are more relevant for fuel-economy.

How can the developed methodology used in the optimization of engine start for warm start conditions?

- The methodology can be used to individually investigate and analyze engine starts for either fuel consumption (efficiency) optimization or emission reductions.
- With relevant assumptions, for the engine setup used in the second experimental campaign of phase two, analysis of a vast amount of collected data with the developed methodology, demonstrated a reduction of approximately 1.75 g in CO_2 per km, when the engine was started with the most efficient engine start condition compared to the standard calibration condition.

Uniqueness and Contribution to the Field

The work presented in this thesis has contributed to the knowledge of benefits, mechanisms, and application of water injection technology in SI engines. The uniqueness of the work on water injection includes mapping of water injection benefits with different octane rating gasoline; explanation of the mechanisms behind the effect of water injection and the effect of relative ambient humidity, both resulting in the conclusion that it is the total water amount in the induced air that affects the combustion caused mainly by dilution, not evaporation. Additionally, the assessment on the feasibility and benefits of the technology in a hybrid vehicle was also performed via simulations in GT-Suite showing the potential of water injection in fuel consumption reduction. The work provides evidence that in the cases when the engine is operating on a low RON fuel, injecting water can achieve power levels similar to the case when it is operating on a high RON fuel. Additionally, the results from the study of relative humidity contributes to the knowledge explaining working mechanism of water injection. From the second phase of the work, an interesting/useful way to analyze engine starts in a powertrain system - *Drive Cycle Analysis* was demonstrated. In addition to this, a methodology was developed to better understand, investigate and optimize engine starts in different powertrain architectures. The methodology can be used to categorize engine starts from a variety of powertrain systems. Depending upon the cold or warm start conditions, experiments can be performed using AVL CAMEO to identify most efficient engine starts for specific hardware and operating conditions. Lastly, a case study demonstrates the potential of CO_2 reduction, only by optimization of start event alone, while comparing the default engine start procedure with the most efficient engine start.

Chapter 8

Future Work and Outlook

This chapter presents some opportunities for future research building on the work presented in this thesis along with some insights and thoughts about the future of the automotive industry.

8.1 Future Work

8.1.1 Water Injection

- **Fundamental study of water injection:**
  - To continue the work presented in Paper 2, it would be helpful to develop a chemical kinetics model to study the influence of different competing effects on the mechanisms responsible for the beneficial impact of water injection in combustion engines.
  - Additionally, the fundamental study can be supplemented by investigating the behaviour of water injection on combustion properties under optical experiments.
- **Water injection combustion model:** A validated combustion model of water injection as diluent could be used to understand and investigate the effect of different injecting quantity on knock supression and in-cylinder combustion. This model could be imported into various powertrain architectures to perform systems analysis.
- **Water and bio-fuels:** Due to time limitations in this project, the effect of injecting water with other diluents such as glycol or alcohol fuels (e.g., methanol or ethanol) was not studied. However, such a strategy could offer interesting opportunities for further improvement of water injection technology.

8.1.2 Engine Starts

- **Validation of developed methodology:** The tests conducted on the engine test bed at AVL were performed with a 4-cylinder gasoline direct injection (GDI) engine whereas the engine used in the hybrid system was a 3-cylinder port-fuel injected (PFI) engine. It would therefore be desirable to validate the methodology developed using data from the engine test bed against experimental data obtained using the hybrid setup and potentially also other engine setups.

- **Optimization of engine starts on the HEV Powertrain:** The validated method could be used to optimize engine start conditions for the hybrid system available at Chalmers and extended to encompass Energy Management Strategy (EMS) optimization.

- **Sensitivity analysis of parameters:** A detailed analysis of the variables used in the optimization section of engines starts, can be performed to identify the sensitivity and competing-effects of different variables on engine starts.

- **Hybrid System study with bio- and e-fuels** Similar investigations could be conducted to optimize engine start conditions when using second generation bio-fuels or carbon neutral fuels produced with renewable electricity (so called e-fuels). Combining the conclusions of this project with the work of Andersson and Börjesson [5] could enable an interesting evaluation of the potential for improving engine starts using second-generation renewable fuels.

- **Development and validation of a simulation model:** Simulation studies have several advantages over experiments, so it would be beneficial to use the experimental data presented herein to develop a GT Suite model for studying engine starts and EMS optimization strategies. AVL CAMEO offers a platform for integrating simulation models and running optimization tests in a simulation environment. The data from this study could be used to validate predictions of fuel consumption, emissions, and other key performance indicators (KPI).

8.2 Outlook

Global concern over climate change and the enormous impact of emissions associated with road transport (particularly greenhouse gases) on our planet has quite rightly led to the introduction of stringent emission control policies. This has led to major changes in the transport sector, especially for passenger cars, with the aim of partly or completely replacing the internal combustion engine with electrified propulsion systems. When the author started his PhD studies in 2017, there was significant interest among industry and other research organisations to investigate ways to improve the efficiency of engines and consequently hybrid powertrains. However, less than four and a half years later, the interest in IC engine research & development has shrunk greatly; due to the anticipated "sustainable" transport solution offered by pure electric vehicles. The move towards sustainable electric vehicles is welcome, since transition to a pure renewable transport system should be the ultimate goal. However, given the limitations of current technology and infrastructure, plans based on completely eliminating the combustion engine and shifting to pure electric vehicles to reduce greenhouse gas emissions are flawed and will remain so for the foreseeable future.

As shown in figure 1.3 in Chapter 1: until we have developed technologies for more sustainable battery production & recycling, and most importantly, until the world's electric grids are dominated by sustainable energy sources, replacing conventional combustion engine vehicles with pure electric vehicles is pointless. This will simply shift the problem from one source to another. A viable alternative to this problem is hybrid vehicles, which can function as a bridge between our current circumstances and the ideal we pursue. Andersson and Börjesson [5] showed that the total life cycle CO_2 reduction potential of hybrid vehicles when used with second generation bio-fuels or carbon neutral e-fuels is significantly higher than that of pure electric vehicles. Additionally, the conclusions from the work presented in this dissertation indicate that the efficiency of a powertrain system equipped with an internal combustion engine can be further improved using a combination of different technologies. So, the conclusions from [5] and this study, can be integrated to further investigate and enhance the efficiency and sustainability of future powertains. To the author, this path appears to be more viable and realistic in addressing the issue of greenhouse gas emissions in passenger cars.

Bibliography

[1] O Edenhofer et al. *JM (eds.), Climate change 2014: Mitigation of climate change*. Tech. rep. Tech. rep., Working Group III Contribution to the Fifth Assessment Report of ..., 2014.

[2] European Environment Agency. *Greenhouse gas emissions from transport in Europe*. [Online; accessed 24-September-2021]. 2017. URL: https://www.eea.europa.eu/data-and-maps/indicators/transport-emissions-of-greenhouse-gases/transport-emissions-of-greenhouse-gases-12.

[3] Troy R Hawkins et al. "Comparative environmental life cycle assessment of conventional and electric vehicles". In: *Journal of industrial ecology* 17.1 (2013), pp. 53–64.

[4] Christian Bauer et al. "The environmental performance of current and future passenger vehicles: Life cycle assessment based on a novel scenario analysis framework". In: *Applied energy* 157 (2015), pp. 871–883.

[5] Öivind Andersson and Pål Börjesson. "The greenhouse gas emissions of an electrified vehicle combined with renewable fuels: Life cycle assessment and policy implications". In: *Applied Energy* 289 (2021), p. 116621.

[6] John B Heywood. *Internal combustion engine fundamentals*. McGraw-Hill Education, 2018.

[7] Zhi Wang, Hui Liu, and Rolf D Reitz. "Knocking combustion in spark-ignition engines". In: *Progress in Energy and Combustion Science* 61 (2017), pp. 78–112.

[8] G Konig and CGW Sheppard. "End gas autoignition and knock in a spark ignition engine". In: *SAE transactions* (1990), pp. 820–839.

[9] Stefano Fontanesi et al. "Analysis of knock tendency in a small VVA turbocharged engine based on integrated 1D-3D simulations and auto-regressive technique". In: *SAE International Journal of Engines* 7.1 (2014), pp. 72–86.

[10] T Eckl and E Kirchner. "The Long Path from Discomfort to Customer Acceptance: Start-Stopp: Yesterday, Today and Tomorrow". In: *Schaeffler Technologies AG & CO. KG (Hrsg.): Solving the Powertrain Puzzle* (2014), pp. 346–359.

[11] I. Scholten et al. "Geely's Modular Hybrid Propulsion System". In: *42. International Vienna Motor Symposium* (2021).

[12] T Pauer et al. "Optimization of gasoline engines by water injection". In: *37th International Vienna Motor Symposium*. 2016.

[13] Bruce D Peters and Russell F Stebar. "Water-gasoline fuels—their effect on spark ignition engine emissions and performance". In: *SAE Transactions* (1976), pp. 1832–1853.

[14] Wei Mingrui et al. "Water injection for higher engine performance and lower emissions". In: *Journal of the Energy Institute* 90.2 (2017), pp. 285–299.

[15] Alberto Boretti. "Water injection in directly injected turbocharged spark ignition engines". In: *Applied Thermal Engineering* 52.1 (2013), pp. 62–68.

[16] Abhijeet M Nande, Thomas Wallner, and Jeffrey Naber. *Influence of water injection on performance and emissions of a direct-injection hydrogen research engine*. Tech. rep. SAE Technical Paper, 2008.

[17] Hakan Özcan and MS Söylemez. "Thermal balance of a LPG fuelled, four stroke SI engine with water addition". In: *Energy conversion and management* 47.5 (2006), pp. 570–581.

[18] V Subramanian, JM Mallikarjuna, and A Ramesh. "Effect of water injection and spark timing on the nitric oxide emission and combustion parameters of a hydrogen fuelled spark ignition engine". In: *International Journal of Hydrogen Energy* 32.9 (2007), pp. 1159–1173.

[19] S Brusca and R Lanzafame. *Evaluation of the effects of water injection in a single cylinder CFR cetane engine*. Tech. rep. SAE Technical Paper, 2001.

[20] Franz X Tanner, Matthias Brunner, and German Weisser. *A computational investigation of water injection strategies for nitric oxide reduction in large-bore DI diesel engines*. Tech. rep. SAE Technical Paper, 2001.

[21] Matthieu Cordier et al. *Water Injection to Improve Direct Injection Spark Ignition Engine Efficiency*. Tech. rep. SAE Technical Paper, 2019.

[22] Addison M Rothrock, ALOIS EESEK Jr, and Anthony W Jones. "The induction of water to the inlet air as a means of internal cooling in aircraft-engine cylinders". In: *Annual Report-National Advisory Committee for Aeronautics* 752-773 (1943), p. 59.

[23] Rinaldo J Brun, H Lowell Olsen, and Cearcy D Miller. *End-Zone Water Injection as a means of suppressing knock in a spark-ignition engine*. Aircraft Engine Research Laboratory, 1944.

[24] AT Colwell, RE Cummings, and DE Anderson. "Alcohol-water injection". In: *SAE Transactions* (1945), pp. 358–372.

[25] MR Rowe and GT Ladd. "Water injection for aircraft engines". In: *SAE Transactions* (1946), pp. 26–44.

[26] DC Eaton. "Cruising economy by use of water injection". In: *SAE Transactions* (1946), pp. 81–92.

[27] John Christopher. *Race for Hitler's X-Planes: Britain's 1945 Mission to Capture Secret Luftwaffe Technology*. The History Press, 2012.

[28] Graham White. *R-2800 Pratt & Whitney's Dependable Masterpiece*. SAE, 2001.

[29] United Aircraft Corporation. *The Pratt & Whitney Aircraft Story*. 1952.

[30] The Aviation History Online Museum. *Pratt & Whitney R-2800*. [Online; accessed 7-October-2019]. 1996. URL: http://www.aviation-history.com/engines/pr-2800.htm.

[31] Wikipedia contributors. *Daimler-Benz DB 605 — Wikipedia, The Free Encyclopedia*. [Online; accessed 7-October-2019]. 2019. URL: https://en.wikipedia.org/w/index.php?title=Daimler-Benz_DB_605&oldid=916974720.

[32] Wayback Machine. *The Daimler-Benz DB605*. [Online; accessed 7-October-2019]. URL: https://web.archive.org/web/20050916000302/http://w1.1861.telia.com/~u186104874/db605.htm.

[33] Wikipedia contributors. *Oldsmobile V8 engine — Wikipedia, The Free Encyclopedia*. [Online; accessed 7-October-2019]. 2019. URL: https://en.wikipedia.org/w/index.php?title=Oldsmobile_V8_engine&oldid=904194546.

[34] Wikipedia contributors. *Saab 99 — Wikipedia, The Free Encyclopedia*. [Online; accessed 7-October-2019]. 2019. URL: https://en.wikipedia.org/w/index.php?title=Saab_99&oldid=919554869.

[35] Matt Kimberley. *Oldsmobile's Jetfire Was A World First Turbo Car With A Fatal Flaw*. [Online; accessed 7-October-2019]. 2018. URL: https://www.carthrottle.com/post/oldsmobiles-jetfire-was-a-world-first-turbo-car-with-a-fatal-flaw/.

[36] Fabian Hoppe et al. "Water injection for gasoline engines: Potentials, challenges, and solutions". In: *International Journal of Engine Research* 17.1 (2016), pp. 86–96.

[37] Corinna Netzer et al. "Numerical analysis of the impact of water injection on combustion and thermodynamics in a gasoline engine using detailed chemistry". In: *SAE International Journal of Engines* 11.6 (2018), pp. 1151–1166.

[38] R Lanzafame. *Water injection effects in a single-cylinder CFR engine*. Tech. rep. SAE Technical Paper, 1999.

[39] Ingo Hermann et al. "Water Injection for Gasoline Engines-Quo Vadis?" In: *International Conference on Knocking in Gasoline Engines*. Springer. 2017, pp. 299–321.

[40] B Durst et al. "BMW water injection: initial experience and future potentials". In: *38th International Vienna Motor Symposium*. 2017.

[41] Martin Böhm et al. "Functional integration of water injection into the gasoline engine". In: *MTZ worldwide* 77.1 (2016), pp. 36–41.

[42] D TSURU, H KATO, and H TAJIMA. "Numerical and Experimental Study of Reduction of NOx on Diesel Combustion by Using Water Injection Systems". In: ().

[43] Charles F Taylor. "The internal combustion engine in theory and practice, 1985". In: *Volume* 1 ().

[44] Arthur W Gardiner. *Atmospheric Humidity and Engine Performance*. Tech. rep. SAE technical Paper, 1929.

[45] Jayesh Khatri et al. *Water Injection Benefits in a 3-Cylinder Downsized SI-Engine*. Tech. rep. SAE Technical Paper, 2019.

[46] John C Ingamells et al. *Effects of Atmospheric Variables on Passenger Car Octane Number Requirements*. Tech. rep. SAE Technical Paper, 1966.

[47] Yunus A Cengel and Michael A Boles. "Thermodynamics: an engineering approach". In: *Sea* 1000 (2002), p. 8862.

[48] Bin Chen et al. "Thermodynamic and numerical analysis of intake air humidification of a turbocharged GDI engine". In: *Sādhanā* 43.5 (2018), p. 79.

[49] Mahammad A Hannan, FA Azidin, and Azah Mohamed. "Hybrid electric vehicles and their challenges: A review". In: *Renewable and Sustainable Energy Reviews* 29 (2014), pp. 135–150.

[50] J Wade and RJ Farrauto. "Controlling emissions of pollutants in urban areas". In: *Metropolitan Sustainability*. Elsevier, 2012, pp. 260–291.

[51] Deboshree Mukherjee and Benjaram M Reddy. "Significance of Oxygen Storage Capacity of Catalytic Materials in Emission Control Application". In: *Emission Control Science and Technology* 6.4 (2020), pp. 381–389.

[52] Arvind Kumar et al. *Optimization of Performance of Oxygen Storage Component (OSC) for NO Reduction in Three Way Catalysts to Achieve BS VI Emission Norms*. Tech. rep. 2019.

[53] Commissioning Regulation. "Regulation (EC) No 692/2008 as regards emissions from light passenger and commercial vehicles (Euro 6)". In: *European Union* (2016).

[54] Andrew Roberts, Richard Brooks, and Philip Shipway. "Internal combustion engine cold-start efficiency: A review of the problem, causes and potential solutions". In: *Energy Conversion and Management* 82 (2014), pp. 327–350.

[55] Tao Li et al. "Effect of partial-heating of the intake port on the mixture preparation and combustion of the first cranking cycle during the cold-start stage of port fuel injection engine". In: *Experimental Thermal and Fluid Science* 49 (2013), pp. 14–21.

[56] Peiyong Ni, Xiangli Wang, and Shengli Wei. "Effects of intake air temperature on SI engine emissions during a cold start". In: *International Journal of Sustainable Energy* 33.2 (2014), pp. 243–250.

[57] Luis Carlos Monteiro Sales and José Ricardo Sodré. "Cold start emissions of an ethanol-fuelled engine with heated intake air and fuel". In: *Fuel* 95 (2012), pp. 122–125.

[58] JD Trapy and P Damiral. "An investigation of lubricating system warm-up for the improvement of cold start efficiency and emissions of SI automotive engines". In: *SAE transactions* (1990), pp. 1635–1645.

[59] Frank Will and Alberto Boretti. "A new method to warm up lubricating oil to improve the fuel efficiency during cold start". In: *SAE international journal of engines* 4.1 (2011), pp. 175–187.

[60] Roberto Cipollone, Davide Di Battista, and Marco Mauriello. "Effects of oil warm up acceleration on the fuel consumption of reciprocating internal combustion engines". In: *Energy Procedia* 82 (2015), pp. 1–8.

[61] Guang Xin Gao, Zhu Lin Yuan, and Jian Da Yu. "Investigation of cold start engine performance at low temperature fuelled with alternative fuel". In: *Applied Mechanics and Materials*. Vol. 694. Trans Tech Publ. 2014, pp. 39–44.

[62] Ruizhi Song et al. "Combustion characteristics of SI engine fueled with methanol-gasoline blends during cold start". In: *Frontiers of Energy and Power Engineering in China* 2.4 (2008), pp. 395–400.

[63] Paolo Iodice et al. "Effect of ethanol–gasoline blends on CO and HC emissions in last generation SI engines within the cold-start transient: An experimental investigation". In: *Applied energy* 179 (2016), pp. 182–190.

[64] Marcello F Brunocilla and Fernando Lepsch. *Influence of hot fuel injection on air/fuel mixture preparation and effects on Flex Fuel Engines*. Tech. rep. SAE Technical Paper, 2006.

[65] Daniel Kabasin et al. "Emission reduction with heated injectors". In: *SAE International Journal of Engines* 3.1 (2010), pp. 982–995.

[66] C Lohfink, H Baecker, and M Tichy. *Experimental investigation on catalyst-heating strategies and potential of GDI combustion systems*. Tech. rep. SAE Technical Paper, 2008.

[67] Suchitra Sivakumar et al. *Effects of Using an Electrically Heated Catalyst on the State of Charge of the Battery Pack for Series Hybrid Electric Vehicles at Cold Start*. Tech. rep. SAE Technical Paper, 2020.

[68] Dongsuk Kum, Huei Peng, and Norman K Bucknor. "Optimal catalyst temperature management of plug-in hybrid electric vehicles". In: *Proceedings of the 2011 American Control Conference*. IEEE. 2011, pp. 2732–2738.

[69] Paul Chambon et al. "PHEV cold start emissions management". In: *SAE International Journal of Alternative Powertrains* 2.2 (2013), pp. 252–260.

[70] Daisy Thomas et al. *Investigating the engine behavior of a hybrid vehicle and its impact on regulated emissions during on-road testing*. Tech. rep. SAE Technical Paper, 2019.

[71] Thomas Wellmann et al. "Influence of automatic engine stop/start systems on vehicle NVH and launch performance". In: *SAE International Journal of Engines* 8.4 (2015), pp. 1938–1946.

[72] Per Tunestål. "Self-tuning gross heat release computation for internal combustion engines". In: *Control Engineering Practice* 17.4 (2009), pp. 518–524.

[73] Håkan Sandquist, Simon Klacar, and Shubo Li. "Development of a HEV Powertrain for Global Application". In: *28. Aachen Colloquium Automobile and Engine Technology* (2019).

[74] AVL List GmbH. *AVL PUMA 2: Testbed Automation Platform*. [Online; accessed 18-February-2020]. 2021. URL: https://www.avl.com/-/avl-puma-2.

[75] Emmanuel Kasseris and John Heywood. "Charge cooling effects on knock limits in SI DI engines using gasoline/ethanol blends: Part 2-effective octane numbers". In: *SAE International Journal of Fuels and Lubricants* 5.2 (2012), pp. 844–854.

[76] Trevor Davies et al. *Fuel effects in a boosted DISI engine*. Tech. rep. SAE Technical Paper, 2011.

[77] Gautam T Kalghatgi. "Fuel anti-knock quality-Part I. Engine studies". In: *SAE Transactions* (2001), pp. 1993–2004.

[78] Gautam T Kalghatgi. "Fuel anti-knock quality-Part II. Vehicle Studies-how relevant is Motor Octane Number (MON) in modern engines?" In: *SAE Transactions* (2001), pp. 2005–2015.

[79] Gautam T Kalghatgi et al. "Auto-ignition quality of practical fuels and implications for fuel requirements of future SI and HCCI engines". In: *SAE technical paper* 4 (2005).

[80] Jayesh Khatri et al. "Effect of relative humidity on water injection technique in downsized spark ignition engines". In: *International Journal of Engine Research* (2020), p. 1468087420940854.

[81] Marcus Klein. *A specific heat ratio model and compression ratio estimation*. Division of Vehicular Systems, Department of Electrical Engineering . . ., 2004.

[82] Jayesh Khatri and Lucien Koopmans. *Water Injection System Application in a Mild Hybrid Powertrain*. Tech. rep. SAE Technical Paper, 2020.

[83] Tadahiko Murata, Hisao Ishibuchi, et al. "MOGA: multi-objective genetic algorithms". In: *IEEE international conference on evolutionary computation*. Vol. 1. 1995, pp. 289–294.

[84] S Lu. *Vehicle survivability and travel mileage schedules*. Tech. rep. 2006.

[85] *Greenhouse Gases Equivalencies Calculator - Calculations and References*. https://www.epa.gov/energy/greenhouse-gases-equivalencies-calculator-calculations-and-references. Accessed: 2021-10-19.

Appendices

Appendix A

Drive Cycle Analysis

In this chapter, the figures from the tests performed with the hybrid setup when operated under different drive cycles are presented. The tests were conducted under the first campaign of the second phase (engine starts investigation) of the work at Chalmers university's powertrain test bed. The figures show engine start categories for the six drive cycles, including RTS95, US06 and NEDC.

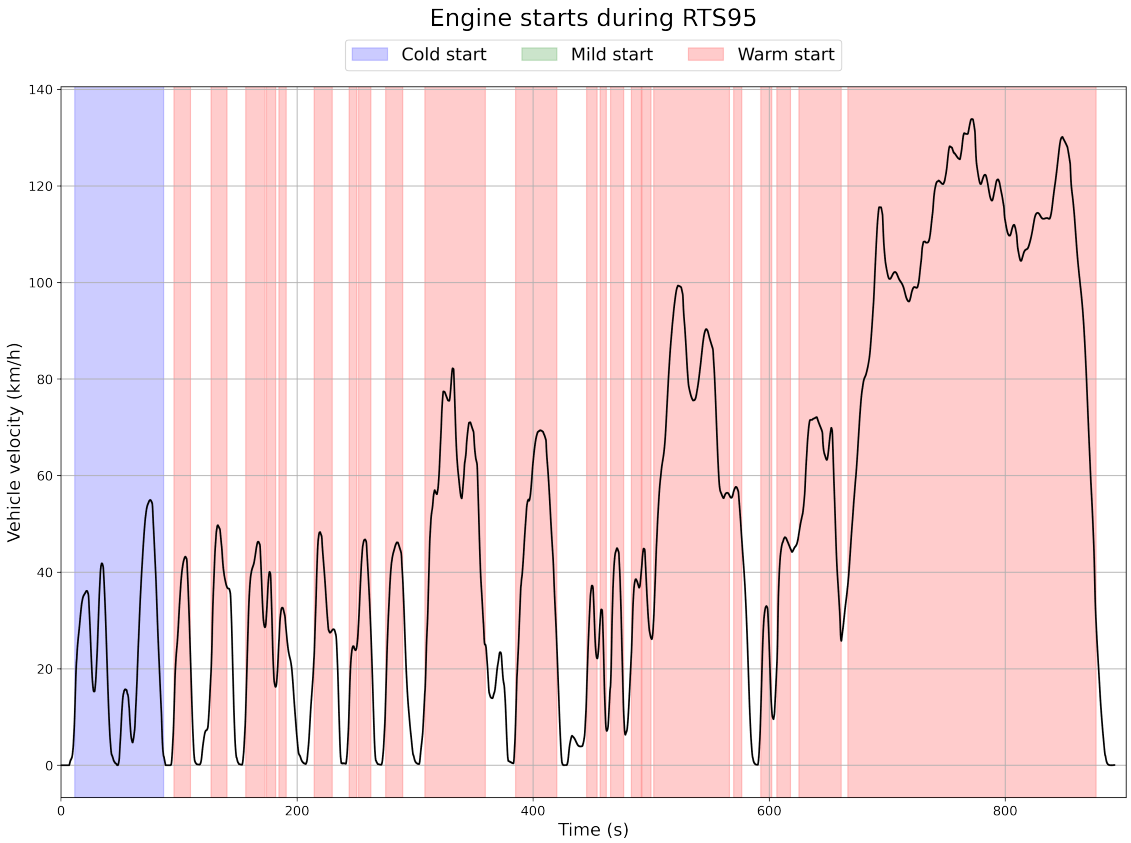

Figure A.1: Engine Starts during RTS95

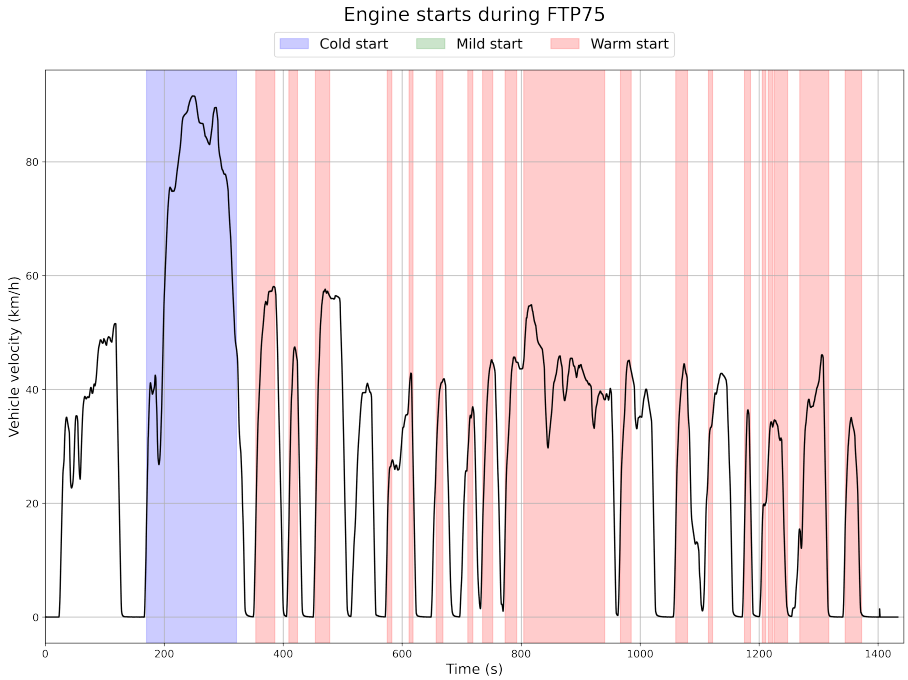

Figure A.2: Engine Starts during FTP75

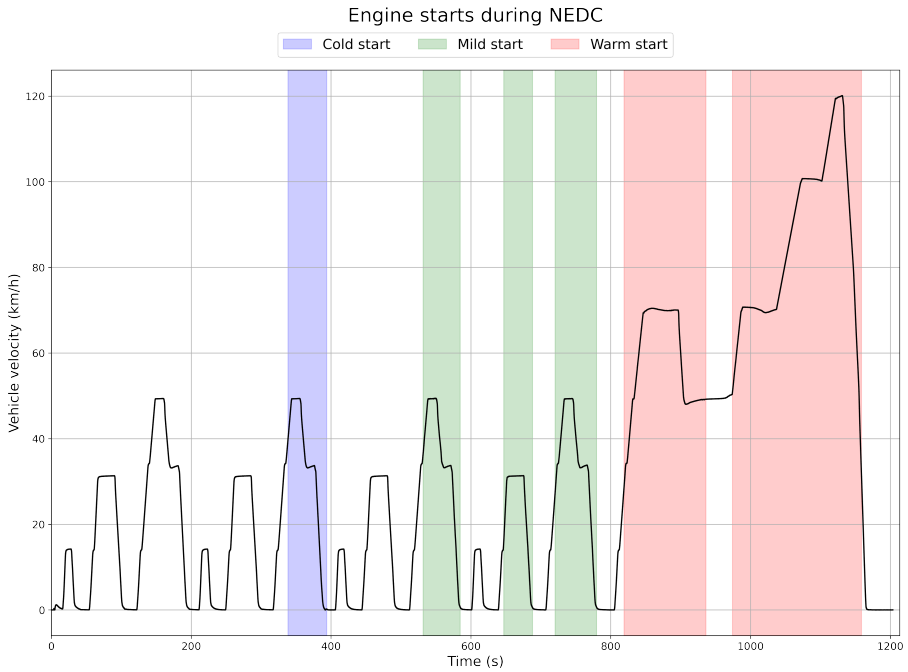

Figure A.3: Engine Starts during NEDC

Figure A.4: Engine Starts during SC03

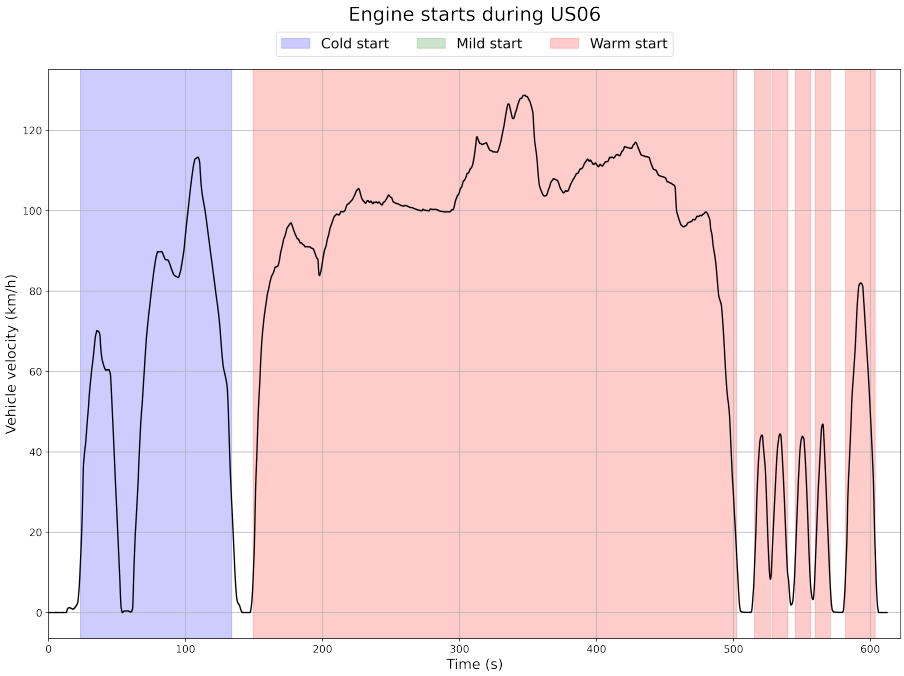

Figure A.5: Engine Starts during US06

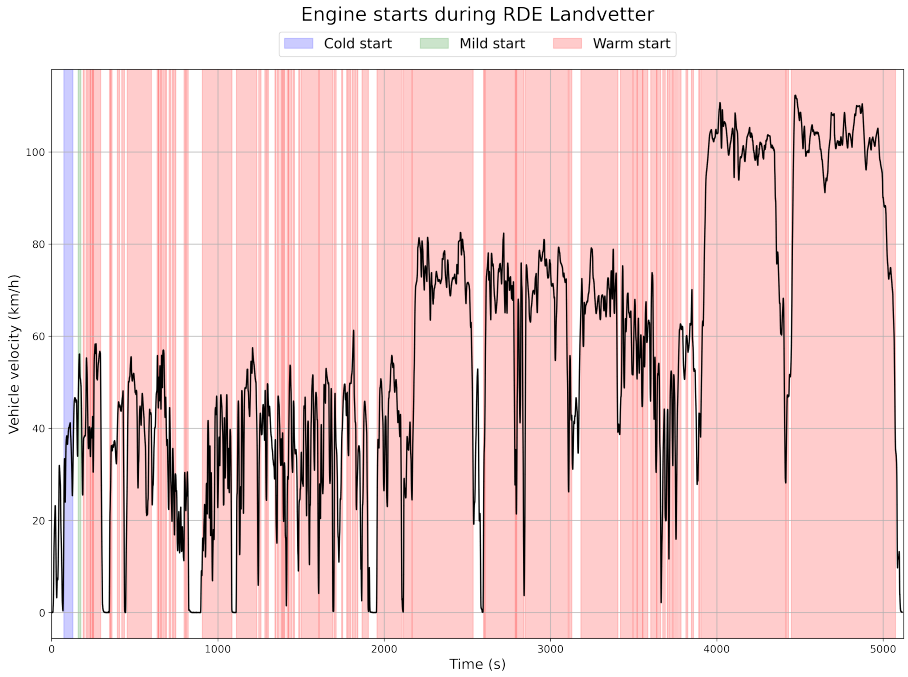

Figure A.6: Engine Starts during a Real Drive Cycle

Appendix B

Engine Start Optimization

This chapter demonstrates an example showing the optimization of engine start based on the results presented in section 6.2 using AVL tool CAMEO. AVL CAMEO is a calibration software, supporting

- intelligent and automated testing in order to get behavior models of a system under test
- These behavior models are used in a later step to support optimization decisions based on these models.
- Finally, decided values might be used to recalculate or define ECU-Parameter sets like single values, curves or maps.

So finally, using all these steps, a target oriented and traceable calibration of a mechatronic unit is supported. While CAMEO was used in this study for test automation, in this section a demonstration is provided to identify optimal engine starting conditions (speed and torque) when the target was set to minimize the integrated tailpipe NOx and integrated fuel mass. A constraint, that at least 10 kW engine power should be delivered right after the start, was applied during the optimization.

Figure B.1 shows the trade-off diagram for mass integrated tailpipe NOx and fuel consumption, after asking the optimizer to use both channels to be minimized in a multi objective approach. The blue points in the figure depicts measured values and the orange points are the values generated by the optimizer, predicted by the behavior-models – based on the experimental data. The R2 value for fuel mass integrated and tailpipe NOx was 0.9886 and 0.9477, respectively. The grey points also depic the predicted values, however, the grey points violate either one of the optimization constraints set in the Optimizer. A *pareto front* can be noted close to the horizontal axis – outlined with “blue diamonds” and the selected optimum point marked as “green diamond”.

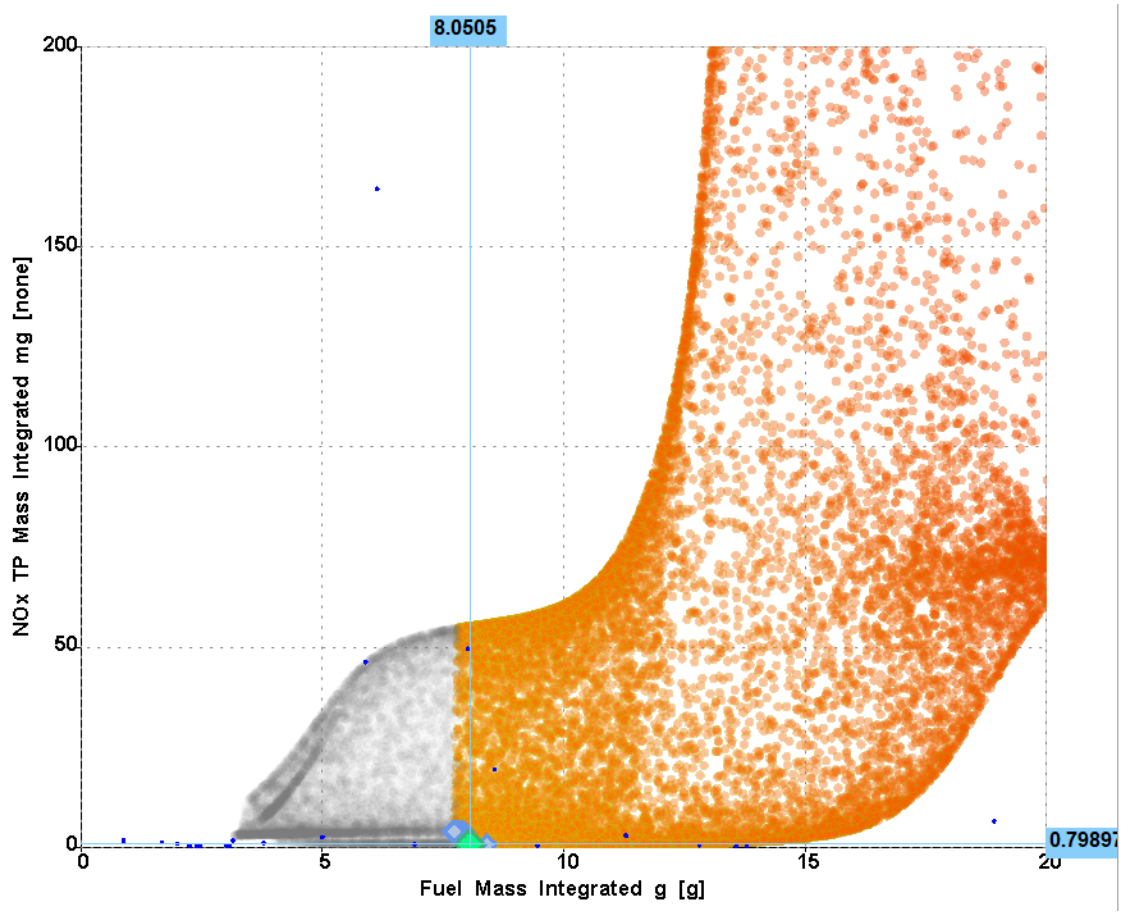

Figure B.1: Trade-off between integrated fuel mass and tailpipe NOx for the starting condition when the TWC temperature is 400°C at the engine start. The plot is generated in AVL CAMEO.

The results from the figure suggest that, for this condition - a start with catalyst temperature of 400°C, it is most beneficial to start the engine with 1540 rpm as engine speed and an alpha value of 21.5% - expecting a torque of 62 Nm and thus the desired 10 kW. This can also seen from the intersection plot in figure B.2. The behavior and confidence interval of different responses (tailpipe NOx and fuel mass) against parameters - engine speed, torque and catalyst temperature, can also be seen in figure B.2.

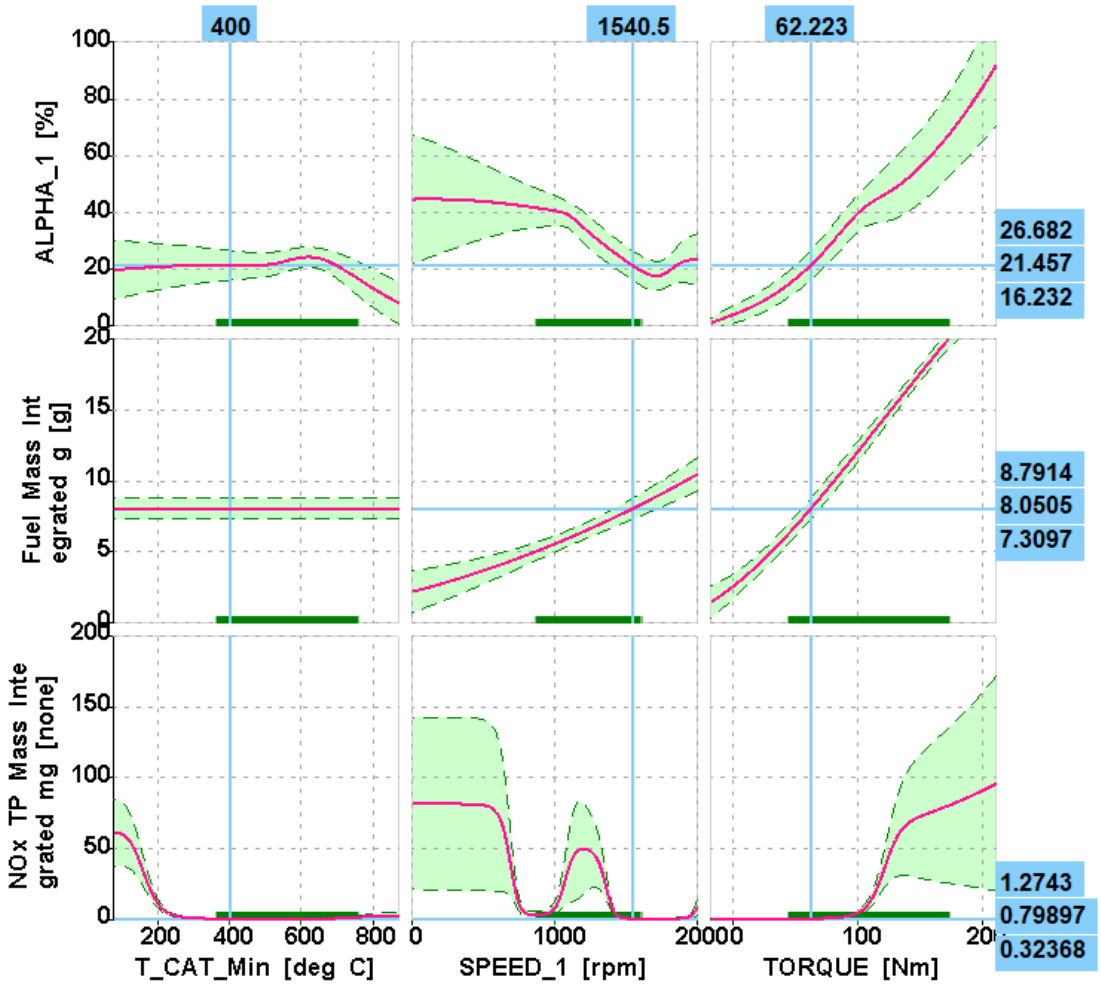

Figure B.2: Intersection plot in AVL CAMEO showing the behavior of different parameters on target functions and responses